NAVAL POSTGRADUATE SCHOOL
Monterey, California

DTIC
ELECTE
S FEB 26 1992 D
B

THESIS

HIGH FREQUENCY ANALYSES OF COASTAL METEOROLOGICAL PHENOMENA AFFECTING REFRACTIVITY

by

Anthony A. Martinez

December 1991

Thesis Advisor: Carlyle H. Wash

92 2 21 004

92-04590

REPORT DOCUMENTATION PAGE

1a. REPORT SECURITY CLASSIFICATION Unclassified			1b. RESTRICTIVE MARKINGS			
2a. SECURITY CLASSIFICATION AUTHORITY			3. DISTRIBUTION/AVAILABILITY OF REPORT Approved for public release; distribution is unlimited.			
2b. DECLASSIFICATION/DOWNGRADING SCHEDULE						
4. PERFORMING ORGANIZATION REPORT NUMBER(S)			5. MONITORING ORGANIZATION REPORT NUMBER(S)			
6a. NAME OF PERFORMING ORGANIZATION Naval Postgraduate School		6b. OFFICE SYMBOL (If Applicable) 35	7a. NAME OF MONITORING ORGANIZATION Naval Postgraduate School			
6c. ADDRESS (city, state, and ZIP code) Monterey, CA 93943-5000			7b. ADDRESS (city, state, and ZIP code) Monterey, CA 93943-5000			
8a. NAME OF FUNDING/SPONSORING ORGANIZATION		6b. OFFICE SYMBOL (If Applicable)	9. PROCUREMENT INSTRUMENT IDENTIFICATION NUMBER			
8c. ADDRESS (city, state, and ZIP code)			10. SOURCE OF FUNDING NUMBERS			
			PROGRAM ELEMENT NO.	PROJECT NO.	TASK NO.	WORK UNIT ACCESSION NO.

11. TITLE (Include Security Classification)
HIGH FREQUENCY ANALYSES OF COASTAL METEOROLOGICAL PHENOMENA AFFECTING REFRACTIVITY

12. PERSONAL AUTHOR(S)
Anthony A. Martinez

13a. TYPE OF REPORT Master's Thesis	13b. TIME COVERED FROM TO	14. DATE OF REPORT (year, month, day) December 1991	15. PAGE COUNT 100

16. SUPPLEMENTARY NOTATION
The views expressed in this thesis are those of the author and do not reflect the official policy or position of the Department of Defense or the U.S. Government.

17. COSATI CODES			18. SUBJECT TERMS (continue on reverse if necessary and identify by block number)
FIELD	GROUP	SUBGROUP	Coastal Meteorology, Refraction, Ducting, Evaporation Duct

19. ABSTRACT (Continue on reverse if necessary and identify by block number)

An eastern Pacific Ocean survey was conducted 7-10 May 1991 along the California coast to determine temporal and spatial variability in refractive conditions. Refractive profiles obtained from high frequency radiosonde measurements at shore sites and a ship plus continuous shipboard surface measurements found a high degree of refractive variability to be present. Local and synoptic scale conditions were found to have a major impact on the degree of refractive variability. The variability was in the occurrence of elevated layers and the evaporation duct height. With passage of the cold front, the evaporation duct height increased from values that would not affect shipboard sensors to those that would. Survey soundings and refractive profiles were also compared with subjective refractive analyses and forecast profiles from the Navy Atmospheric Boundary Layer model. In situ measurements revealed significant variability in refractive profiles that were not revealed in the model forecasts.

20. DISTRIBUTION/AVAILABILITY OF ABSTRACT [X] UNCLASSIFIED/UNLIMITED ☐ SAME AS RPT. ☐ DTIC USERS	21. ABSTRACT SECURITY CLASSIFICATION Unclassified		
22a. NAME OF RESPONSIBLE INDIVIDUAL Carlyle H. Wash	22b. TELEPHONE (Include Area Code) (408) 646-2295	22c. OFFICE SYMBOL MR/WX	

High Frequency Analyses
of Coastal Meteorological Phenomena
Affecting Refractivity

by

Anthony A. Martinez
Lieutenant Commander, United States Navy
B.S., United States Naval Academy, 1981

Submitted in partial fulfillment of the requirements for
the degree of

MASTER OF SCIENCE IN METEOROLOGY AND
PHYSICAL OCEANOGRAPHY

from the

NAVAL POSTGRADUATE SCHOOL
December, 1991
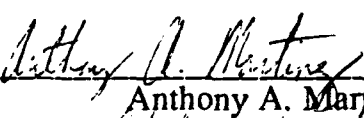
Author: _____
Anthony A. Martinez

Approved by: _____
Carlyle H. Wash, Thesis Advisor
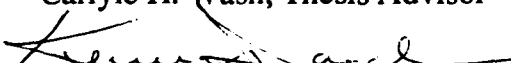
_____
Kenneth L. Davidson, Second Reader
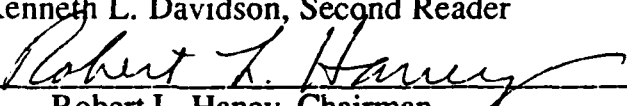
_____
Robert L. Haney, Chairman,
Department of Meteorology

ii

ABSTRACT

An eastern Pacific Ocean survey was conducted 7-10 May 1991 along the California coast to determine temporal and spatial variability in refractive conditions. Refractive profiles obtained from high frequency radiosonde measurements at shore sites and a ship plus continuous shipboard surface measurements found a high degree of refractive variability to be present associated with frontal passage. Local and synoptic scale conditions were found to have a major impact on the degree of refractive variability. The variability was in the occurrence of elevated layers and the evaporation duct height. With passage of the cold front, the evaporation duct height increased from values that would not affect shipboard sensors to those that would. Survey soundings and refractive profiles were also compared with subjective refractive analyses and forecast profiles from the Navy Atmospheric Boundary Layer model. In situ measurements revealed significant variability in refractive profiles that were not revealed in the model forecasts.

iii

TABLE OF CONTENTS

LIST OF TABLES

LIST OF FIGURES

ACKNOWLEDGMENTS

I. INTRODUCTION

The performance of modern naval weapon systems, sensors and communications equipment can be impacted significantly by a marine environment. With an awareness of these effects, the Navy is exploring ways of placing environmental measurement and display systems aboard its small combatants to more easily monitor and assess the surrounding environment.

IOTA (Integrated Oceanographic Tactical Aid) is one such system being developed for fleet use. It is intended to acquire, process and display in situ environmental data in an automated fashion to aid in the tactical decision-making process. An environmental system already in use by the Navy is TESS (Tactical Environmental Support System). TESS is designed to meet the need for an improved environmental support capability aboard major combatants and at selected shore activities. IOTA is intended to extend the TESS concept to smaller Navy ships. However, while TESS is designed for operation only by environmental support personnel (e.g., Aerographer's Mates), IOTA is intended for use by personnel with little or no training in the environmental sciences.

IOTA will have the capability to receive raw and preprocessed environmental data via afloat communications systems plus support requests and data inputs from other

1

systems. IOTA will also have the ability to receive local environmental sensor data and satellite data.

Atmospheric refraction is one important factor which affects modern communications, sensors and weapon systems. Formation of and changes in elevated or surface ducts affect a ship's ability to detect incoming missiles and aircraft as well as the performance of onboard sensors and communications systems. Aircraft operating in concert with other naval forces also find their sensors and communications affected by these phenomena. In an environment where refractive conditions are subject to rapid change due to constantly changing environmental conditions, it is vital that a naval unit be able to measure refractive conditions continuously. This ability to receive local environmental data will allow a steady determination to be made of constantly changing refractive conditions surrounding a ship. Depending on these conditions, the performance of communications, weapons systems and sensors can be enhanced or adversely affected.

In support of this IOTA effort, the objectives of this thesis will be:

1) to evaluate continuous measurement systems and satellite systems for their use as tactical aids within IOTA.

2) to observe and identify coastal meteorological phenomena which could have a direct impact on refractive conditions.

3) to compare a refractive layer model, refractive assessments and sounding forecasts against actual observations.

Chapter II will discuss meteorological parameters affecting refraction, atmospheric refractive layers and ducts, and the minimum radio frequency which can be trapped in a duct. Chapter III will describe the organization of an in situ survey to measure refractive changes in the eastern Pacific Ocean along the California coast. Chapter IV discusses results of the survey. These results demonstrate the importance of meteorological phenomena on atmospheric refraction as well as the temporal and spatial variability of refractive conditions. A comparison of refractive layers observed is made against layers expected from a proposed working model by Rosenthal and Helvey (1979). Chapter V compares refractive assessments made by the Naval Western Oceanography Center (NWOC) for the eastern Pacific Ocean against those obtained during the survey. NABL (Naval Atmospheric Boundary Layer) 12 and 24 hour forecast soundings for the eastern Pacific Ocean are also compared against radiosonde soundings obtained by the survey's at sea platform.

II. ASSESSMENT OF REFRACTION

When an electromagnetic (EM) signal propagates through a medium, it interacts with that medium through the absorption and re-emission or scattering of EM energy. The efficiency of the interaction is related to the amount of signal absorption. Changes in propagation velocity due to this interaction result in a bending of the signal path. This bending is called refraction.

A. METEOROLOGICAL VARIABLES AFFECTING REFRACTIVE LAYERS

A measure of refraction is the index of refraction (n). For Very High Frequency (VHF), Ultra High Frequency (UHF), and microwave frequency propagation in the atmosphere, n ranges between 1.00025 and 1.00040. Since these values are very close to one, another measure of refraction used, from Patterson (1988), is the refractivity (N) which is given as:

$$N = (n-1) \times 10^6 = \frac{77.6P}{T} + \frac{3.73 \times 10^5 e}{T^2}$$

where P = atmospheric pressure (mb)

e = partial pressure of water vapor (mb) or

$$e = \frac{-RH}{100} \times 6.105 \exp(a)$$

$$a = 25.22 \times \frac{(T - 273.2)}{T} - 5.31 \times \log_e \frac{T}{273.2}$$

T = atmospheric temperature (K)

4

RH = atmospheric relative humidity (%)

In the atmosphere, N is generally between 250 and 400. From the above equation, it can be seen that N is dependent on pressure, temperature, and moisture. Since these variables vary throughout the troposphere, there are gradients of refractivity and, as a consequence, EM rays bend as they pass through the troposphere. Since these variables usually vary much less in the horizontal than in the vertical, horizontal gradients of refractivity are usually negligible compared to those in the vertical.

Fig. 1 illustrates how propagation of an EM ray is affected by various types of refractive conditions. Under normal refractive conditions, some bending of an EM ray will occur due to changes in refractivity encountered by the EM ray as it propagates through the atmosphere. In other than normal refractive conditions, greater upward or downward bending of an EM ray can occur. Excessive bending of an EM ray upward and away from the earth is the refractive condition called subrefraction. In the case of superrefraction, a propagating EM ray will be bent downward from a straight line more than under normal conditions. It can be bent to the extent that the radius of curvature of the EM ray approaches the radius of curvature of the earth. Another refractive condition, known as trapping, occurs when rapidly varying refractivity causes the radius of curvature of the EM ray to become smaller than the radius of the earth. This results in the EM ray either

5

striking the earth and undergoing surface reflection, or entering a region of standard refraction and being refracted back upward, only to reenter the area of rapidly changing refractivity which causes downward refraction. This results in a trapping of the EM ray in a duct as the EM ray is confined and channeled between the top and bottom of the duct.

To depict more clearly the presence of these trapping conditions or ducts in the atmosphere, a modified index is used. This modified index, called the M-index, is defined as

$$M = N + (.157 \text{ m}^{-1})(z)$$

where N is the value of the refractivity at any height z (m). When the M-gradient (dM/dz) is zero the EM ray curvature equals the earth's curvature. This is another way of stating that when the N-gradient (dN/dz) is minus .157 units per meter, the EM ray has the same curvature as the earth. For a standard atmosphere, M increases with height. The importance of M is that dM/dz must be negative for a duct to form. In addition, plotting the M-index as a function of height allows the location of the top and bottom of a duct to be quickly recognized. Table I, adapted from Patterson et al. (1990), classifies the various refractive conditions, their relationship to dM/dz, and the distance to surface horizon of a propagating EM ray.

PC-IREPS (Personal Computer-Integrated Refractive Effects Prediction System) Version 2.0, from Patterson (1990), a

Table I: REFRACTIVE CONDITIONS

Refractive Condition	$\frac{dM}{dz}$ (m^{-1})	Distance to surface horizon
Subrefraction	> .157	Reduced
Normal	.079 to .157	Normal
Superrefraction	0 to .079	Increased
Trapping	< 0	Greatly Increased

system designed to predict EM propagation properties was used in this thesis to determine the presence of refractive layers and ducts based on temperature, pressure, and relative humidity data received from survey radiosonde measurements.

From Table I, a trapping layer is defined as a region where dM/dz < 0. Fig. 2 displays examples of a trapping layer with its associated duct which could be an elevated duct (Fig. 2a) or a surface duct (Figs. 2b and 2c). The top of each type of duct will always be at the same height as the top of the trapping layer. However, the bottom of each duct will usually extend below the bottom of the trapping layer. The elevated duct will have its lower boundary above the surface while that of the surface-based duct will be at the surface.

To have trapping layers, a positive vertical temperature gradient (inversion) and/or a negative vertical humidity gradient are required, i.e. a trapping layer is likely to form where temperature increases rapidly with height and/or humidity decreases rapidly with height. Fig. 3 illustrates the typical marine atmospheric boundary layer (MABL) which

exists between the surface and the free troposphere above it. The top of the MABL, the interfacial layer, is characterized by a large drop in specific humidity (q) and a large increase in potential temperature (θ) which is ideal for formation of a trapping layer. A trapping layer which remains above the surface is sometimes referred to as an elevated layer. Fig. 4 illustrates how a trapping layer can affect propagation of a radar signal leading to long range detection of the signal and errors in aircraft tracking.

Over the ocean, trapping layers and their associated ducts are usually found in two areas as shown in Fig. 5. One is just above the sea surface (the evaporation duct) and the other is at the top of the MABL which can usually be found at heights from 100 - 2000 m. In addition, ducts can also be found in any other area of the atmosphere where a strong positive vertical temperature gradient and/or a strong vertical negative humidity gradient are present.

B. EVAPORATION DUCT

Over the sea surface, a very thin surface-based duct often forms with typical heights of 2-30 m. It is characterized by a rapid vertical decrease of relative humidity from 100% (at the water surface itself) to 80-90% (in the atmosphere) resulting in a rapid vertical decrease of refractivity. The distinction between this duct and a surface-based duct is that it is produced solely from evaporation over the sea surface,

8

hence the name evaporation duct. The top of this duct is at a height called the evaporation duct height, Z_*. Z_* cannot be determined from radiosonde or refractometer measurements because the evaporation duct occurs over heights too small for these instruments to obtain accurate measurements.

Aboard the Research Vessel (R/V) Point Sur, the at sea platform used in this survey, Z_* was computed employing the bulk method used by Fairall et al. (1978). This method uses Monin-Obukhov Similarity (MOS) theory, which is based upon the relationship of the surface layer profiles of temperature, wind speed, water vapor, and turbulence with the surface fluxes of momentum and sensible and latent heat. In computing Z_*, measurements of only four quantities--air temperature, wind velocity, and relative humidity measured at a single level plus sea surface temperature--were required utilizing this method. Fig. 6 shows where these single level measurements were made on the R/V Point Sur to determine the evaporation duct M-profile. Assumptions made in using the bulk method were that relative humidity at the sea surface is 100% and wind speed at the surface is zero. Using the bulk method, Z_* is computed using an iterative approach to solving the following equation:

$$Z_* = - \frac{[7.2\ \Delta q - 1.2\ \Delta T]}{.125[Ln\ Z/Z_0 - \psi(\xi)} \cdot \phi_s(\xi_*)$$

where ΔT = air-surface temperature difference (K)

9

Δq = air-surface specific humidity difference ($gmkg^{-1}$)

Z = measurement height (m)

Z_o = roughness length (m)

$\phi_s(\xi_*)$ = stability function

$\psi(\xi)$ = profile stability function

C. MINIMUM FREQUENCY (f_{min})

If a transmitter is located within a duct, the thickness of the duct will determine the range of frequencies which can be trapped. The following equation from Farrell (1989) is used to determine the minimum frequency (f_{min}) that will be trapped by a duct:

$$f_{min} \text{ (GHz)} = CG^{-1/2}d^{-3/2}$$

where $C = 1.1933 \times 10^2$ for a surface-based duct

$C = 7.8947 \times 10^2$ for an elevated duct

$$G = \frac{M_B - M_T}{d}$$

M_B = modified refractivity at the bottom of the trapping layer

M_T = modified refractivity at the top of the trapping layer

d = depth of trapping layer (m)

In the case of the evaporation duct, f_{min} is calculated using the equation from Fairall et al. (1978):

$$f_{min} \ (GHz) = 3.6 \times 10^2 Z_*^{-3/2}$$

where Z_* is in meters.

F_{min} is only an approximate value since frequencies slightly less than f_{min} will still be somewhat trapped. However, as the frequencies decrease further below f_{min}, the effects of trapping diminish for these lower frequencies.

III. EAST PACIFIC OCEAN REFRACTION SURVEY

From 7-10 May 1991, a survey was conducted using six shore stations and one at sea platform to determine the degree of refractive changes caused by MABL and lower tropospheric variability along the California coast. These stations were the University of California at Santa Cruz (UCSC) in Santa Cruz, CA; the Naval Postgraduate School (NPS) and Monterey Bay Aquarium (MBA) in Monterey, CA; Vandenberg Air Force Base (VBG), CA; Point Mugu (MUGU), CA; San Nicolas Island (NSI) off the Southern California coast; and the R/V Point Sur (PSUR). The PSUR is owned by the National Sciences Foundation (NSF) and operated by the Moss Landing Marine Laboratory. Funding for the use of this vessel by NPS is provided by the Oceanographer of the Navy.

Vertical profiles were measured with radiosondes at four shore sites and the PSUR and with the HIS (High Resolution Interferometer Sounder) aboard the PSUR. Automated surface observation systems were used to obtain measurements of evaporation duct height, Z_*. Satellite imagery was used to monitor the survey area. Table II displays the systems used at each station.

Upon commencement of the survey (0000Z 8 May), simultaneous radiosonde launches were conducted every six

12

Table II: MEASUREMENT SYSTEMS

	UCSC	MBA	NPS	VBG	MUGU	NSI	PSUR
Radiosonde			x	x	x	x	x
Automated surface observation system	x	x					x
HIS							x

hours by PSUR, NPS, and VBG. Additional launches were also conducted at MUGU and NSI. Normally, radiosondes are launched only twice a day from VBG and other National Weather Service sites. Fig. 7 displays the location of the launch sites as well as the track of PSUR during the survey period. The pressure, temperature, and relative humidity profile data from these radiosonde launches allowed in situ refractivity assessments to be made for each location. These assessments included the identification of trapping layers and their associated ducts.

Continuous measurements of Z_* were made using inputs of sea surface temperature as well as continuous single level measurements of wind speed, air temperature, and dewpoint temperature. These measurements were made at PSUR, MBA, and UCSC using an automated surface observation system.

Satellite imagery, received at NPS and consisting of hourly visible and infrared GOES (Geostationary Operational Environmental Satellite) images, was used to monitor the movement and location of weather systems which could affect atmospheric refraction. Also available from GOES was water

vapor imagery useful for monitoring the evolution of water vapor content in the mid-troposphere. Any abrupt changes in water vapor content for a given area could indicate possible changes in refractive conditions.

Finally, the HIS, which is a passive remote sensing system designed for surface-based atmospheric soundings, was used aboard PSUR to conduct continuous temperature and moisture profiles of the atmosphere. These data were then compared against radiosonde measurements.

The goals of utilizing the above-described systems were to measure and detect small scale and rapidly changing meteorological phenomena which could affect atmospheric refraction and to demonstrate tne feasibility of using these systems on a small combatant to monitor environmental conditions at sea.

IV. RESULTS

An analysis of observed elevated trapping and superrefractive layers will be presented first followed by a discussion of observed evaporation duct variation. Times presented are UTC or Zulu time (Z) which are seven hours ahead of Pacific Daylight Savings Time. Sounding and IREPS profile dates and times are presented in the format of dd/ttttZ where dd is the date and tttt is time. The earliest sounding time is 072014Z May 1991 and the latest is 101200Z May 1991.

A. REFRACTIVE LAYERS

During the course of this survey, a weak cold front passed southward through the area. This cold front and its associated vertical motions had a major impact on refractive conditions in the MABL and lower troposphere. Radiosonde data and IREPS profiles from PSUR, NPS, VBG, NSI, and MUGU were used to determine changes in refractive conditions. A comparison of ducts and superrefractive layers observed will be made against those expected from a proposed working model by Rosenthal and Helvey (1979) for a cyclone and associated frontal and high pressure systems. Fig. 8 displays a large subtropical high southeast and a continental modified polar high west of the cold front. The regions labeled A-F identify areas where different refractive conditions are expected to be

15

encountered. Therefore, it is useful to describe events in relation to the position of the cold front and its circulation.

1. Prefrontal Inversion

The large scale 07/1200Z 500 mb analysis (Fig. 9) prior to commencement of the survey reveals the presence of an upper level ridge over California and a pronounced trough at 140W. By 08/0000Z, this ridge moves to the east as the East Pacific trough approaches from the northwest. 500 mb winds along the entire coast are southwesterly. The 08/0000Z NMC (National Meteorological Center) northern hemisphere surface analysis (Fig. 10) analyzes a surface cold front approaching California from the northwest. Winds are variable ahead of and northwesterly behind the front. A cloud band associated with this front is clearly evident in the 07/2231Z visible satellite image (Fig. 11). A patch of fog is present well east of the front along the Central California coast. To the west of the front is a large area of open cellular cumulus.

Prior to the onset of frontal activity, initial soundings from the five station radiosonde network reveal the presence of a low-level inversion at each location. These inversions occur at the top of the MABL where the dry air produced by subsidence from the upper level ridge caps the moist air of the MABL. This rapid drying of the atmosphere and inversion at the top of the MABL leads to a strong negative vertical

16

humidity gradient and a positive vertical temperature gradient which favor duct formation. Although these conditions occur at the top of the MABL, the presence of a duct is dependent on the magnitude of these temperature and moisture changes. At four of the five stations, (Fig. 12) ducts are present with a superrefractive layer present at the remaining station. Also, duct thicknesses and heights are found to vary.

The 07/2014Z sounding (Fig. 13a) from NSI, the southernmost station, illustrates this strong inversion and negative humidity gradient at a height of 300-500 m. The IREPS profile (Fig. 13b) for this station reveals the presence of a duct at a height of 500 m. The PSUR 08/0000Z sounding (Fig. 14a) indicates a weaker inversion 500 Km to the north of NSI between 200-700 m. Its IREPS profile (Fig. 14b) reveals the presence of a duct at about 500 m. Other stations have ducts at heights from 200 to 450 m.

It can also be seen that the PSUR duct in Fig. 14b is about twice as thick as the NSI duct in Fig. 13b. These different thicknesses indicate that the minimum frequency (f_{min}) which can be trapped in each duct will be different.

Following Rosenthal and Helvey (1979), region E (Fig. 8) best describes the survey area at this time. It calls for superrefractive layers to be present. Survey station observations show superrefractive layers to be present at all

stations. In addition, ducts are also found at four of the five stations.

2. Prefrontal Activity

As the cold front approaches the Central California coast, the frontal circulations modify the subsidence inversions. The 08/0531Z IR satellite image (Fig. 15) and 08/0600Z surface analysis (Fig. 16) show the cold front and associated cloud band approaching closer to the survey area. The position of the cold front in the IR image is shown by the band of high and mid-level clouds extending southwestward from Northern California. The frontal upward vertical motions lead to a weakening or elimination of MABL inversions near the surface. This is evident when comparing the 08/0000Z and 08/0600Z soundings for NPS (Figs. 17a and 18a) and PSUR (Figs. 14a and 19a).

However, the influence of the front causes other duct regions to form. At a height from about 1100 to 1700 m, dry layers not present in the NPS 08/0000Z sounding (Fig. 17a) are present in the 08/0600Z sounding (Fig. 18a). A comparison of the NPS 08/0600Z IREPS profile (Fig. 18b) with its 08/0000Z profile (Fig. 17b) shows the formation of multiple ducts due to these dry layers.

A dry layer not present in the PSUR 08/0000Z sounding (Fig. 14a) also shows up in its 08/0600Z sounding (Fig. 19a). A comparison of the PSUR 08/0000Z and 08/0600Z IREPS profiles

(Figs. 14b and 19b) reveals the formation of a duct due to this dry layer at a height of about 900 m. These dry layers are likely advected over the region ahead of the front. This shows that prefrontal activity has eliminated the original ducts at the top of the MABL in a period of six hours and has caused the formation of ducts at other levels.

At this point, region F (Fig. 8) best describes the survey area. Expected refractive conditions are near standard conditions with refractive layers rising and weakening with proximity to the front. What is actually observed is some rising of refractive layers with ducts and superrefractive layers continuing to be present. Also observed is the formation and disappearance of ducts and superrefractive layers due to frontal circulation.

3. Frontal Passage

The cold front passes over PSUR and NPS at approximately 08/1400Z, over VBG at 08/1800Z, and over MUGU and NSI at approximately 08/2100Z. The 08/1500Z surface analysis and data (Fig. 20) indicates that the front has already passed over PSUR and NPS and is headed towards the southern radiosonde sites.

Immediately ahead of the front, 08/1200Z soundings from NPS and PSUR (Figs. 21a and 22a) show a very moist layer from the surface up to approximately 2000 m due to the frontal upward vertical motion. In both cases, the IREPS profiles

(Figs. 21b and 22b) show a duct forming where the well-mixed moist layer is capped by the drier air above.

The net impact of the frontal zone on the soundings is the disappearance of the dry layers which were evident in the 08/0600Z soundings (Figs. 18a and 19a). Instead, what is now seen is a lower troposphere which is generally well-mixed due to frontal circulation.

Rosenthal and Helvey's (1979) model indicates near standard refractive conditions are expected for the frontal area. Survey station observations show only PSUR with normal conditions. Ducts and superrefractive layers continue to be present at the other coastal stations even as the front passes.

It is interesting to note the rapid changes in refractive layers during this 24 hour period. The initial low level inversion, present along the coast, lifts and weakens, new layers appear due to dry air advection, followed by a higher layer due to subsidence behind the front.

4. Postfrontal Subsidence

By 08/2100Z, the cold front has completed its passage through the area. Strong mid-tropospheric subsidence, evident by the dark area in the 08/2101Z water vapor satellite image (Fig. 23), follows immediately behind it and now becomes the primary factor affecting refractivity. This subsidence eventually extends to the surface. An example of the effects

of subsidence on refraction is demonstrated by the NPS sounding at 08/1800Z (Fig. 24a). Note the very dry air subsiding to a height of 1400 m compared to moist conditions just six hours earlier (Fig. 21a). As this subsiding air caps the moist air beneath it, a strong negative vertical humidity gradient forms as well as an inversion. The respective 08/1800Z IREPS profile (Fig. 24b) reveals the presence of a duct in this region. By 09/0000Z, the NPS sounding (Fig. 25a) shows subsidence extending all the way to the surface. This results in the elimination of the strong negative vertical humidity gradient and the inversion. The impact on refractivity is that the duct present in the 08/1800Z IREPS profile (Fig. 24b) no longer exists in the 09/0000Z IREPS profile (Fig. 25b).

Although subsidence reaching the surface at NPS eventually results in elevated duct elimination, its effects at VBG are not enough to eliminate the ducts. The VBG 09/0000Z sounding (Fig. 26a) shows dry subsiding air over moist air at a height of about 1000 m. Also evident is a second layer of dry air at a height of about 500 m. The result is two areas with negative vertical humidity gradients and inversions are present and the 09/0000Z IREPS profile (Fig. 26b) shows ducts to be present in these two areas. Similar duct behavior was present at NSI and MUGU. What is demonstrated in these cases is that after the cold front

passes, subsidence behind it becomes the major factor affecting refractivity.

5. Postfrontal Moistening

As the major subsidence area behind the cold front moves east, moistening due to advection starts to occur throughout the lower troposphere. This cool moist air advection has the effect of eliminating ducts as areas of negative humidity gradients and/or inversions are weakened or eliminated. The advection of cool moist air into the region is clearly shown by the 09/0000Z and 09/1200Z 850 mb analyses (Figs. 27 and 28) and soundings. The 850 mb analyses show cooler air moving into the survey region from the north while soundings show moistening and temperature drops in the lower troposphere.

The NPS 09/0600Z sounding (Fig. 29a) clearly shows an increase in moisture levels and a decrease in temperature throughout the lower troposphere when compared to the sounding six hours earlier (Fig. 25a). The 09/0600Z NPS IREPS profile (Fig. 29b) shows a duct at a height of 1700 m where a layer of drier air is present. By 09/1200Z, as advection of cool moist air continues, the NPS 09/1200Z sounding (Fig. 30a) shows this area with its negative vertical humidity gradient and slight inversion being eliminated. The final result, as shown in the NPS 09/1200Z IREPS profile (Fig. 30b), is the disappearance of the duct. This advection of cool moist air continues through

09/1800Z with the associated NPS sounding and IREPS profile (Figs. 31a and 31b) showing essentially the same conditions as were present at 09/1200Z. Similar conditions are also found at the other stations.

6. Postfrontal Inversions

By 10/0000Z, the inversions which existed at the top of the MABL prior to movement of the cold front into the area appear once again. This is due to the reestablishment of the MABL under the subsidence of the upper level ridge following the frontal passage and occurs at all five stations. The inversion and negative vertical humidity gradient at the top of the MABL cause formation of a duct or a superrefractive layer.

The 10/0000Z, 10/0600Z, and 10/1200Z NPS soundings (Figs. 32a, 33a, and 34a) and IREPS profiles (Figs. 32b, 33b, and 34b) clearly reveal the development of the MABL under large scale subsidence. A comparison of the 10/0600Z sounding (Fig. 33a) with the 10/0000Z sounding (Fig. 32a) shows a strengthening of the inversion and the presence of a negative vertical humidity gradient at the top of the MABL. In the 10/1200Z sounding (Fig. 34a), the inversion is still present, but it is now near the surface. An examination of the IREPS profiles reveals the presence of a duct at 600 m for the 10/0000Z profile (Fig. 32b), a superrefractive layer at 800 m for the 10/0600Z profile (Fig. 33b), and a superrefractive

layer at 100 m for the 10/1200Z profile (Fig. 34b). The duct and superrefractive layers are at the same level as the inversion and negative vertical humidity gradient at the top of the MABL.

The PSUR 10/0000Z, 10/0600Z, 10/1200Z soundings (Figs. 35a, 36a, and 37a) and IREPS profiles (Figs. 35b, 36b, and 37b) also reveal conditions similar to those at NPS. The 10/0000Z sounding (Fig. 35a) shows an inversion and negative vertical humidity gradient starting at approximately 1100 m. In the 10/0600Z sounding (Fig. 36a), the inversion is more pronounced at a height of about 750 m as subsidence acts to lower the MABL. By the 10/1200Z sounding (Fig. 37a), subsidence has forced the top of the MABL, with its inversion and negative vertical humidity gradient, down nearly to the surface. The IREPS profiles reveal no ducts to be present at the top the MABL. However, in each case, a superrefractive layer is present at the top of the MABL where the inversion and negative vertical humidity gradient are present.

The Rosenthal and Helvey (1979) estimate of postfrontal refractive conditions indicates that an initial period of normal refractivity should occur followed by the reestablishment of a low level duct. This survey indicated a more complex postfrontal environment. In particular, strong subsidence following the front produced elevated ducts within 12 hours of frontal passage. The advection of midlevel moisture over the next 12 hours further changed the refractive

24

conditions. Southern observation points measured multiple layers during the postfrontal period.

The central coast temperature and moisture profiles have now returned to the inversion conditions which existed prior to the arrival of the cold front. The typical MABL structure is now present once again with dry air from subsidence above it.

B. EVAPORATION DUCT

During the course of this survey, continuous measurements of parameters used to estimate the evaporation duct height were made from PSUR, MBA, and UCSC using automated surface observation systems. These measurements indicated that evaporation duct height changed significantly with the passage of the cold front. In this section, all measurements referred to are from the automated surface observation system located onboard PSUR although coastal stations measured similar features. Fig. 38 presents continuous wind, temperature and dewpoint measurements and estimates of evaporation duct height and minimum trapped frequencies. Once again, events are described in relation to the cold front.

1. Prefrontal Inversion

The temperature and wind data for the period from 07/2130Z to 08/0000Z show the presence of a very moist marine layer with increasing relative humidity and variable wind speed. The evaporation duct height for this period is

variable varying from a maximum of twelve meters to being z ro by 08/0000Z as the cold front approaches. During this period, f_{min} varies from 10 GHz to greater than 100 GHz.

2. Prefrontal Activity

During this period from 08/0000Z to 08/1300Z, relative humidity above the sea surface approaches 100%. The wind at the surface continues to be variable with speeds from 2-14 ms^{-1}. The net effect of these conditions is to produce an evaporation duct height of three meters or less throughout this period resulting in f_{min} remaining at approximately 100 GHz.

3. Frontal Passage

Immediately following passage of the cold front at approximately 08/1300Z, dramatic changes occur. The wind speed increases to 10-15 ms^{-1} and relative humidity starts to steadily decrease. These changes cause the evaporation duct height to increase from a height of several meters to about nine meters. The two coastal stations reported a marked frontal passage as well. This increase in evaporation duct height results in a decrease of f_{min} from about 100 GHz to a frequency slightly above 10 GHz.

4. Subsidence

As the cold front moves east, a steady decline in dewpoint occurs due to advection of drier air and subsidence discussed earlier. Also, wind speed continues to be above 10

ms^{-1} and slowly increases to about 17 ms^{-1}. The evaporation duct height (Z_*) increases from nine meters to a nearly constant height of thirteen meters. This results in a leveling off of f_{min} at approximately 10 GHz.

5. Postfrontal Period

At approximately 10/0100Z, the MABL is reestablished as relative humidity starts to increase and wind speed decreases to a speed of approximately 12 ms^{-1}. In this period, the evaporation duct height starts to slowly decrease from a height of thirteen meters to a height of approximately nine meters by about 10/0600Z. Once again, f_{min} increases to a frequency greater than 10 GHz. By 10/1000Z, wind speed decreases to about ten ms^{-1} and relative humidity continues its steady increase. The effect of these changes is continued decreases in evaporation duct height from approximately nine meters to seven meters. This results in a further increase in f_{min}.

From the above discussion, it can be seen that frontal passage has a direct impact on evaporation duct height (Z_*) and f_{min}. As the cold front approaches and relative humidity nears saturation, Z_* decreases until it is virtually nonexistent resulting in an increase in f_{min}. After frontal passage occurs (approximately 08/1400Z), Z_* increases dramatically and f_{min} decreases as relative humidity decreases due to subsidence and wind speed increases. By 10/0100Z,

27

relative humidity increases as the MABL is reestablished and wind speed decreases. The results in a decrease in Z_* and an increase in f_{min} to values similar to the start of the survey.

V. REFRACTIVITY ASSESSMENTS AND SOUNDING FORECASTS

In this chapter, experimental refractivity assessments made by NWOC for this eastern Pacific Ocean survey will be compared against radiosonde station IREPS profiles obtained during the survey. NABL forecast soundings for the eastern Pacific Ocean will also be compared against survey soundings.

A. REFRACTIVITY ASSESSMENTS

Refractivity assessments made by NWOC for 08/0000Z, 09/0000Z, and 10/0000Z May 1991 (Figs. 39, 40, and 41), are compared against survey station IREPS profiles (Figs. 12, 42, and 43) for the same period. At 08/0000Z, the NWOC refractivity assessment called *for a superrefractive* layer to exist between 3500-3900 ft (1067-1189 m) at PSUR and NPS; an elevated duct from 500-1200 ft (152-366 m) at NSI and MUGU and to the south of VBG; and an elevated duct at 1800-2200 ft (549-671 m) west of VBG. Table III shows the results for this time. In this table and in Tables IV and V, a superrefractive layer will be abbreviated as SL and an elevated duct as ED. Areas I, II and III in these tables each identify a region with different refractive conditions as shown in the NWOC refractivity assessments (Figs. 39, 40, and 41). Table III, which summarizes the refractivity analysis earlier in chapter IV, shows refractive layers as determined from survey station

measurements to be more extensive and/or at different levels than those made by the NWOC assessment.

Table III: 08/0000Z REFRACTIVITY ASSESSMENT

	AREA I	AREA II	AREA III
NWOC	SL 1067-1189 m	ED 549-671 m	ED 152-366 m
PSUR	ED 475-590 m SL 1455-1480 m		
NPS	ED 430-470 m SL 2440-2540 m		
VBG		ED 230-260 m SL 260-340 m	Same as VBG area II
NSI			SL 285-490 m ED 490-510 m SL 510-550 m
MUGU			SL 130-330 m SL 435-460 m

At 09/0000Z, the NWOC refractivity assessment calls for normal conditions at PSUR, NPS and to the west of VBG; and an elevated duct at 1000-1400 ft (305-427 m) at NSI and MUGU and to the south of VBG. In this case, Table IV presents the comparisons for this time. Once again, the survey station measurements show the number and type of refractive layers present to be more extensive than the NWOC assessment. NWOC analyzed a low elevated duct that was found in the VBG sounding. Superrefractive layers were analyzed by NSI and MUGU at 300-500 m. However, other layers are present above

Table IV: 09/0000Z REFRACTIVITY ASSESSMENT

	Area I	Area II
NWOC	Normal	ED 305-427 m
PSUR	Normal	
NPS	SL 415-640 m SL 1640-1715 m	
VBG	ED 470-605 m ED 1050-1310 m	Same as VBG Area I
NSI		SL 380-450 m SL 540-550 m SL 805-865 m SL 1595-1770 m
MUGU		SL 535-585 m SL 1990-2165 m

this low layer. In addition, superrefractive layers are observed by NPS in the immediate postfrontal area due to subsidence.

At 10/0000Z, the NWOC refractivity assessment calls for normal conditions throughout the survey area. Table V presents the results for this time period. The results from the survey stations differ from the NWOC assessment as refractive layers are found at each station. Inversion conditions have quickly developed at all stations as the postfrontal high pressure system approaches the coast.

These comparisons in Tables III, IV and V show that refractive layers in the lower troposphere are at more levels than the NWOC analysis suggests. It is also evident that these refractive conditions are highly variable spatially. This survey found that refractive conditions are considerably

Table V: 10/0000Z REFRACTIVITY ASSESSMENT

	Area I
NWOC	Normal
PSUR	SL 1095-1195 m
NPS	ED 570-590 m SL 590-840 m
VBG	ED 565-615 m SL 615-715 m
NSI	SL 435-575 m
MUGU	SL 205-465 m SL 2375-2425 m

more complex than the Rosenthal and Helvey (1979) model or NWOC analysis indicate.

B. SOUNDINGS

NABL sounding forecasts for the eastern Pacific Ocean were compared against PSUR soundings. The NABL sounding forecasts consisted of 12 and 24 hour forecasts for 09/1200Z and 10/0000Z. These forecasts were then compared against the PSUR 09/1200Z and 10/0000Z soundings.

The NABL 12 hour forecast for 09/1200Z (Fig. 44)--at 35.6N 124.5W near PSUR--shows a major negative vertical humidity gradient at 950-900 mb while the PSUR 09/1200Z sounding (Fig. 45) shows this same condition above 850 mb. The temperature profile is reasonably well predicted showing a dry adiabatic layer near the surface and a deep stable layer from 850 mb to above 700 mb. However, the detailed inversion structure of

the PSUR sounding was not forecast. Also, moist conditions at the top of the boundary layer were not forecast.

The NABL 24 hour sounding forecast, also for 09/1200Z (Fig. 46), shows saturated conditions near the surface. Above 950 mb, a negative vertical humidity gradient and inversion are shown. This forecast is an improvement upon the 12 hour forecast; however, the negative vertical humidity gradient and slight inversion are still too low.

The 12 hour NABL forecast for 10/0000Z (Fig. 47) shows a negative vertical humidity gradient from about 950 mb to 900 mb and then a second negative vertical humidity gradient at bout 780 mb to 680 mb. The PSUR 10/0000Z sounding (Fig. 48) shows only one broad negative vertical humidity gradient starting at 925 mb. The more moist level from 900 mb to 775 mb illustrated in the NABL forecast is not evident in the PSUR sounding. The general observed temperature profile is indicated in the forecast; however, details, like the inversion at 600 mb are missing.

The NABL 24 hour forecast for 10/0000Z (Fig. 49) also shows a negative vertical humidity gradient starting at about 930 mb. The PSUR 10/0000Z sounding (Fig. 48) also shows the negative vertical humidity gradient at approximately the same level. However, in the PSUR sounding, relative humidity decreases steadily to about 650 mb while it increases in the NABL sounding forecast from 850 to 750 mb.

Although the results from these sounding forecasts are promising, greater vertical resolution and accuracy are necessary to approach the detail of the PSUR soundings. In order to identify the complex refractive environment found in this survey with more accuracy, greater detail is necessary. Such detail cannot be achieved with large scale prediction methods and is currently possible only with in situ measurements.

VI. CONCLUSIONS AND RECOMMENDATIONS

The results of this study, based on in situ observations, support the premise that refractive conditions in a coastal environment are subject to rapid change. Changes in atmospheric conditions such as movement of weather systems through an area have a direct impact on atmospheric refractivity. The survey refractive conditions shown in Tables III, IV and V as well as the PSUR evaporation duct profile (Fig. 38) illustrate this variability in refractivity. These measurements show that refractive conditions vary greatly both temporally and spatially, i.e., for a given location, refractive conditions are highly variable with time and for a number of locations in the same geographical area at a given time, refractive conditions can differ from location to location.

Since naval forces frequently operate in coastal environments, these results indicate that a ship operating in concert with other naval forces could encounter refractive conditions very different from those of other ships operating in the same geographical area. Information on refractive conditions received from another ship or some other source could lead to erroneous assumptions about the expected performance of shipboard communications systems, sensors, and weapons systems.

Comparisons of survey data with a refractive model and NWOC refractivity assessments demonstrated that the refractive environment is much more complex than predicted by the model and assessments. NABL sounding forecasts approximated survey soundings but differed in levels where refractive layers would or would not be expected to form.

From this analysis, it is evident that a refractive model, refractivity assessments and sounding forecasts are not able to approach the accuracy and detail of in situ measurements. Therefore, in situ measurement systems such as those used in this survey aboard the R/V Point Sur may be one way for a naval ship to obtain accurate refractive assessments. Also, refractivity studies of the open ocean and other coastal areas are necessary to determine if the variability in refractive conditions noted in the California coastal region is to be found elsewhere.

APPENDIX

This appendix serves as a convenient location to consolidate all the figures discussed in the text of this thesis.
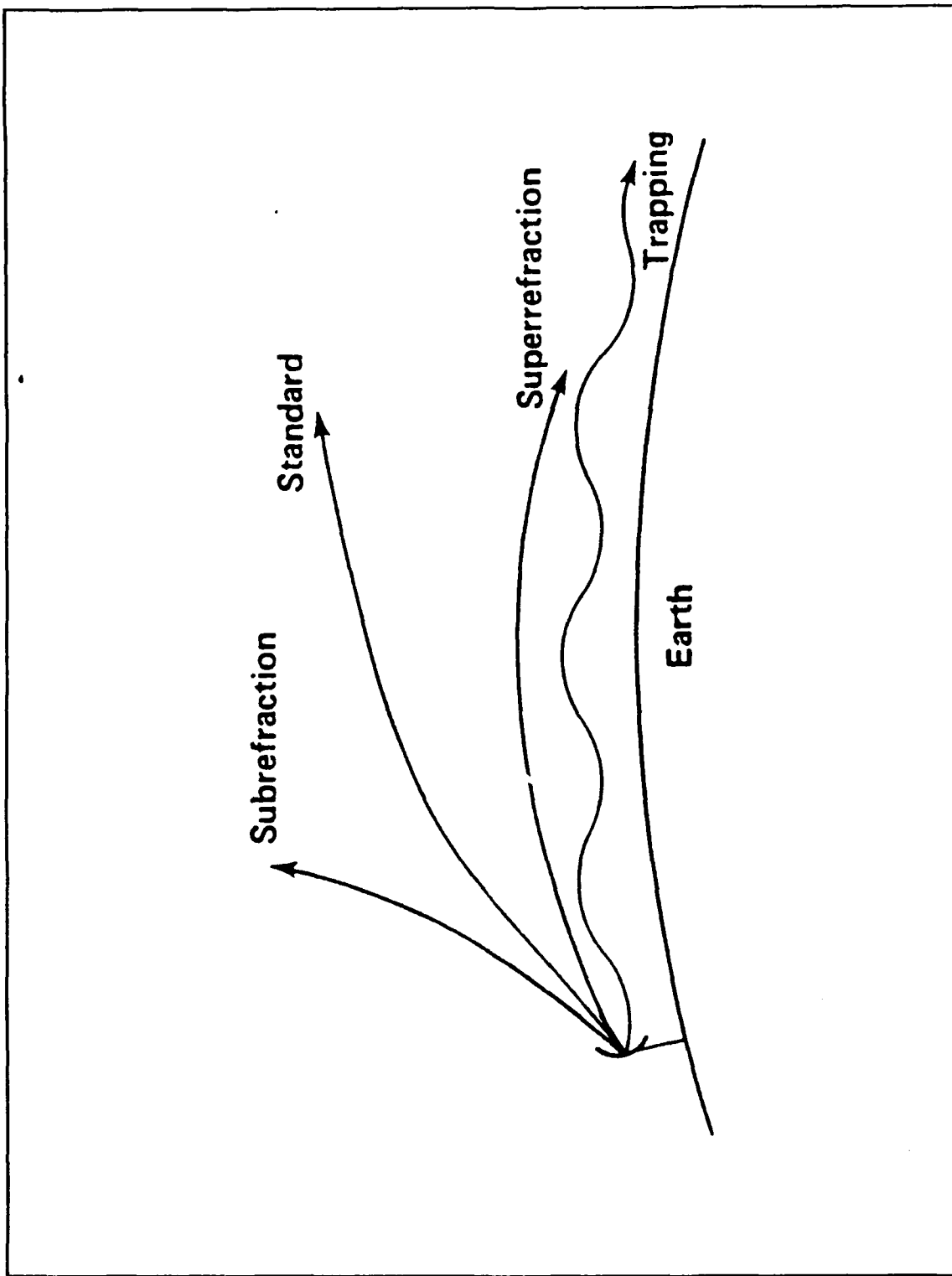
Fig. 1. EM ray propagation under various refractive conditions. From Ko et al. (1983).
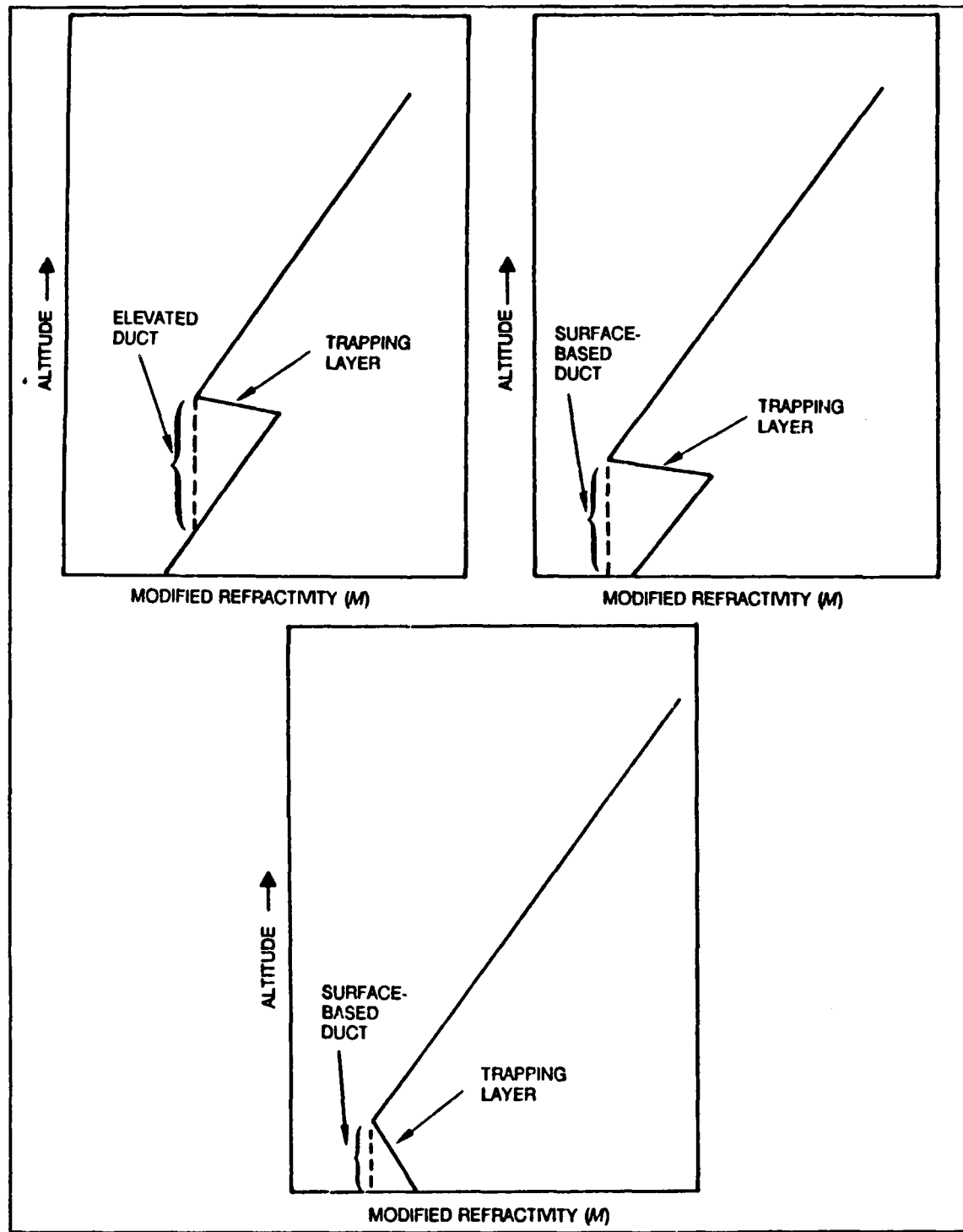
Fig. 2. Examples of ducts. Fig. 2a (upper left) is an elevated duct, Fig. 2b (upper right) is a surface-based duct from an elevated trapping layer, and 2c (bottom) is a surface-based duct from a surface trapping layer. From Paulus (1989).

39
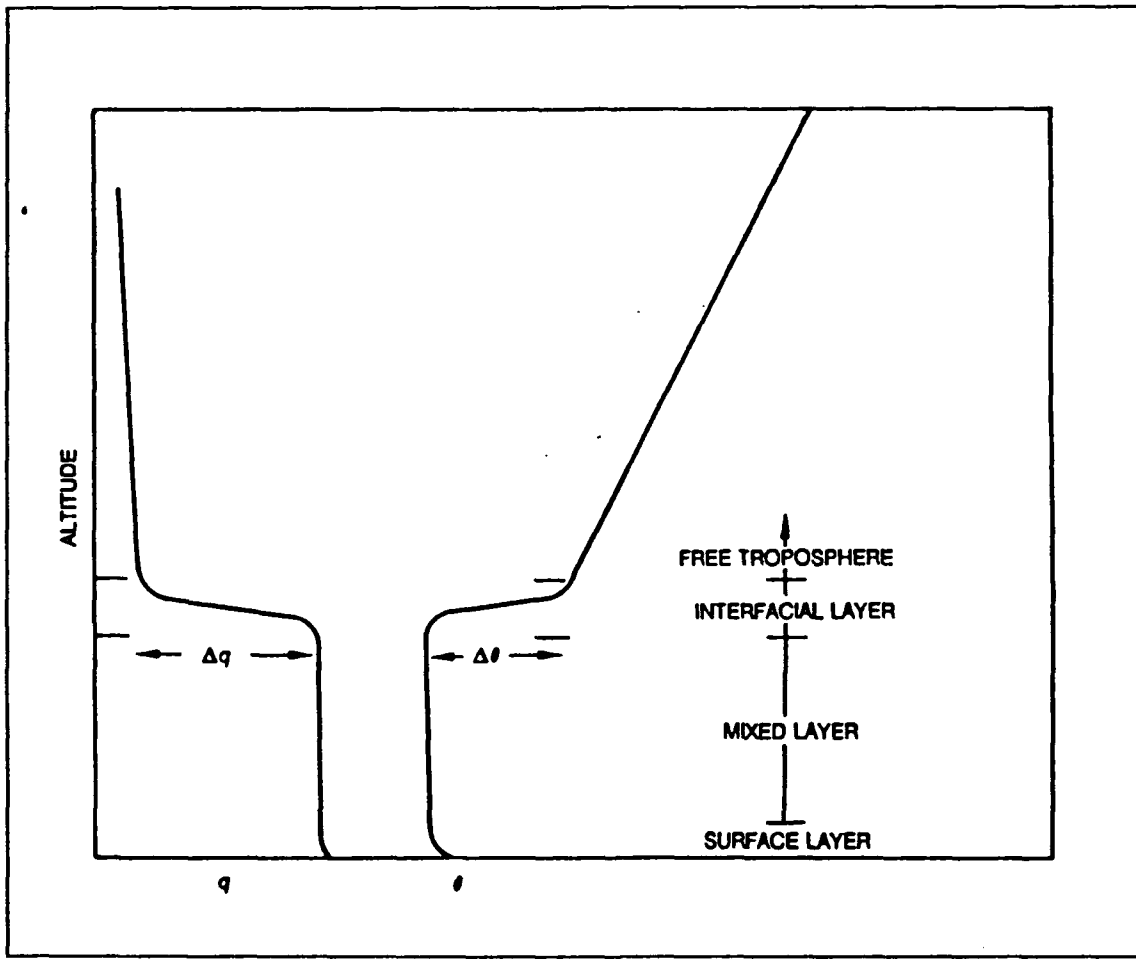
Fig. 3. Marine Atmospheric Boundary Layer (MABL). MABL with negative vertical humidity gradient and positive vertical temperature gradient (inversion) in interfacial layer. From Paulus (1989).

40
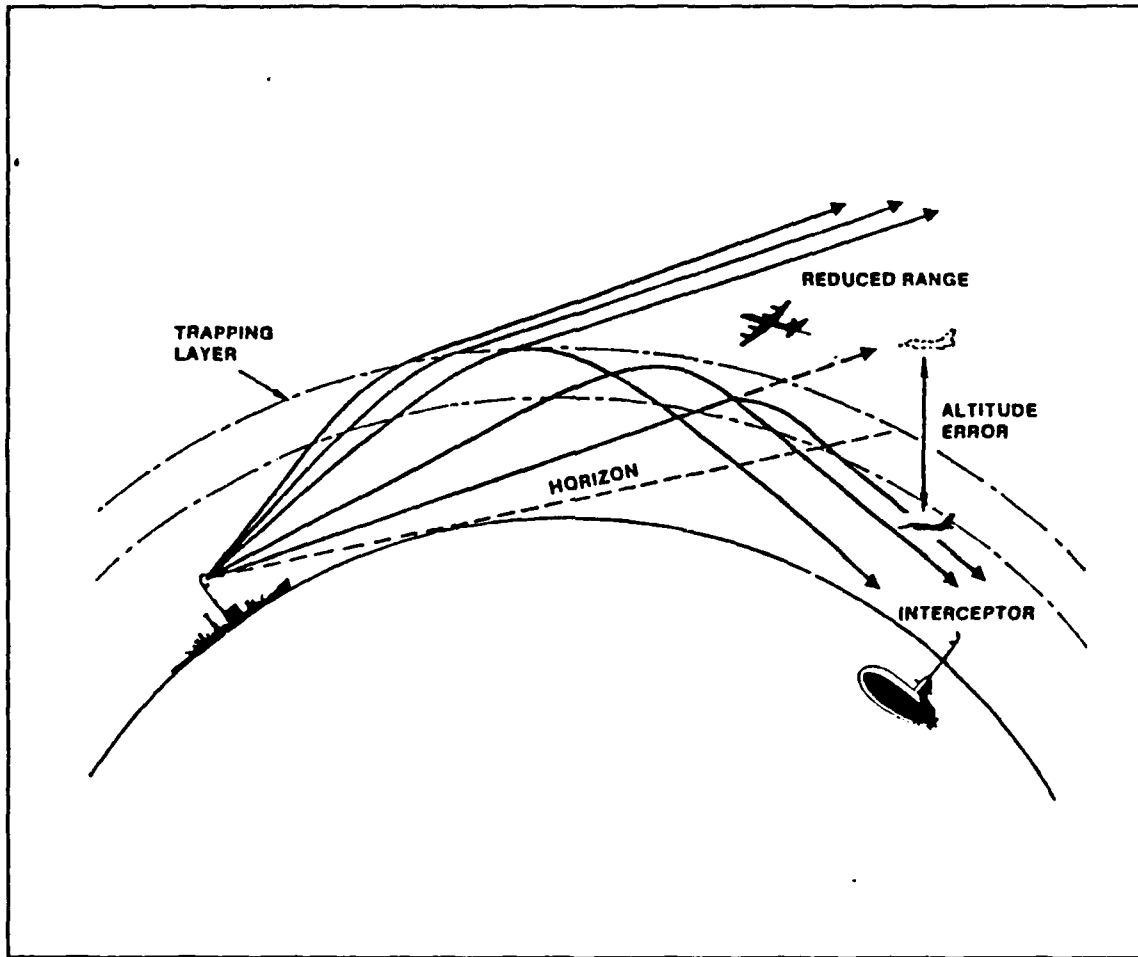
Fig. 4. Example of effects of a trapping layer on radar beam propagation. From Patterson et al. (1990).
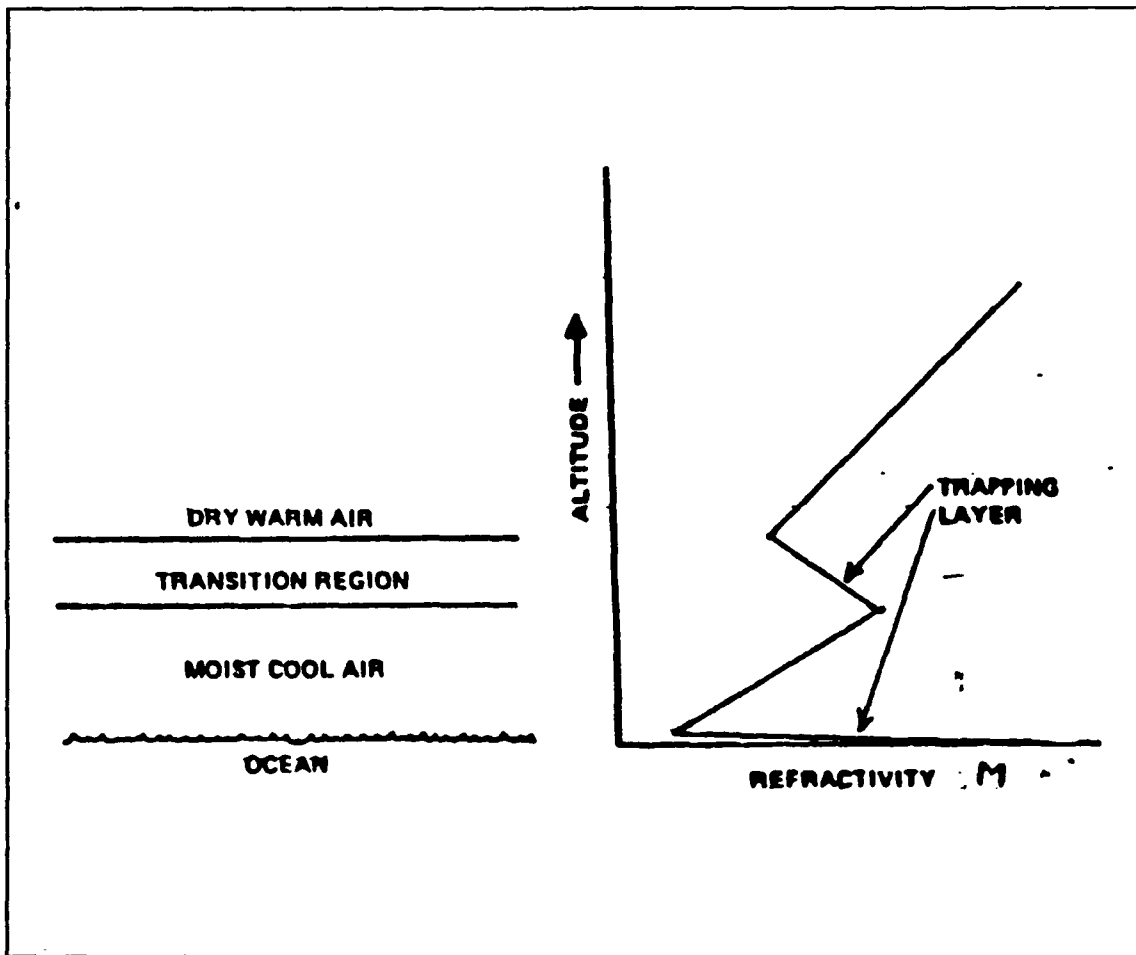
Fig. 5. Ocean M-profile. A typical M-profile over the ocean with trapping layers near the sea surface due to evaporation and at the top of the MABL in the transition region (interfacial layer). From Davidson (1991).
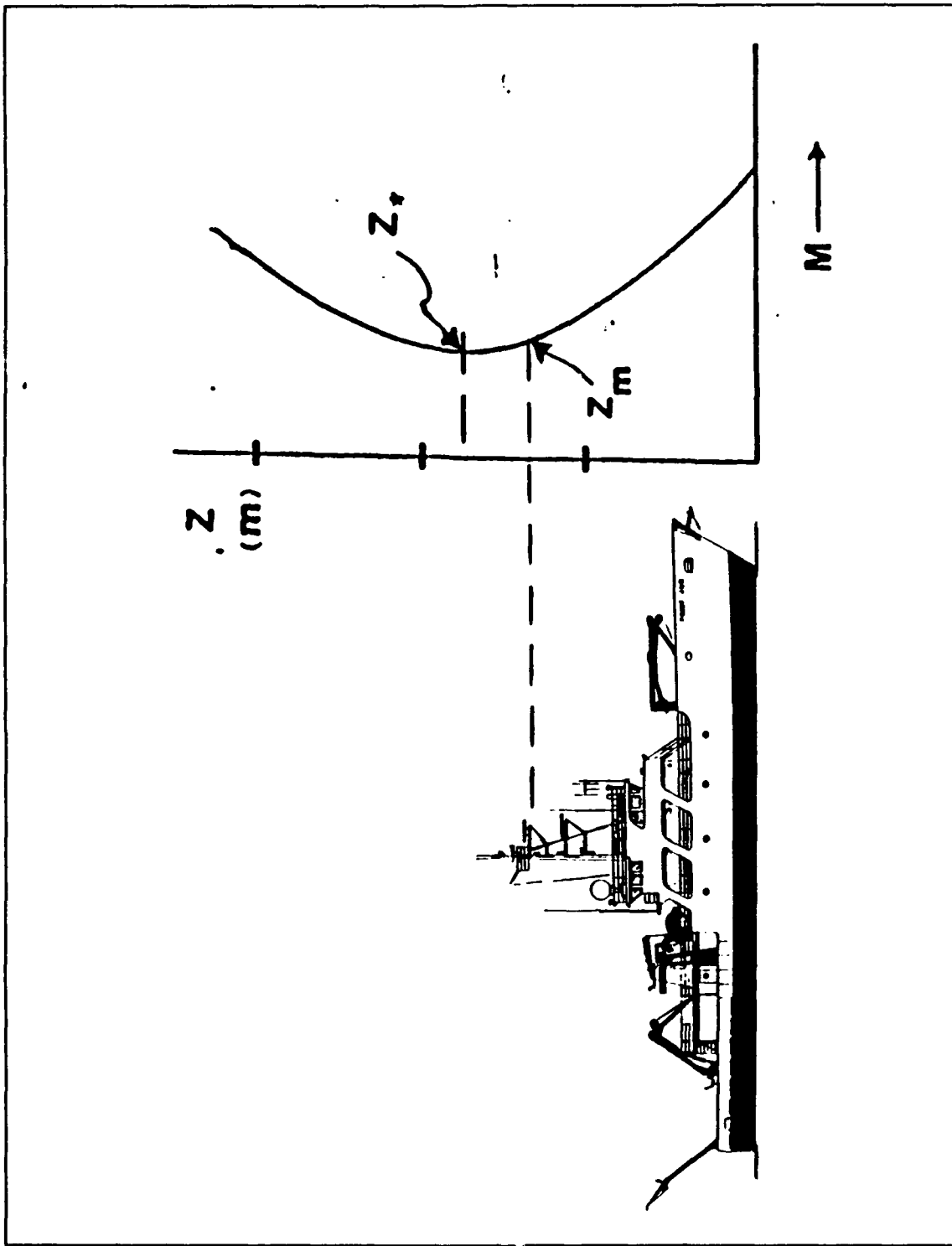
Fig. 6. Single-level measurements. Typical evaporation duct M-profile with Z_m (single-level measurement height) from R/V Point Sur and Z_* (evaporation duct height).

43
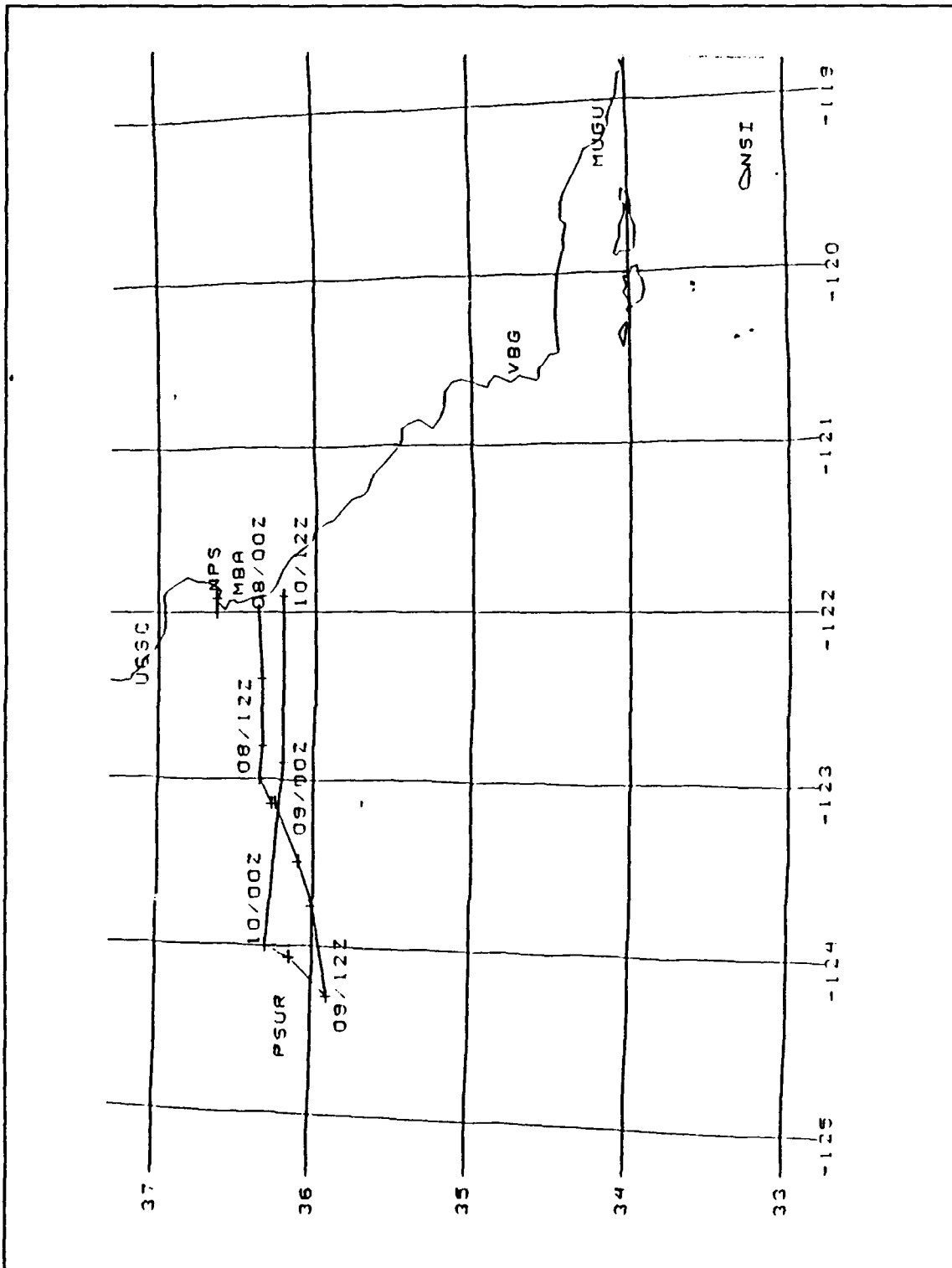
Fig. 7. Survey area map. Map illustrating location of survey stacions and track of PSUR.

44
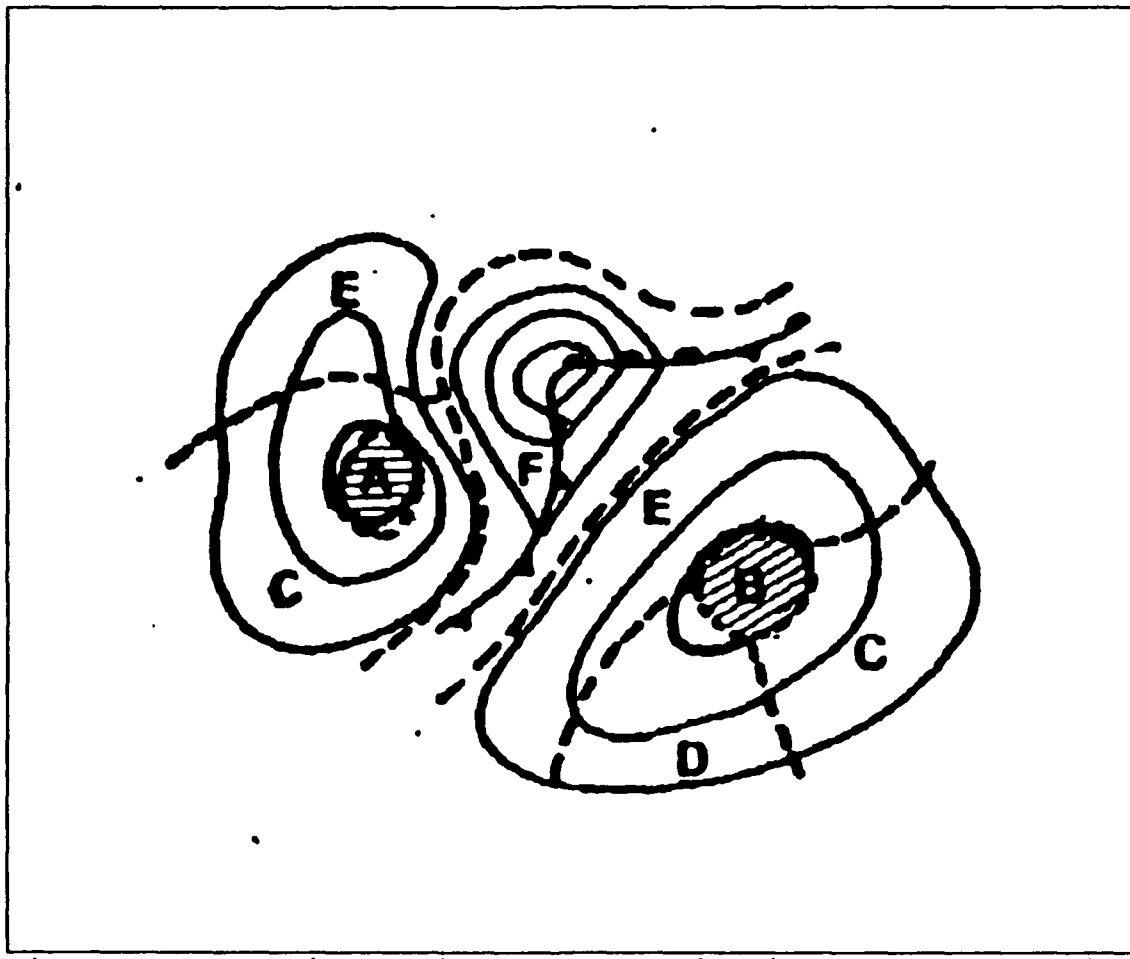
Fig. 8. Refraction regions. Schematic diagram of refraction regions in vicinity of mid-latitude system. From Rosenthal and Helvey (1979).

45
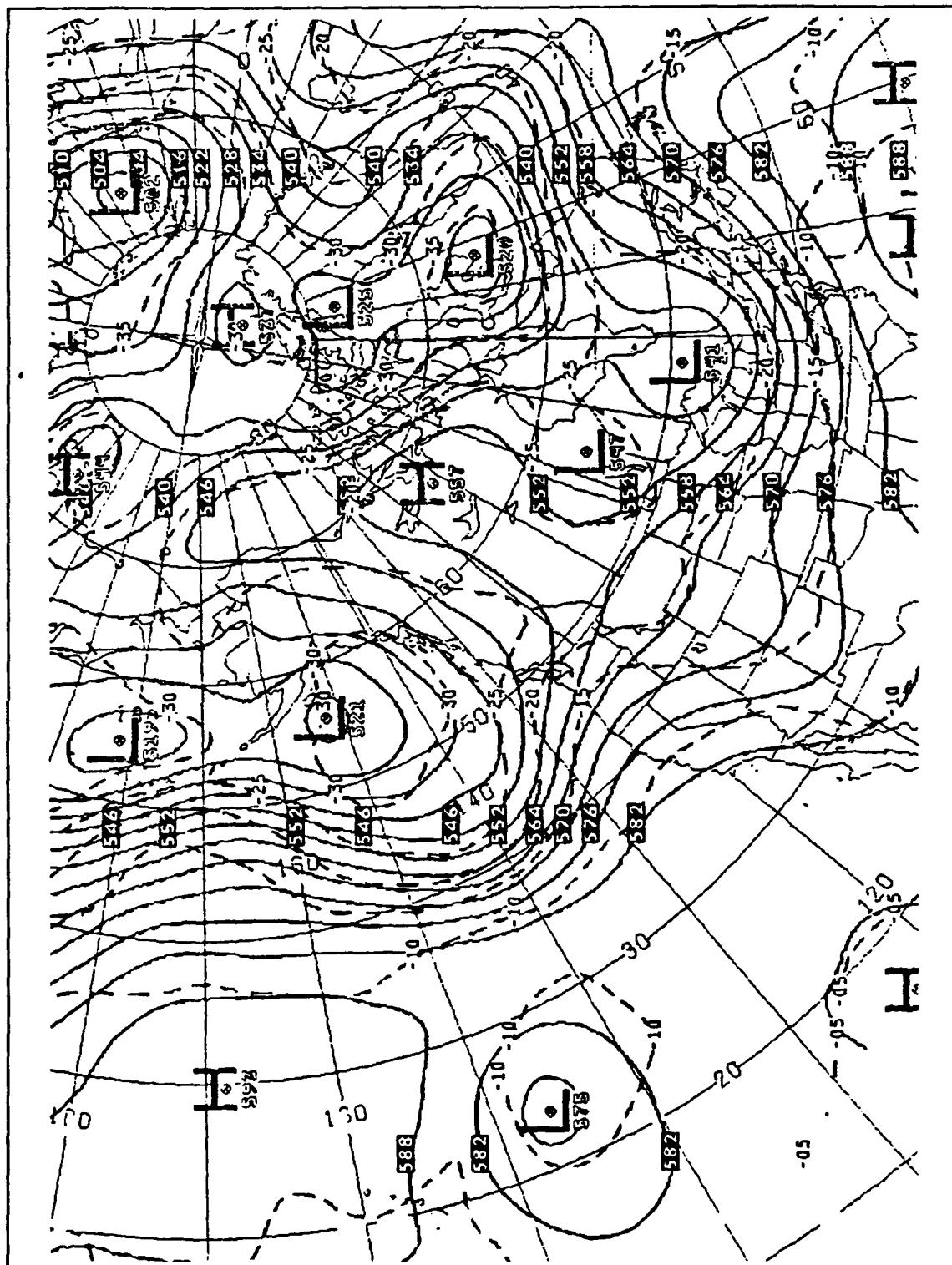
Fig. 9. 07/1200Z National Meteorological Center (NMC) 500 mb analysis of geopotential (dm) and temperature (degrees C).

46
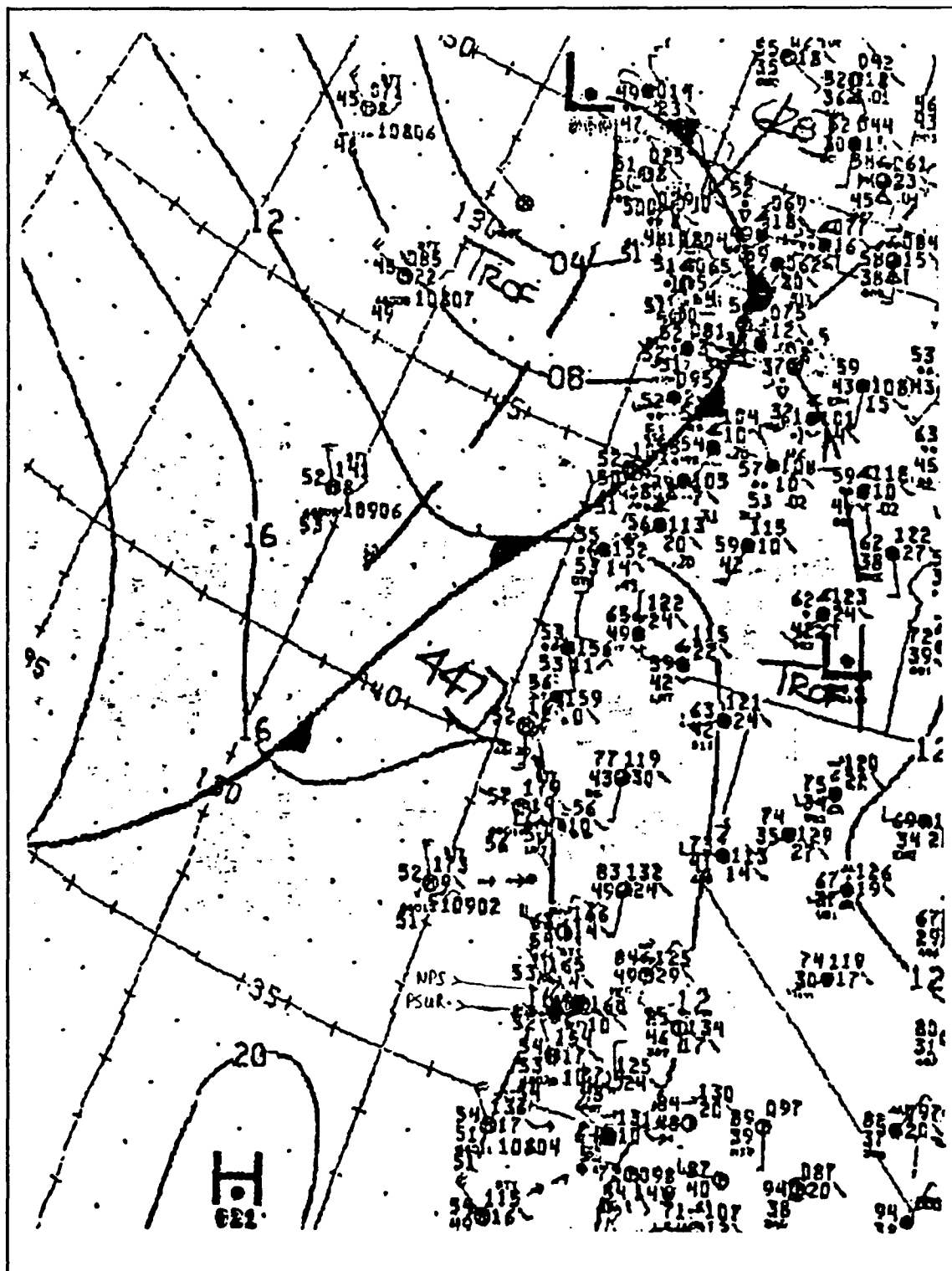
Fig. 10. 08/0000Z NMC surface analysis. Surface analysis showing approach of cold front to California and survey area.

Fig. 11. 07/2231Z visible satellite image. GOES visible image showing approach of cold front.
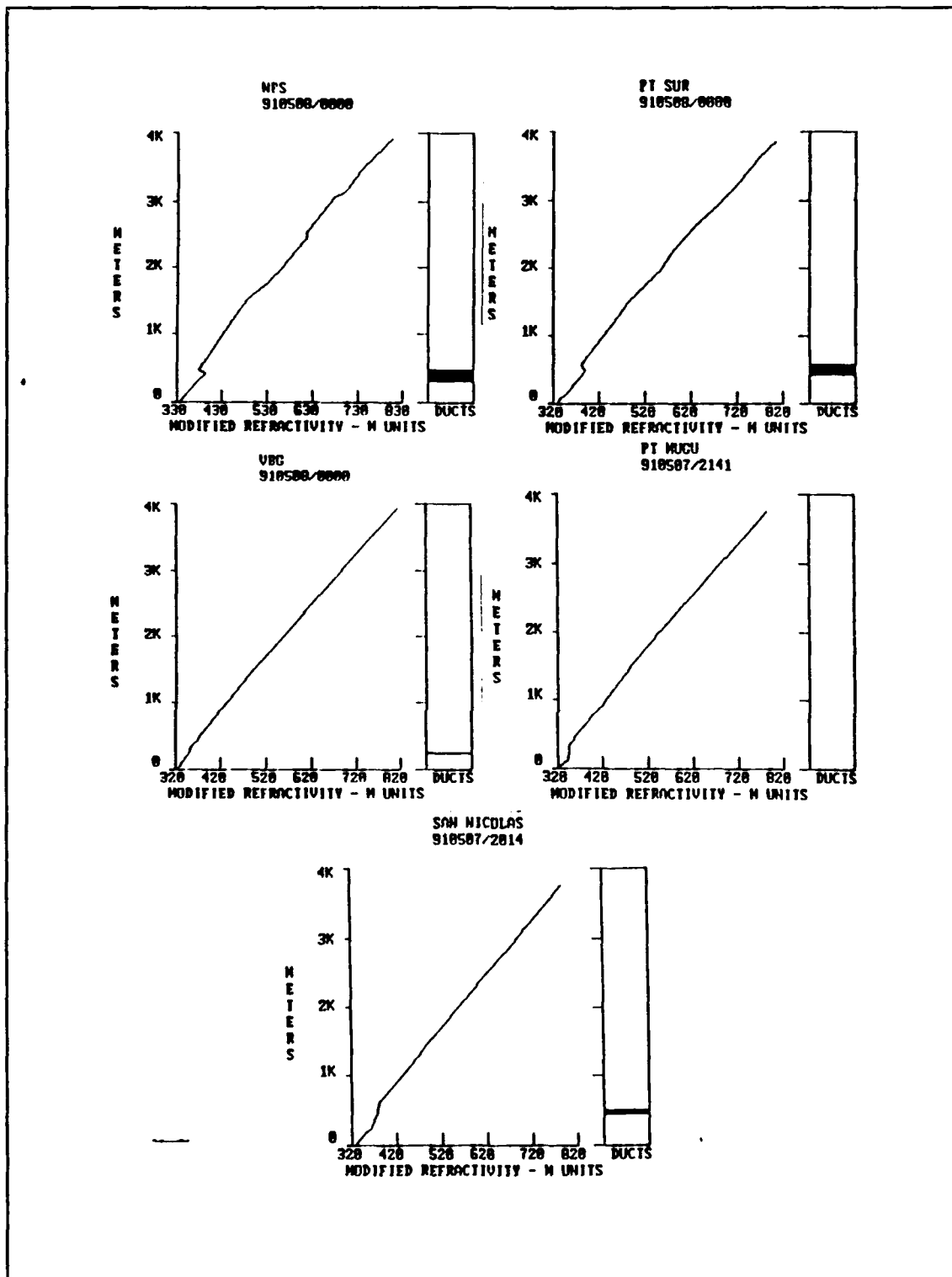
Fig. 12. 08/0000Z IREPS profiles. Survey station IREPS profiles for 08/0000Z time period.
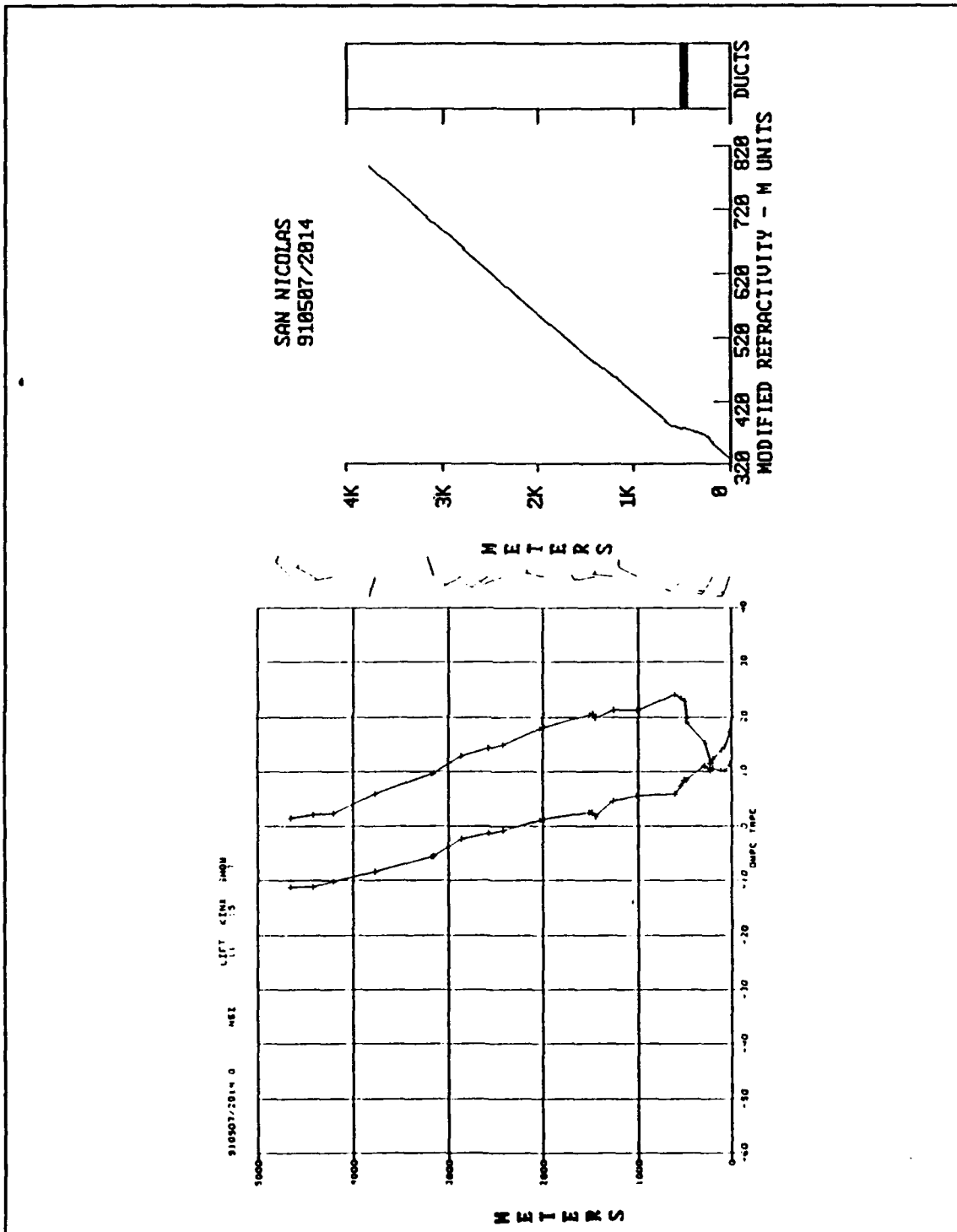
Fig. 13. 07/2014Z NSI sounding and IREPS profile. Fig. 11a (left) is the sounding and Fig. 11b (right) is the IREPS profile.

50
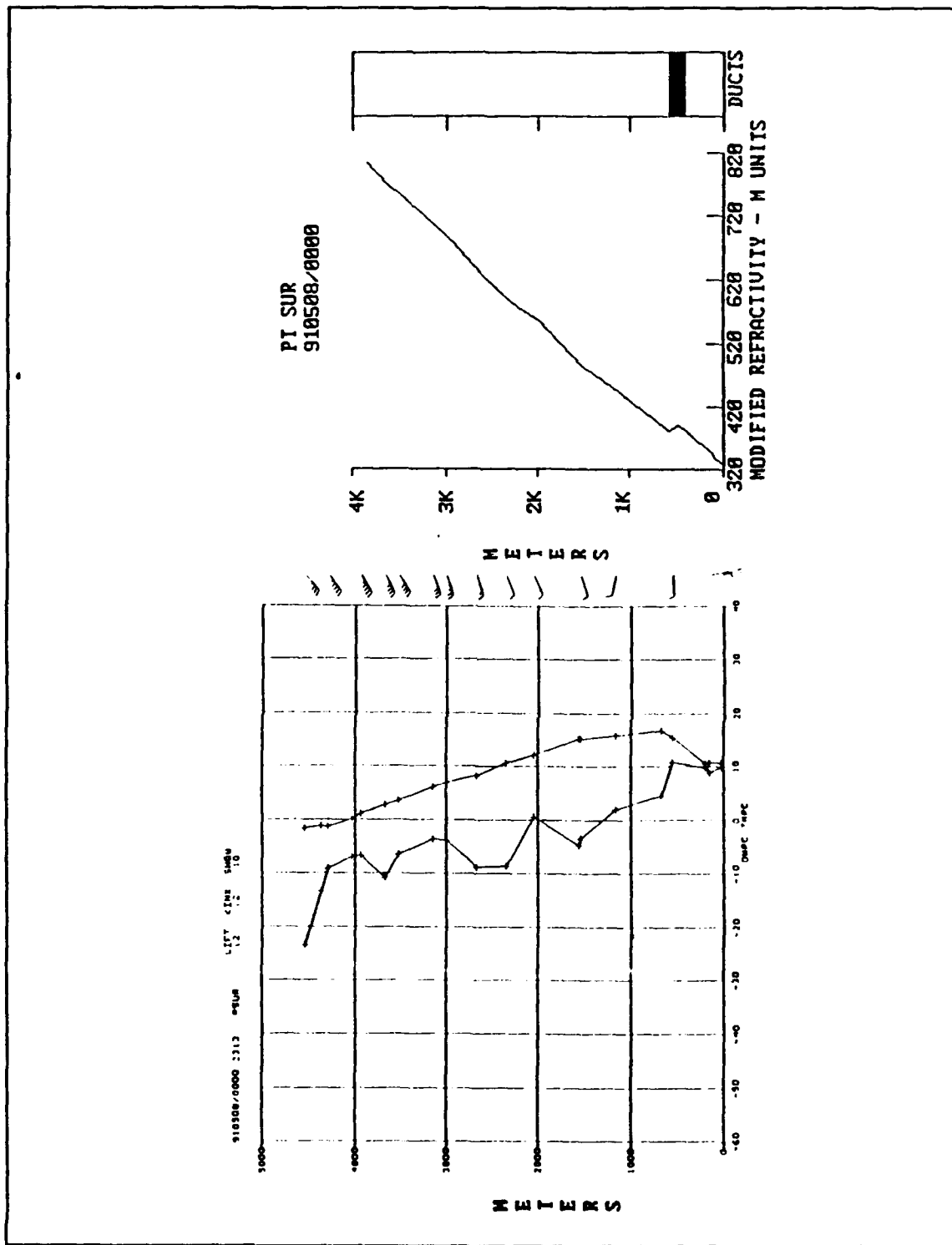
Fig. 14. 08/0000Z PSUR sounding and IREPS profile. Fig. 12a (left) is the sounding and Fig. 12b (right) is the IREPS profile.
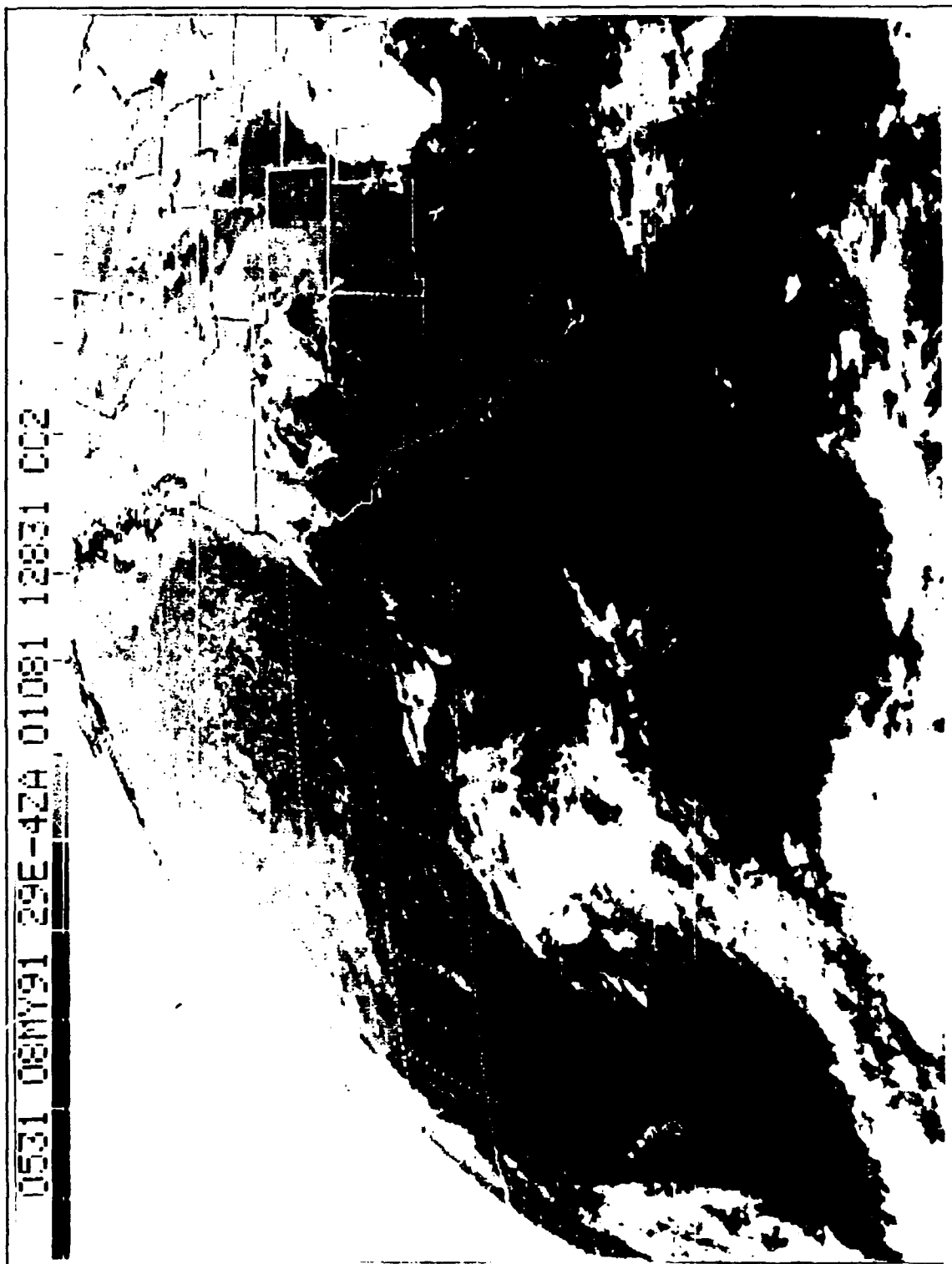
Fig. 15. 08/0531Z IR satellite image. GOES IR image showing cold front movement into survey area.
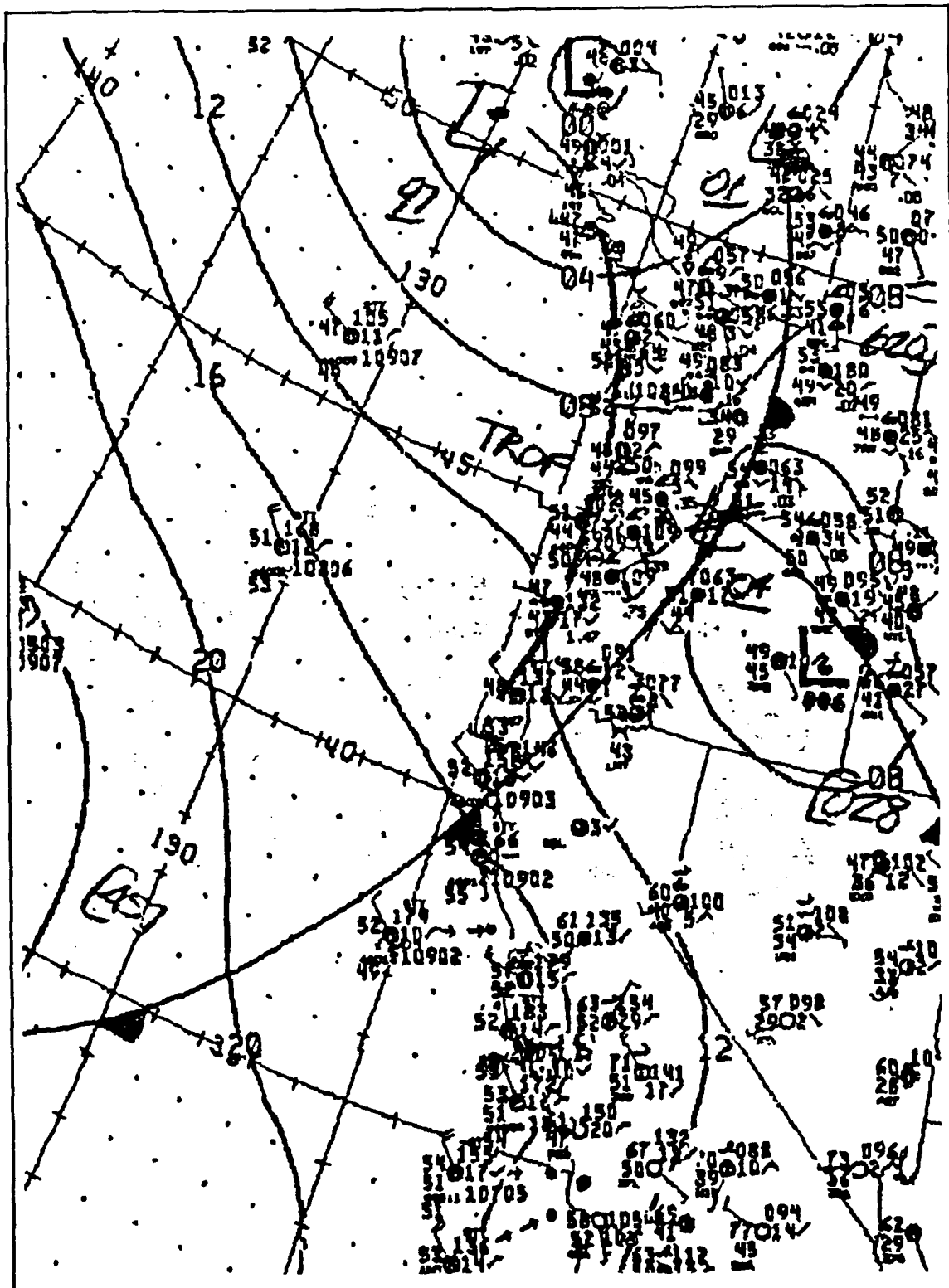
Fig. 16. 08/0600Z NMC surface analysis.
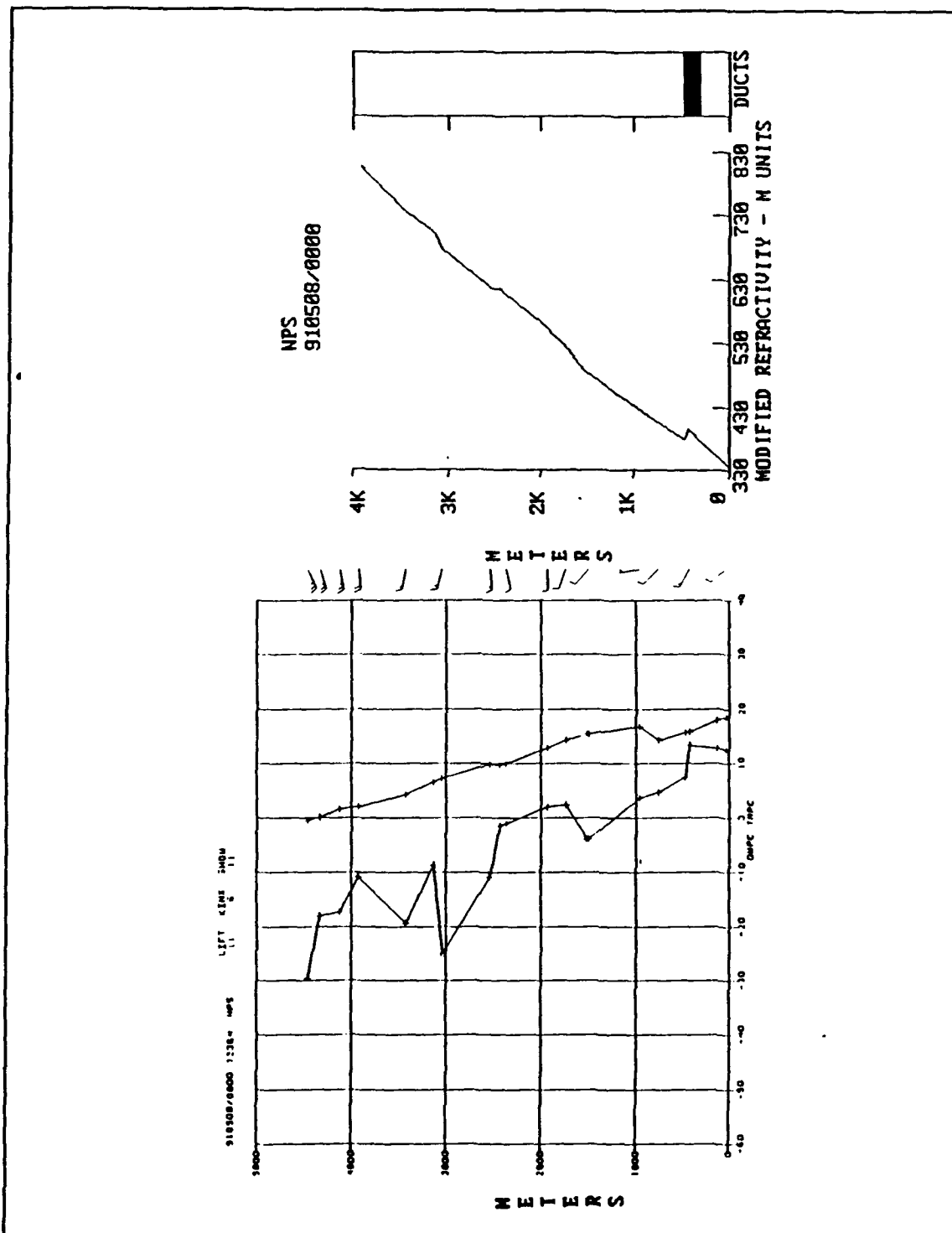
Fig. 17. 08/0000Z NPS sounding and IREPS profile. Fig. 15a (left) is the sounding and Fig. 15b (right) is the IREPS profile.
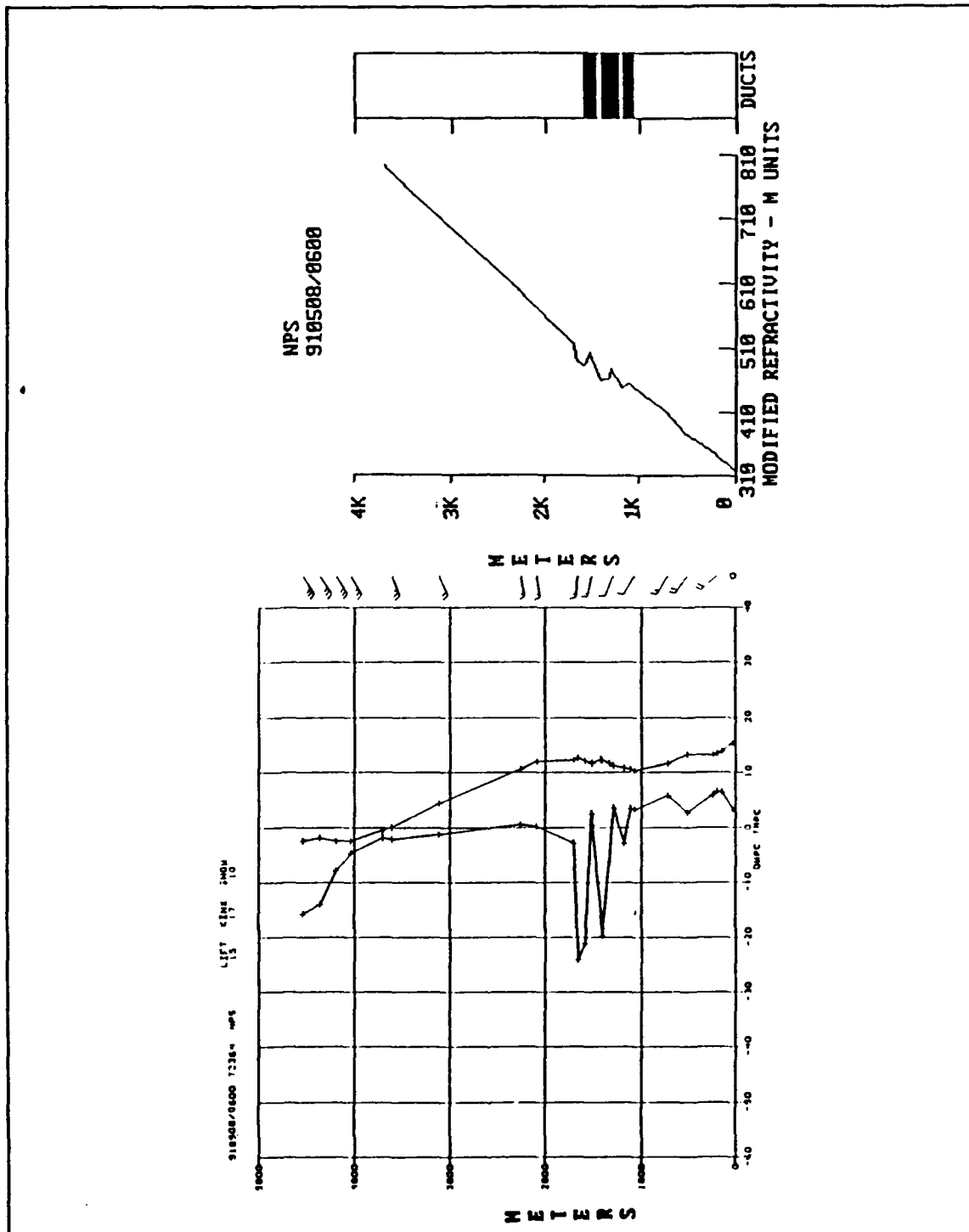
Fig. 18.   08/0600Z NPS sounding and IREPS profile.   Fig. 16a
(left) is the sounding and Fig. 16b (right) is the IREPS
profile.
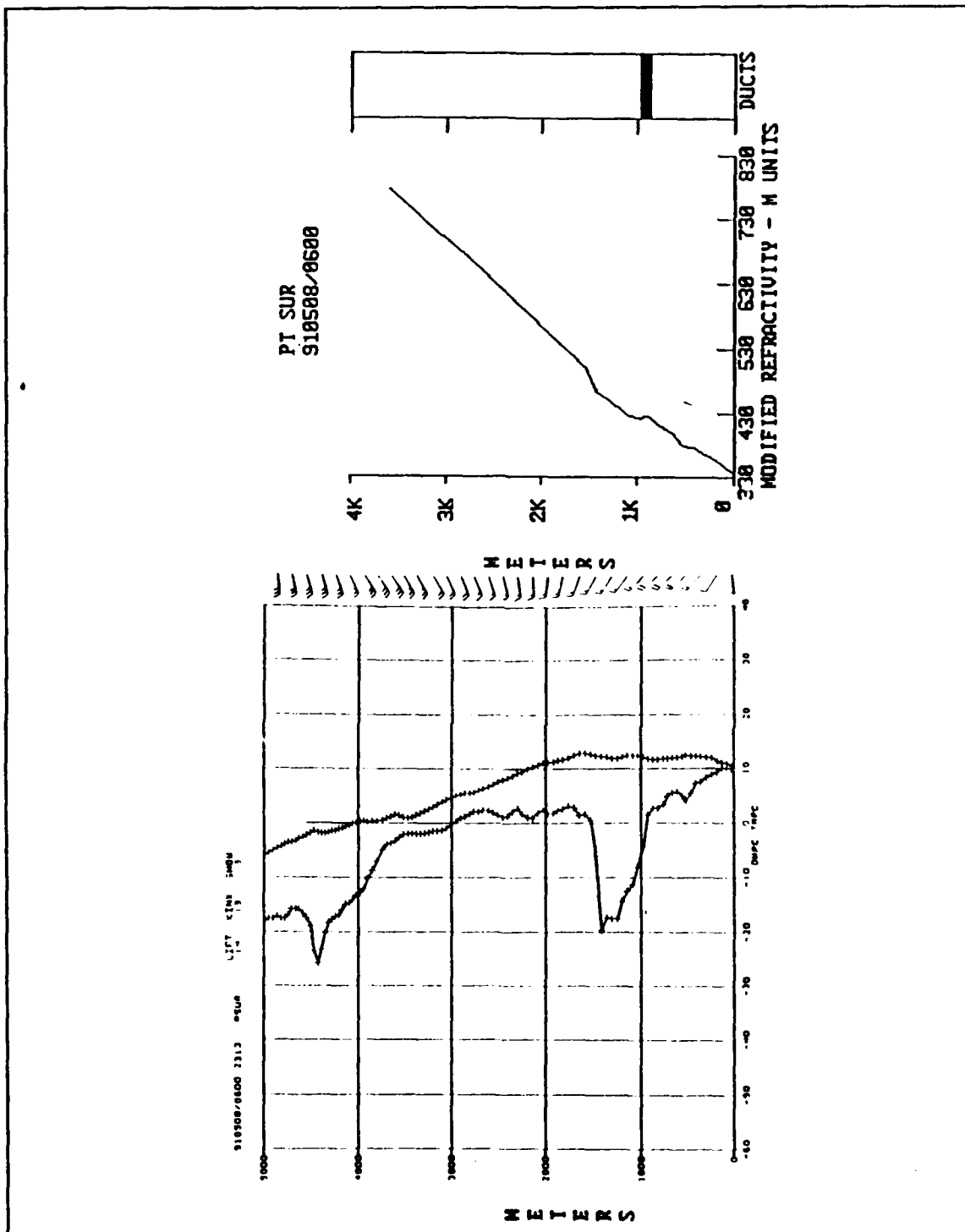
Fig. 19. 08/0600Z PSUR sounding and IREPS profile. Fig. 17a (left) is the sounding and Fig. 17b (right) is the IREPS profile.
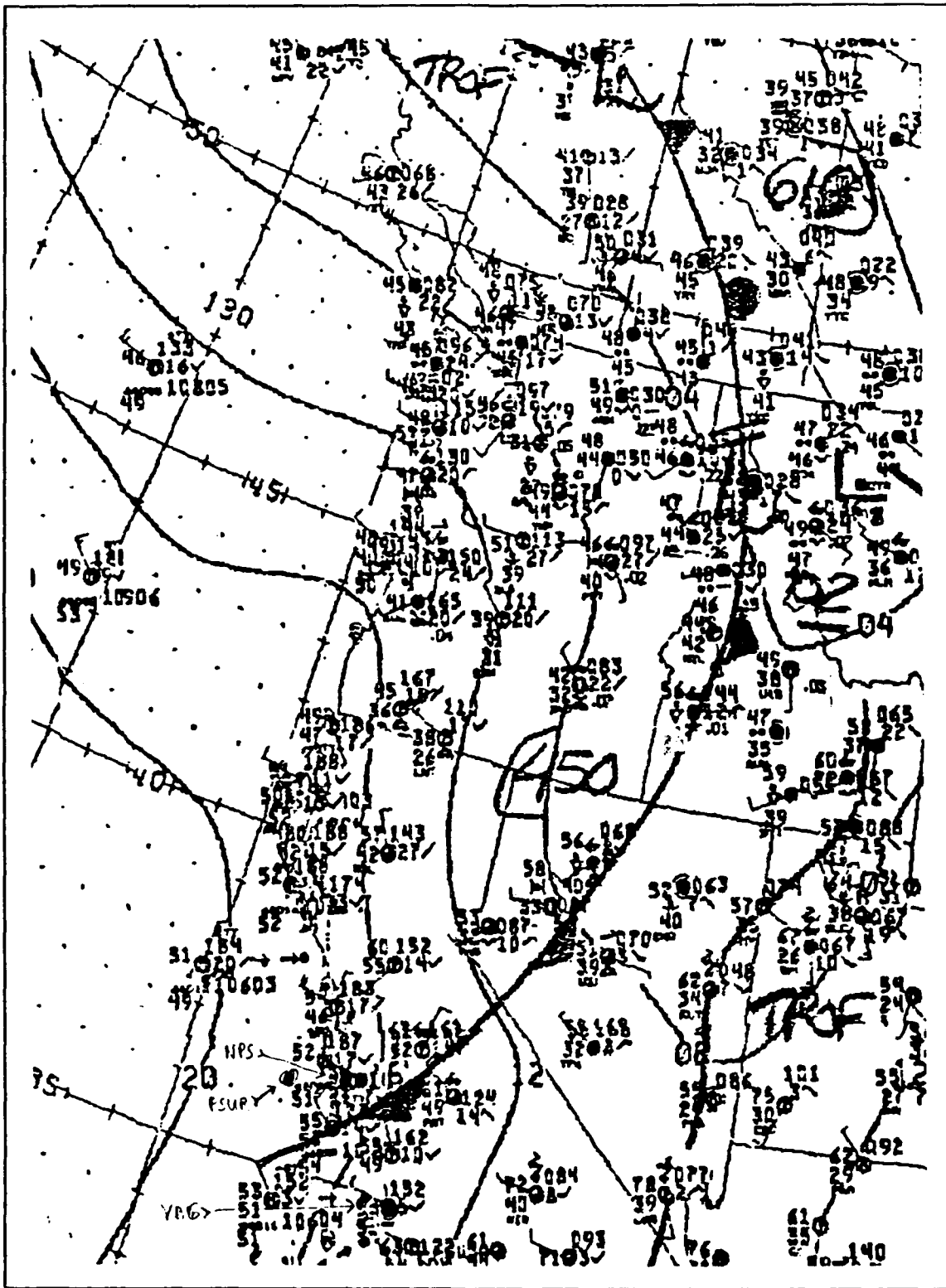
Fig. 20. 08/1500Z NMC surface analysis.
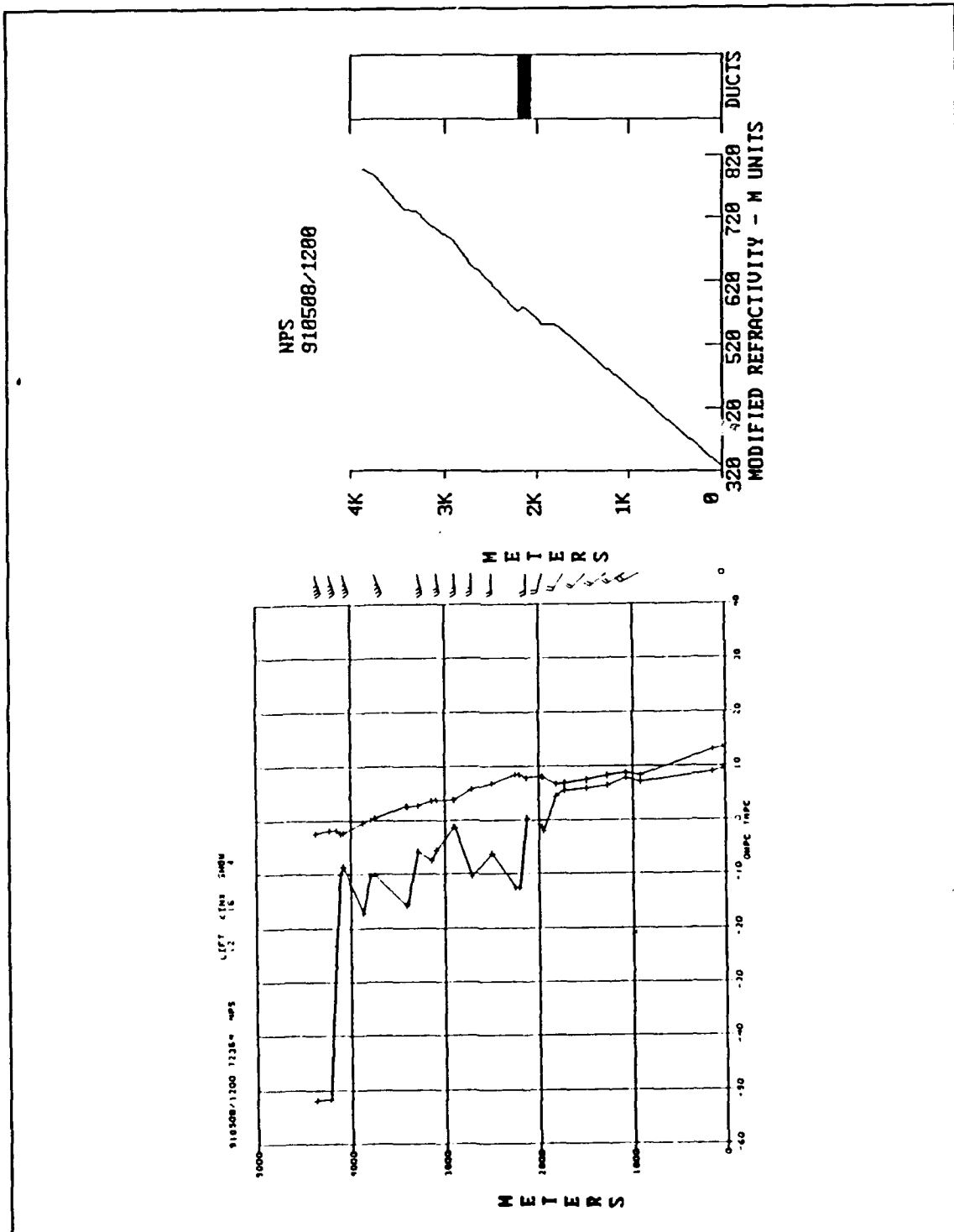
Fig. 21. 08/1200Z NPS sounding and IREPS profile. Fig. 19a (left) is the sounding and Fig. 19b (right) is the IREPS profile.
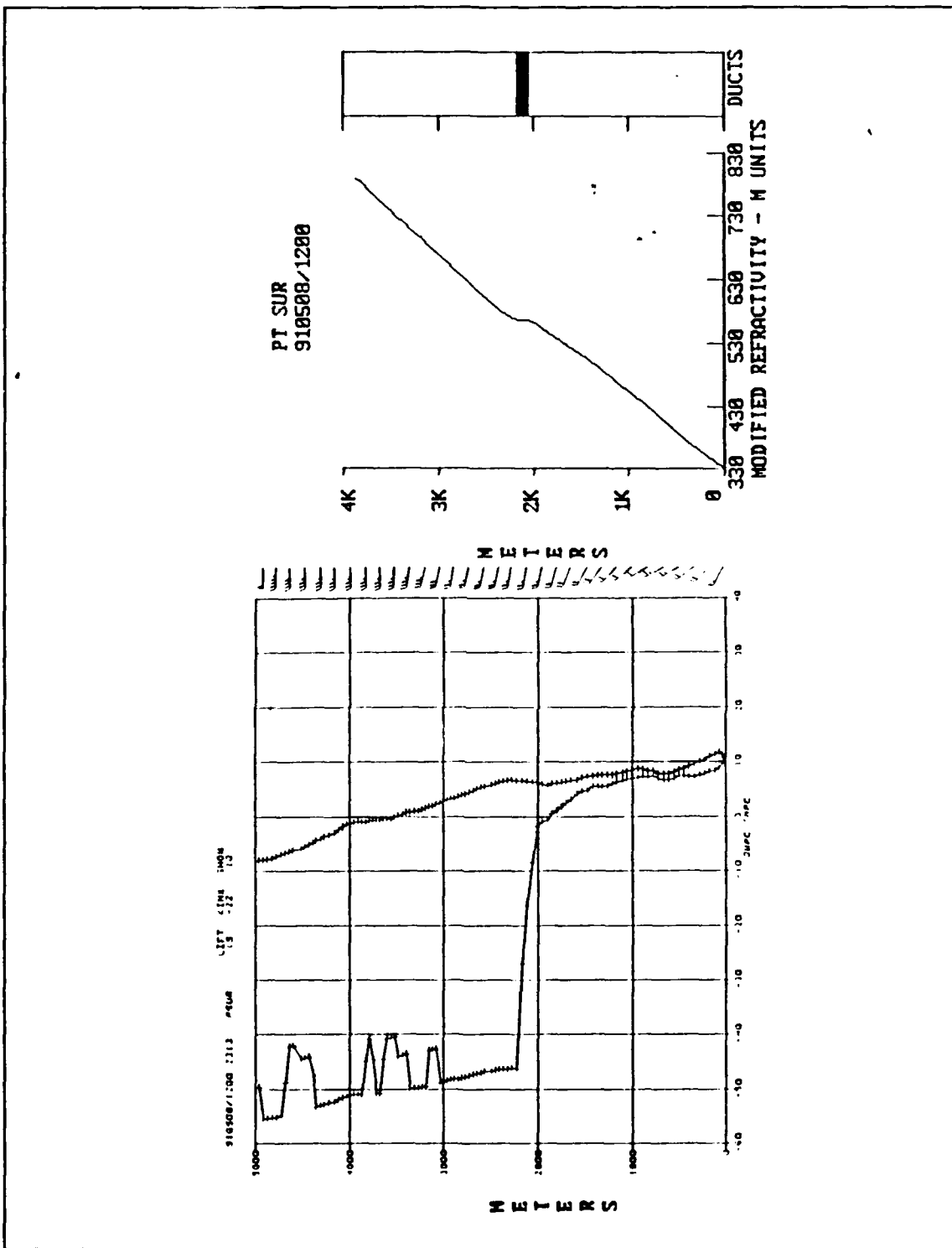
Fig. 22. 08/1200Z PSUR sounding and IREPS profile. Fig. 20a (left) is the sounding and Fig. 20b (right) is the IREPS profile.

Fig. 23. 08/2101Z GOES water vapor satellite image. Image illustrates area of subsidence behind cold front.

60
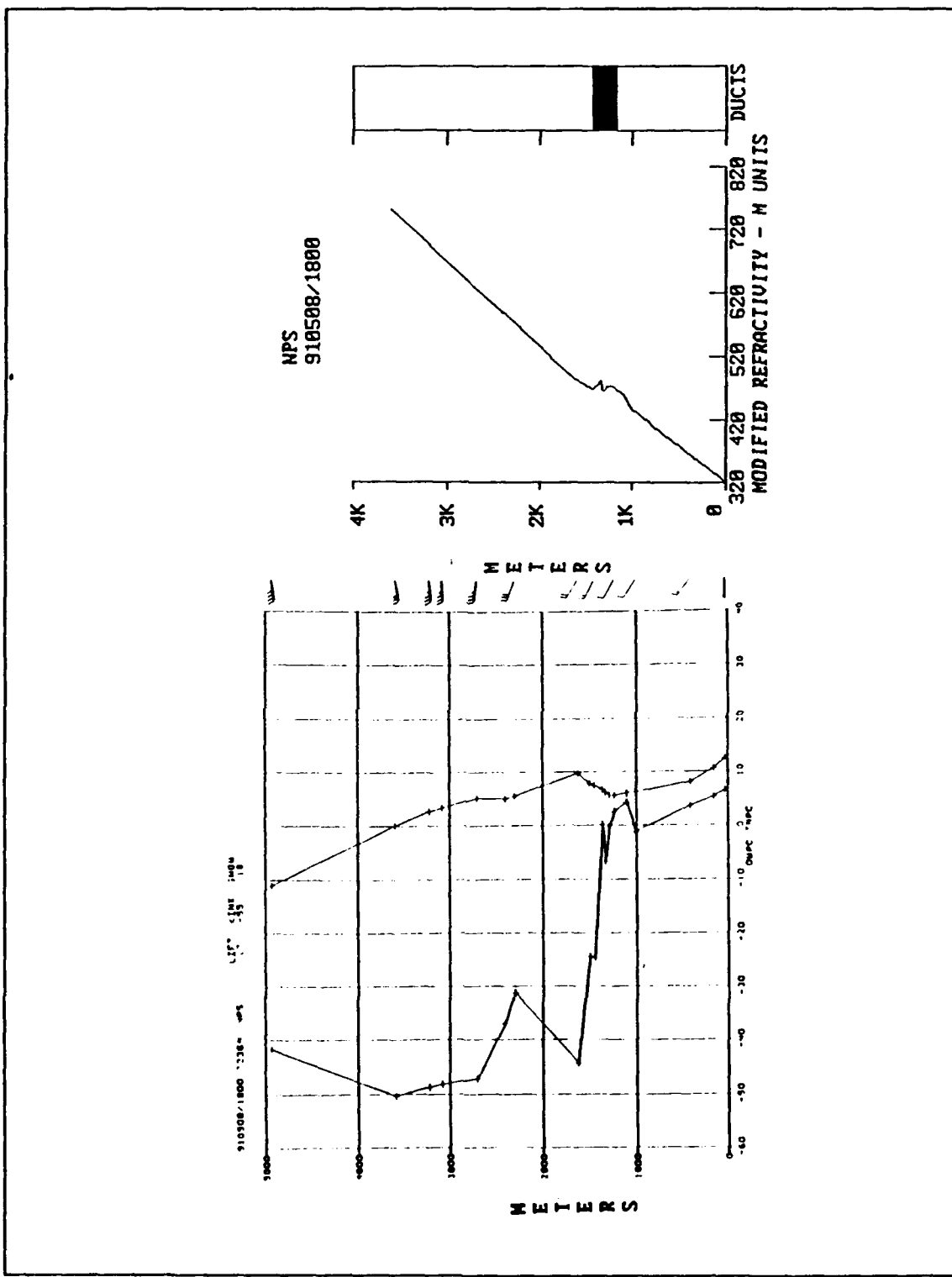
Fig. 24. 08/1800Z NPS sounding and IREPS profile. Fig. 22a (left) is sounding and Fig. 22b (right) is IREPS profile.

61
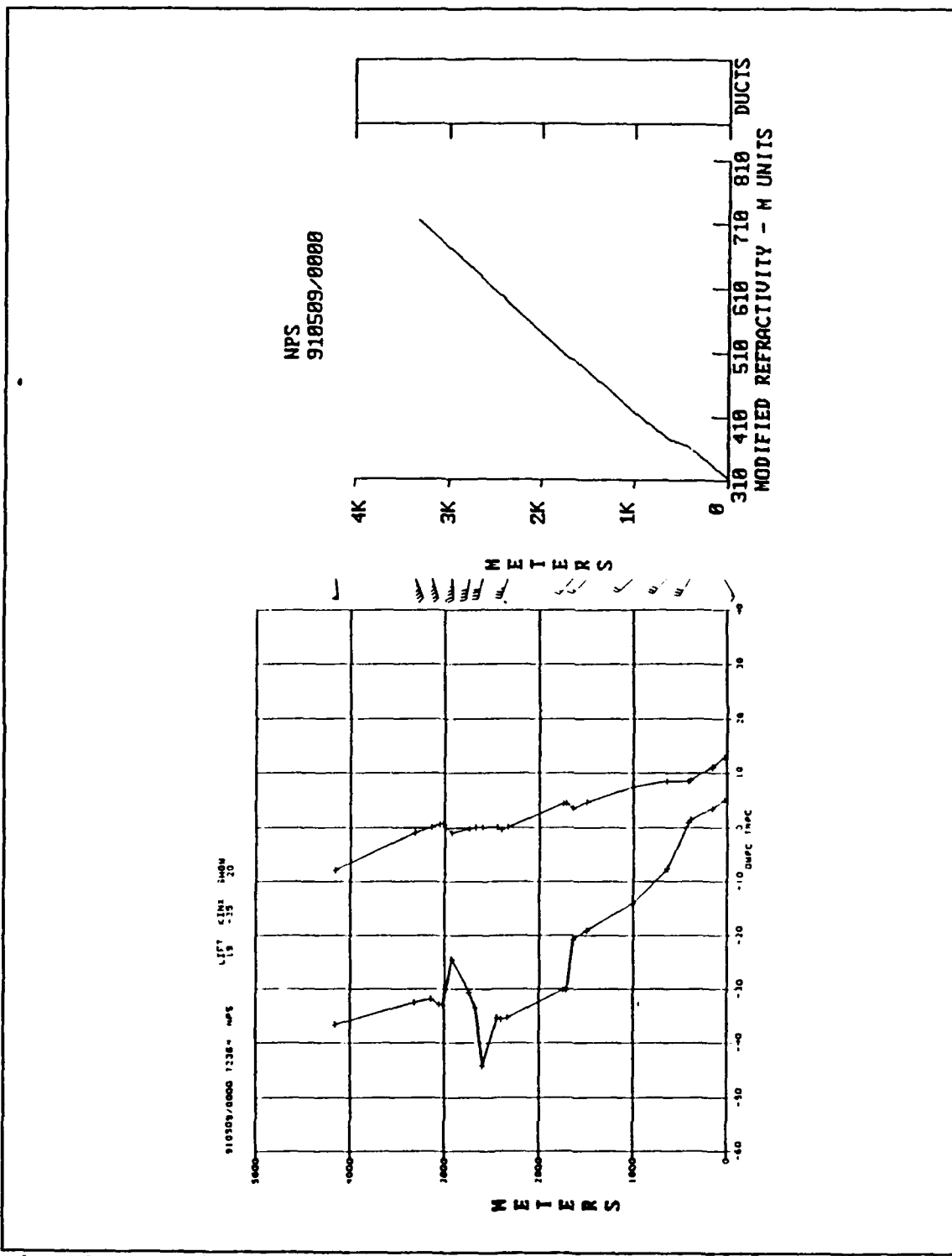
Fig. 25. 09/0000Z NPS sounding and IREPS profile. Fig. 23a (left) is the sounding and Fig. 23b (right) is the IREPS profile.
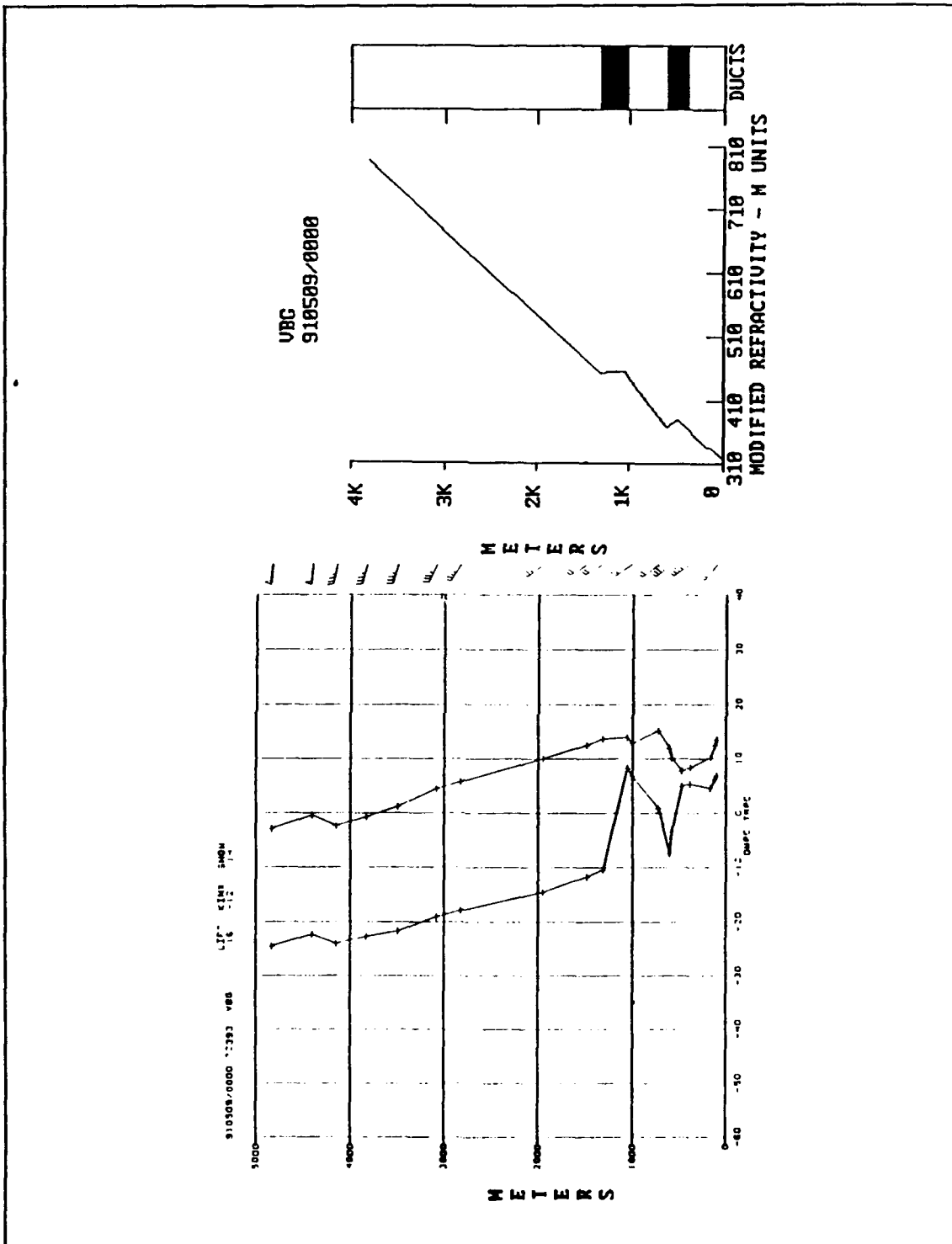
Fig. 26. 09/0000Z VBG sounding and IREPS profile. Fig. 24a (left) is the sounding and Fig. 24b (right) is the IREPS profile.
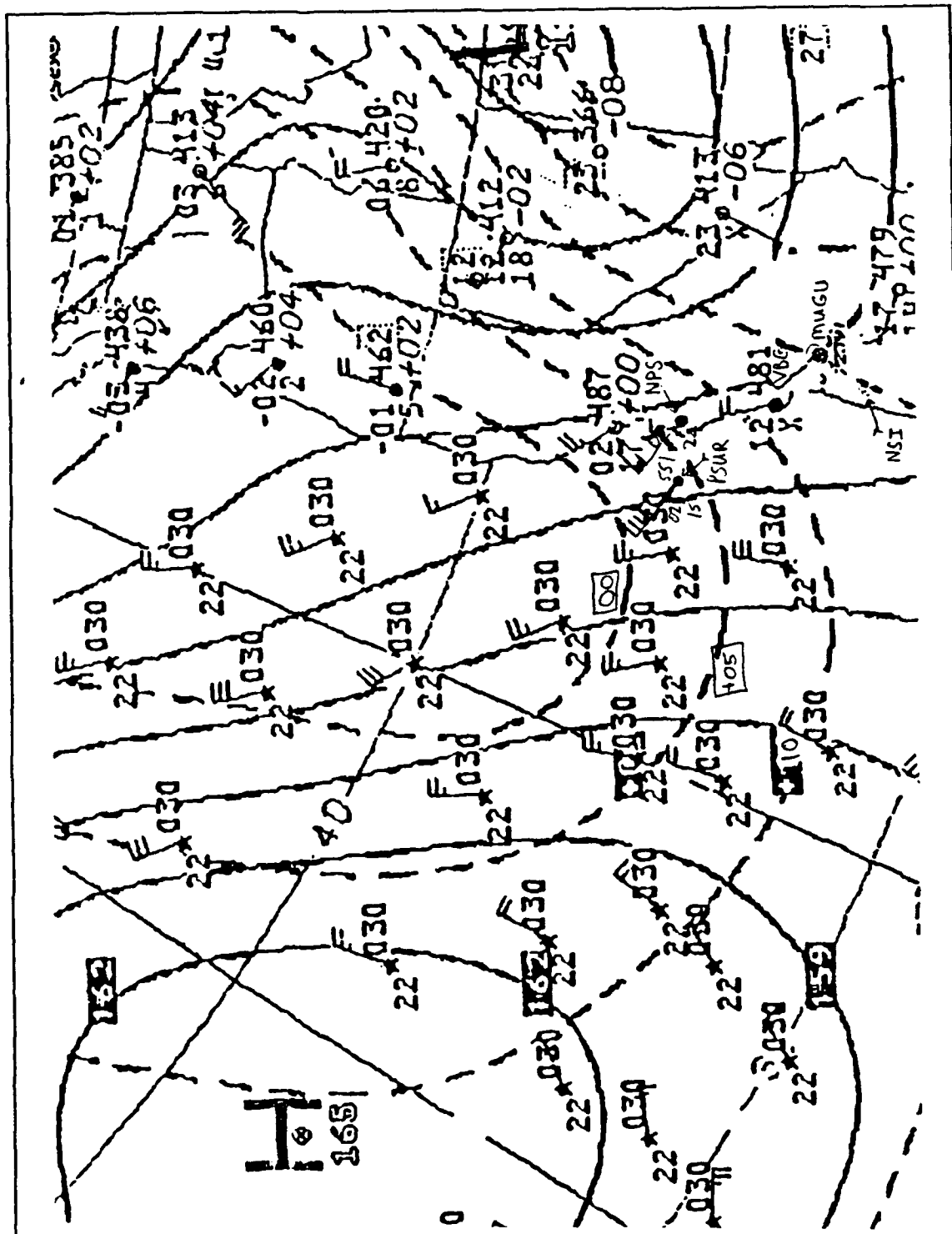
Fig. 27. 09/0000Z NMC 850 mb analysis of geopotential (dm) and temperature (degrees C). PSUR, NPS, VBG, MUGU, and NSI data added.
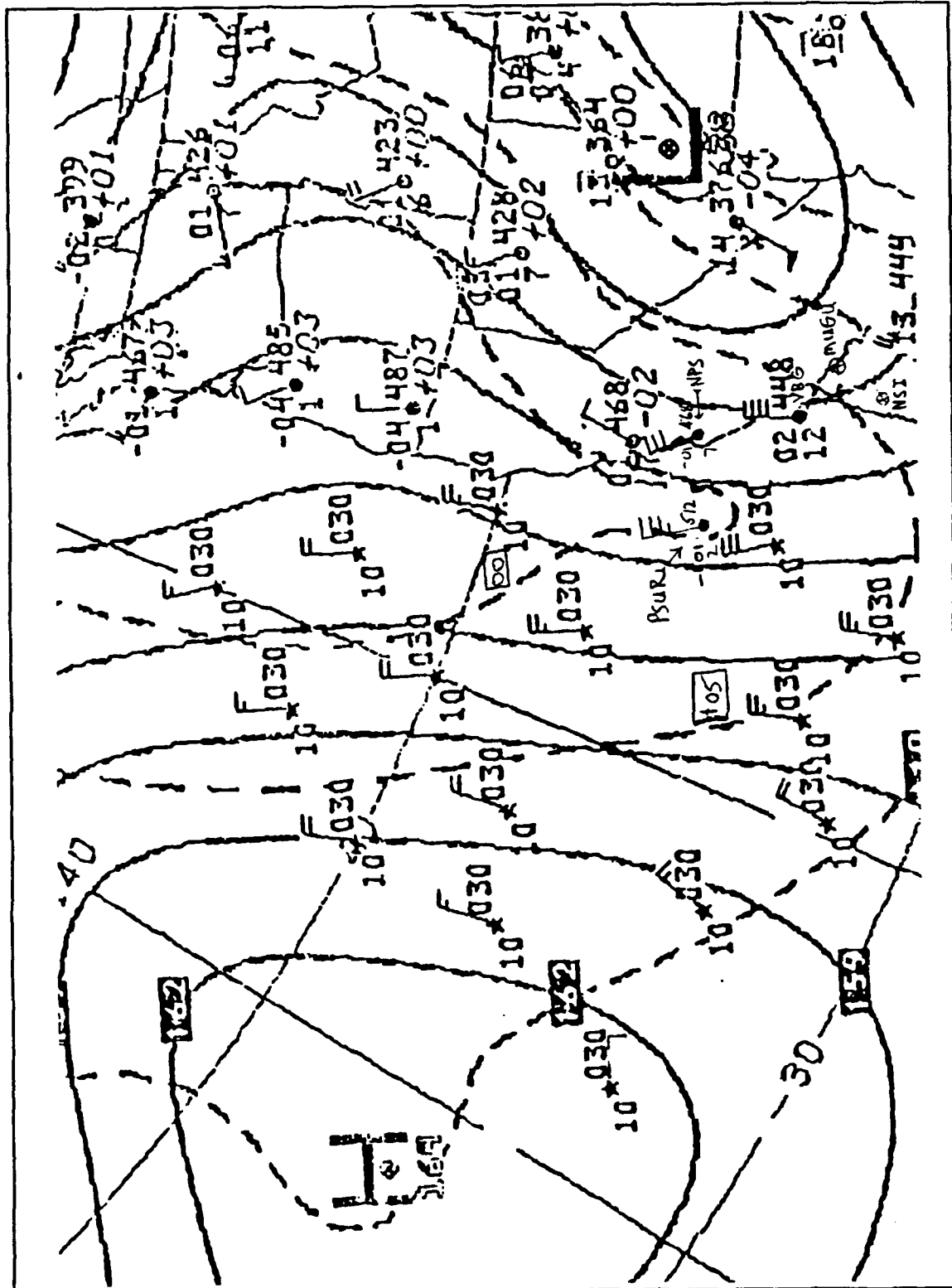
Fig. 28. Same as Fig. 27 but for 09/1200Z.

NPS
910509/0600

MODIFIED REFRACTIVITY – M UNITS

DUCTS
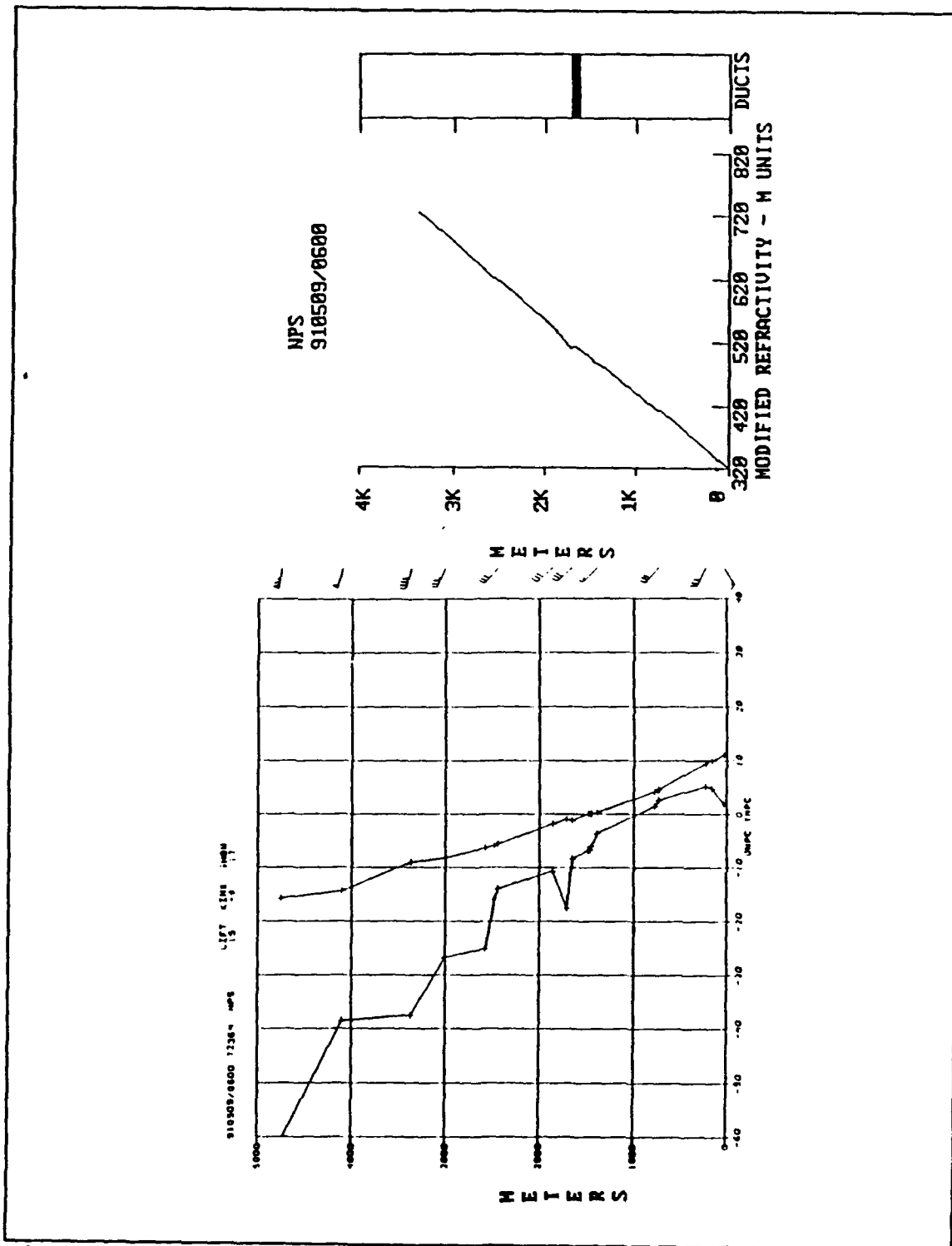
Fig. 29. 09/0600Z NPS sounding and IREPS profile. Fig. 27a
(left) is the sounding and Fig. 27b (right) is the IREPS
profile.
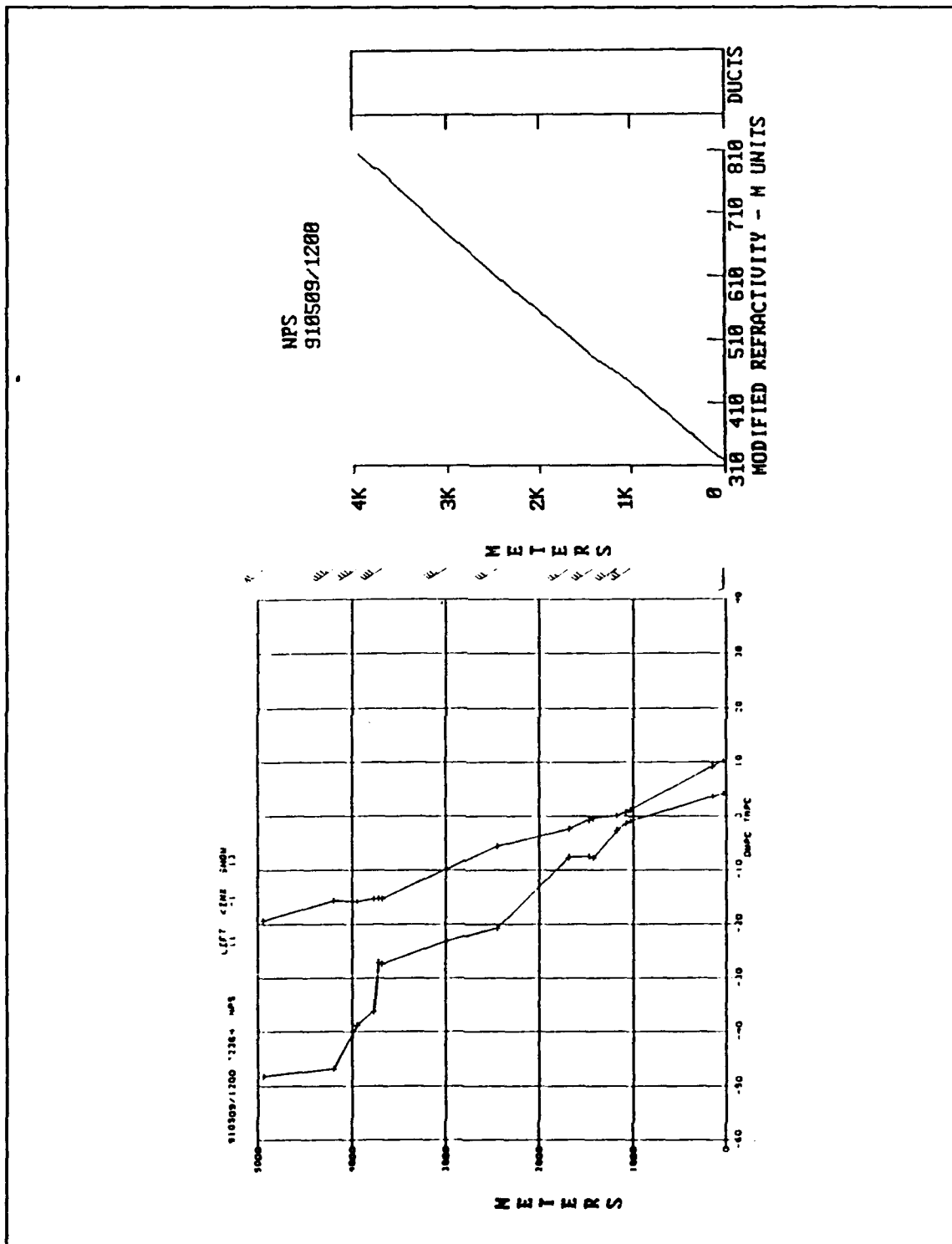
Fig. 30. 09/1200Z NPS sounding and IREPS profile. Fig. 28a (left) is the sounding and Fig. 28b (right) is the IREPS profile.
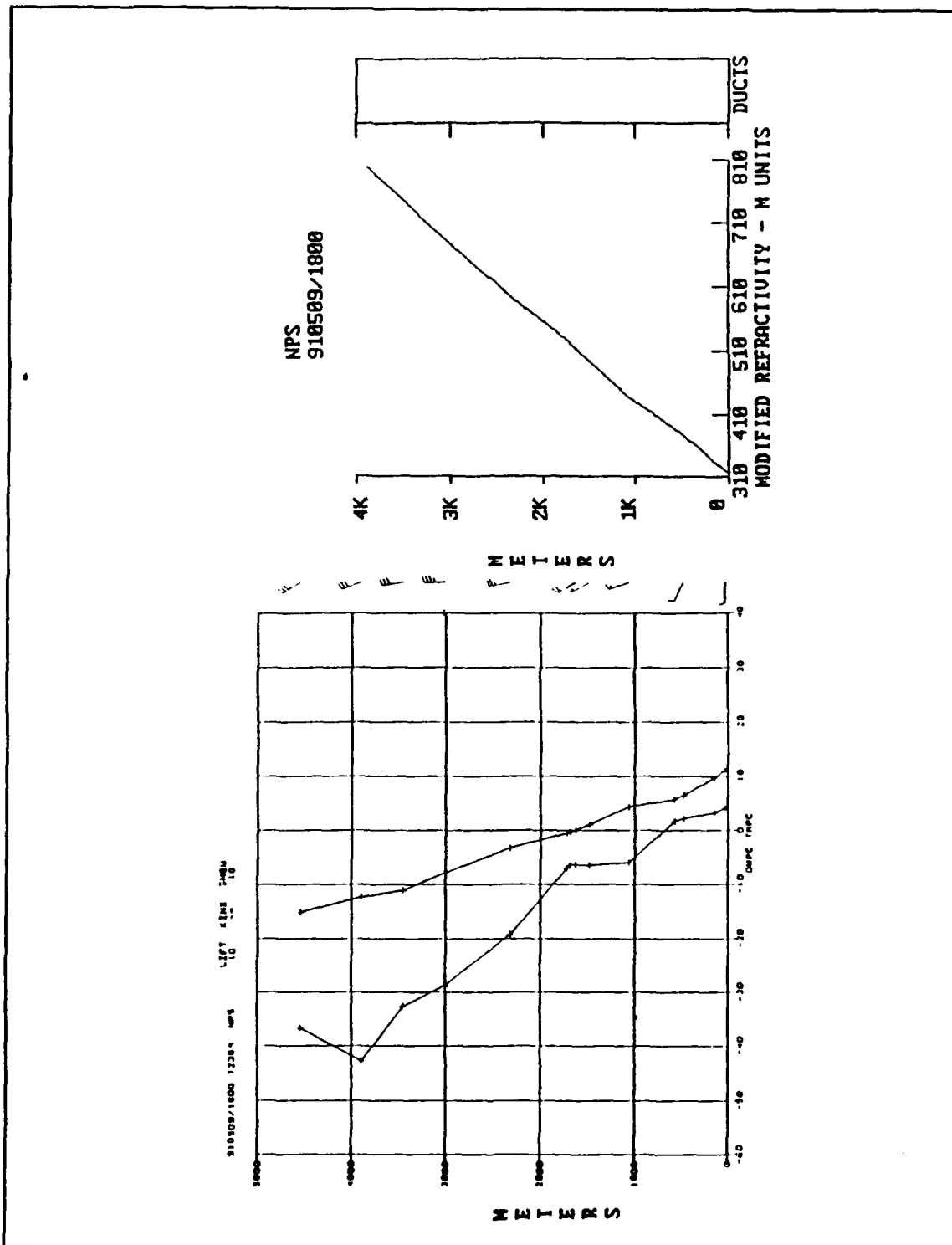
Fig. 31. 09/1800Z NPS sounding and IREPS profile. Fig. 29a (left) is the sounding and Fig. 29b (right) is the IREPS profile.
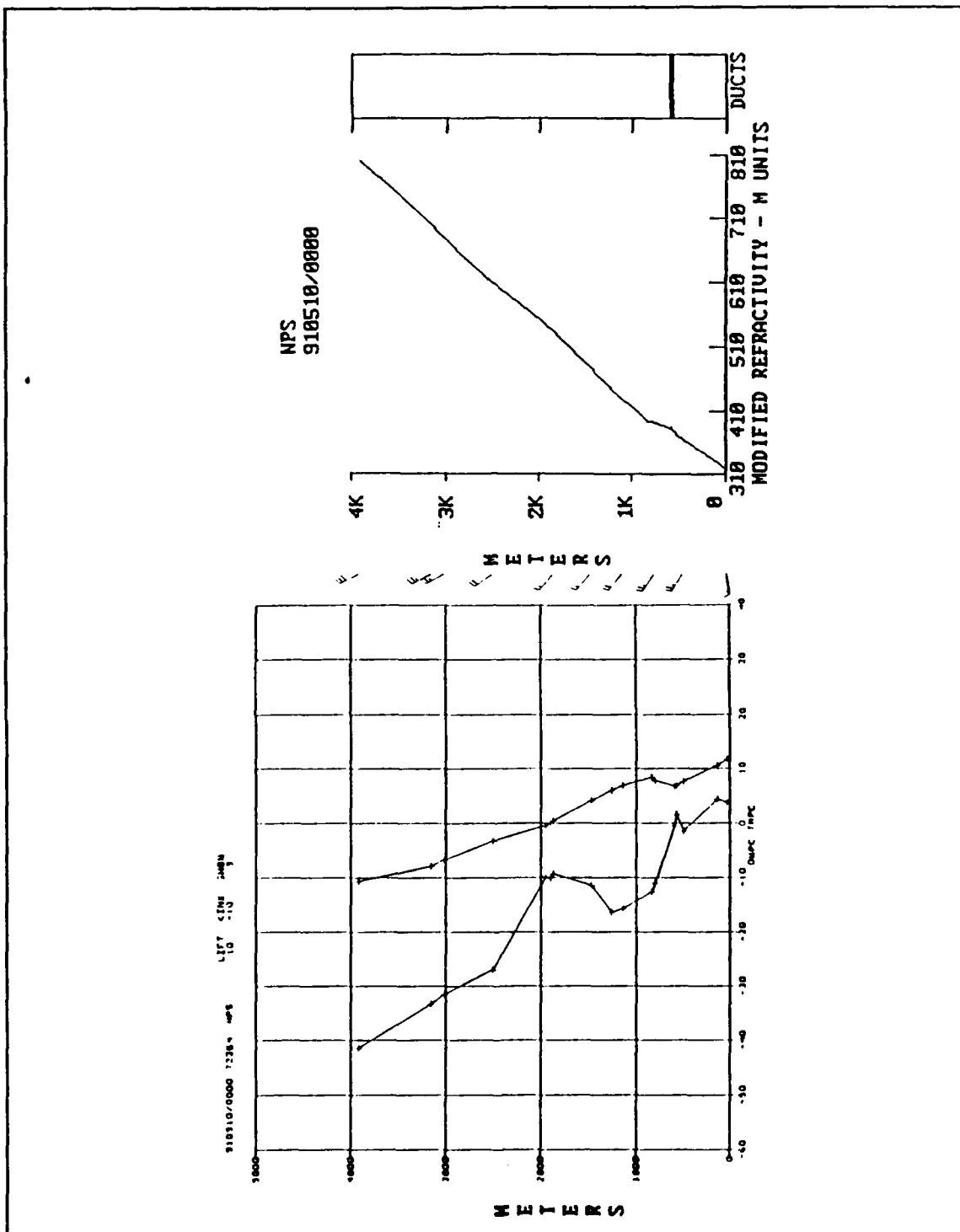
Fig. 32. 10/0000Z NPS sounding and IREPS profile. Fig. 30a (left) is the sounding and Fig. 30b (right) is the IREPS profile.
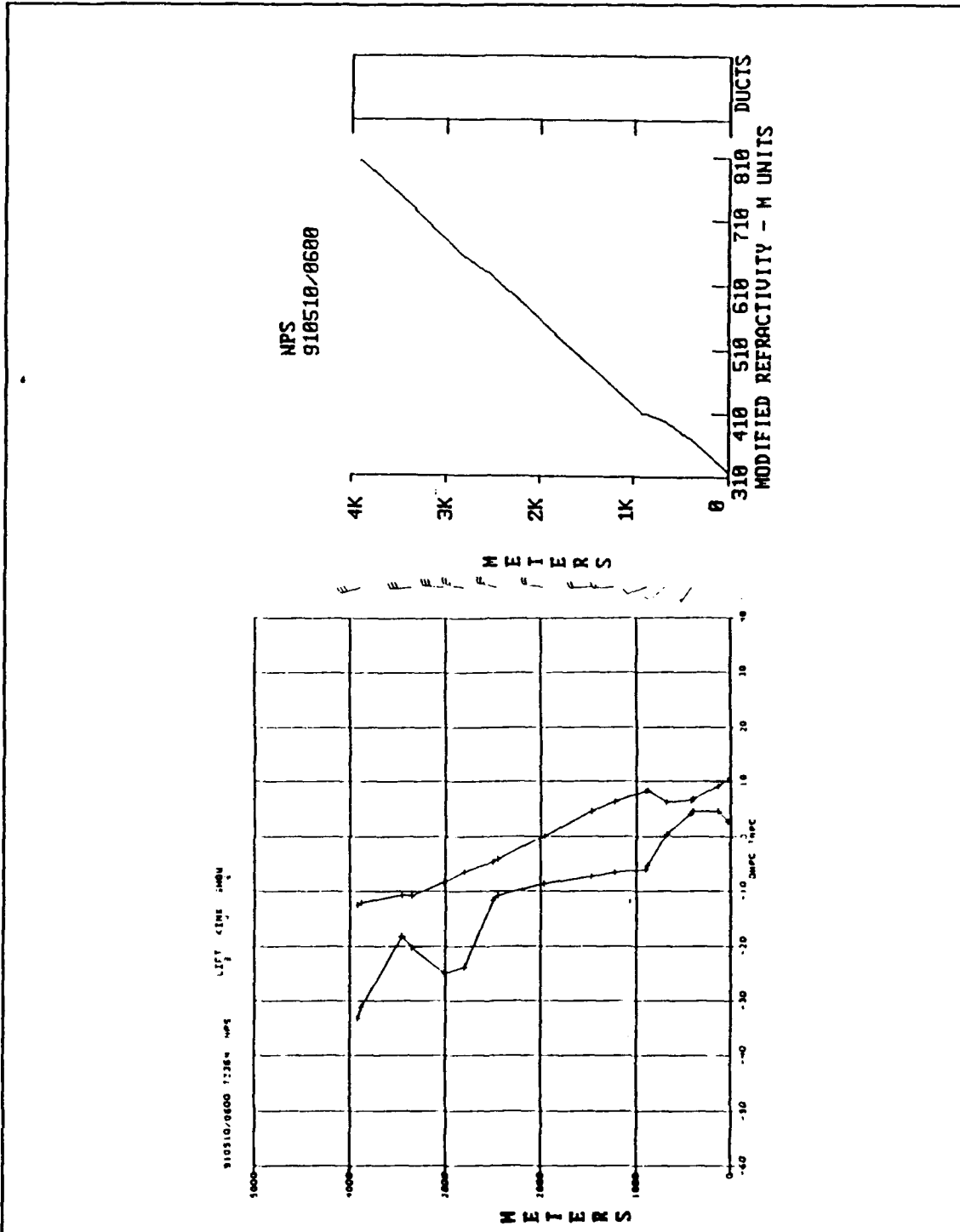
Fig. 33. 10/0600Z NPS sounding and IREPS profile. Fig. 31a (left) is the sounding and Fig. 31b (right) is the IREPS profile.

70
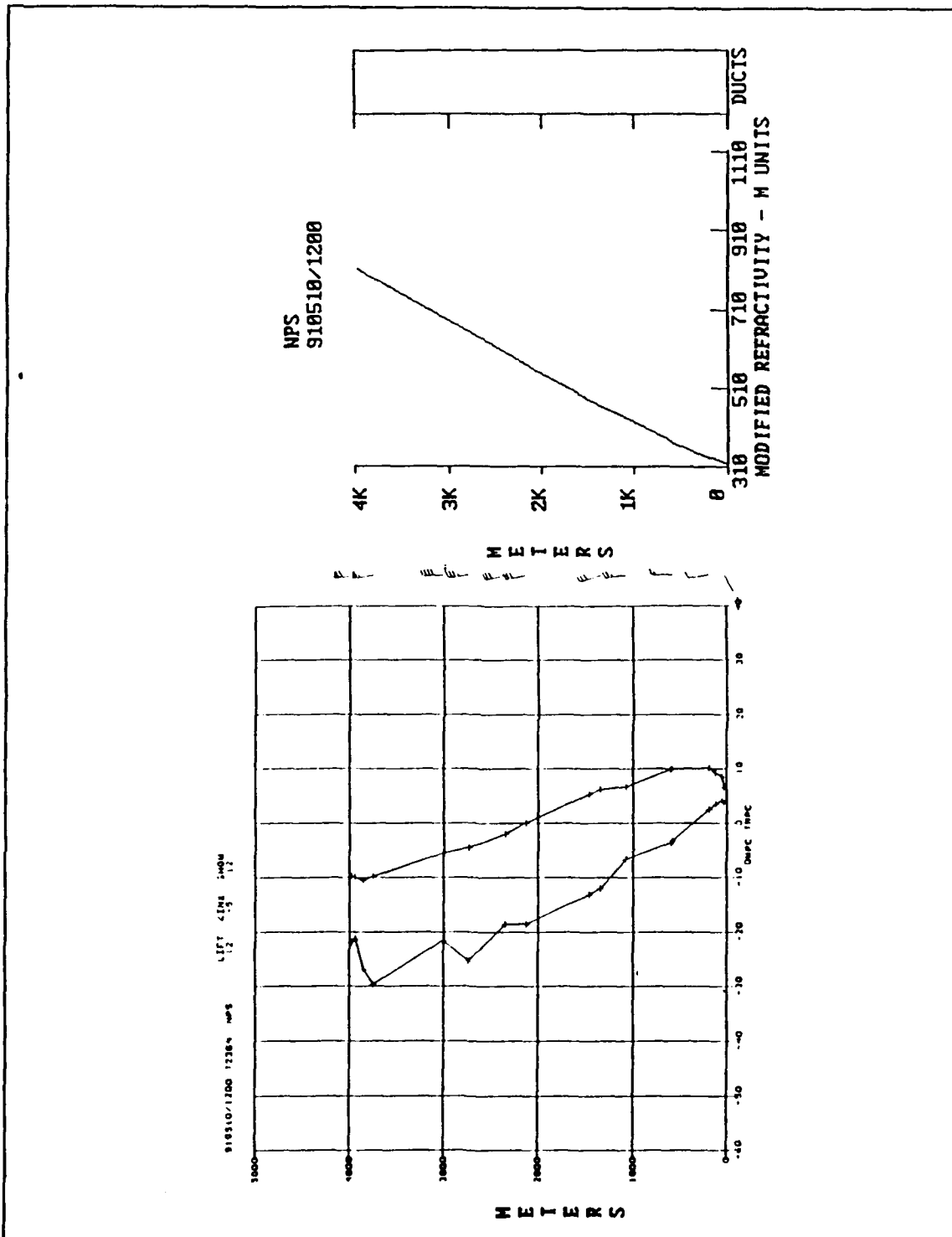
Fig. 34. 10/1200Z NPS sounding and IREPS profile. Fig. 32a (left) is the sounding and Fig. 32b (right) is the IREPS profile.

71
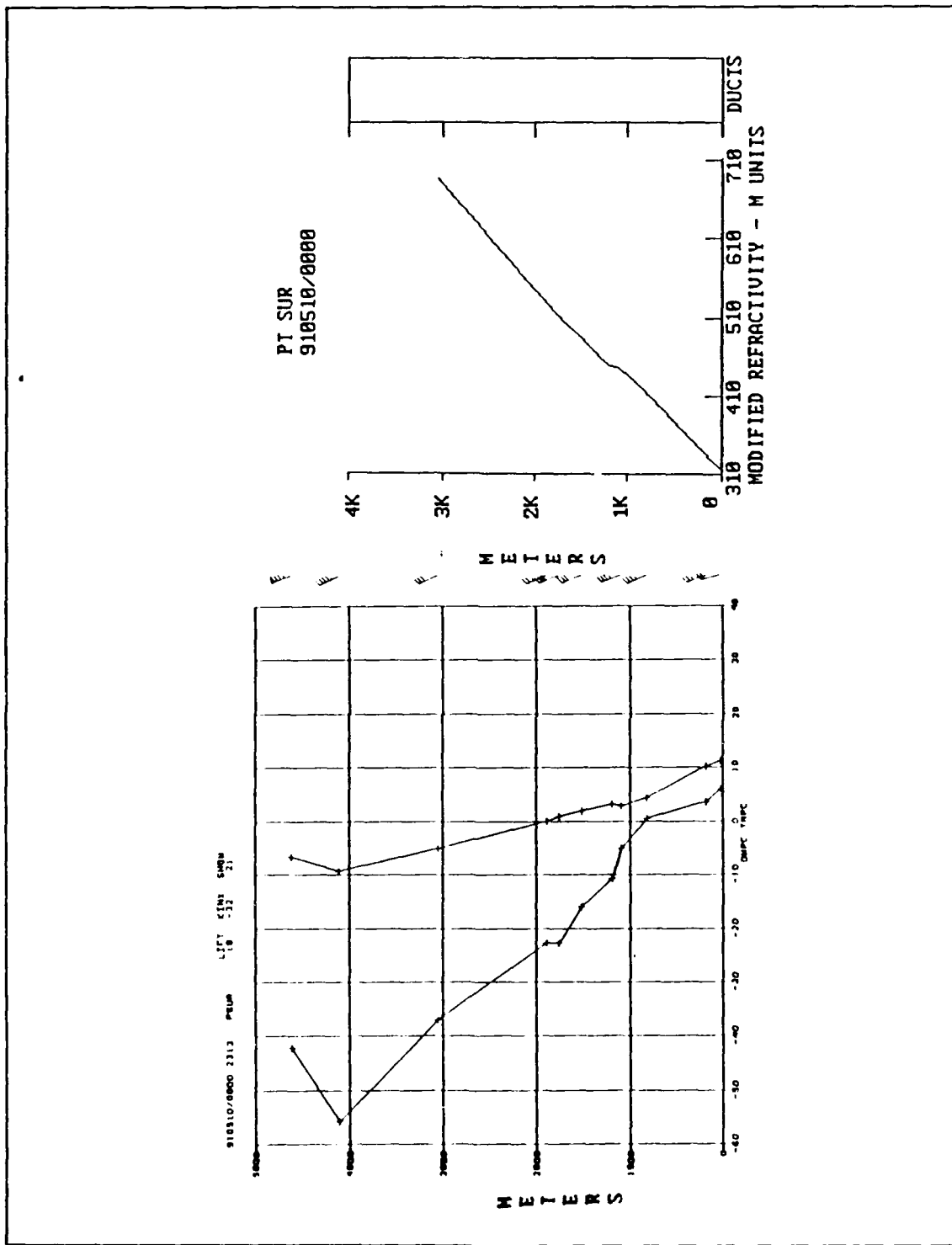
Fig. 35. 10/0000Z PSUR sounding and IREPS profile. Fig. 33a (left) is the sounding and Fig. 33b (right) is the IREPS profile.
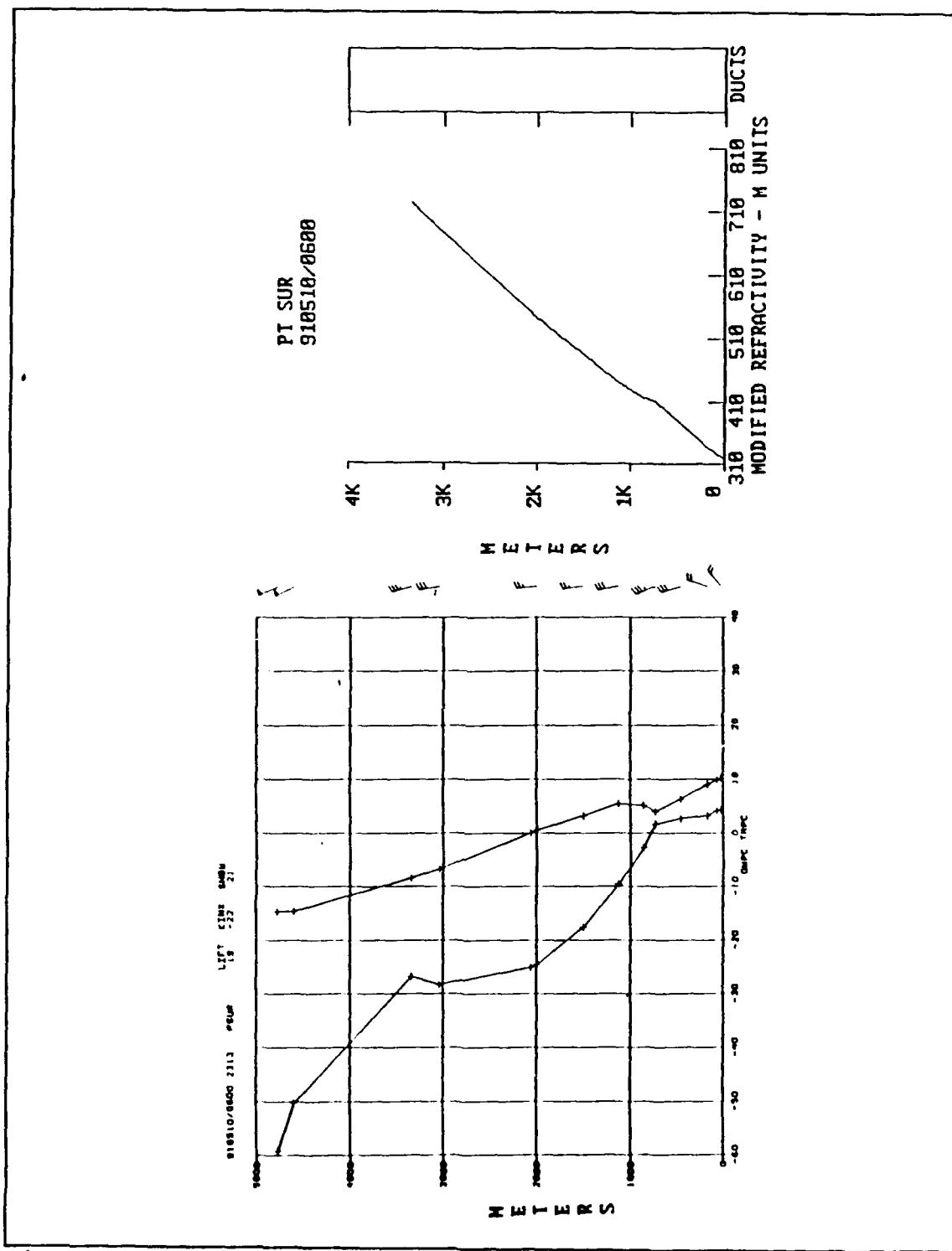
Fig. 36. 10/0600Z PSUR sounding and IREPS profile. Fig. 34a (left) is the sounding and Fig. 34b (right) is the IREPS profile.

73
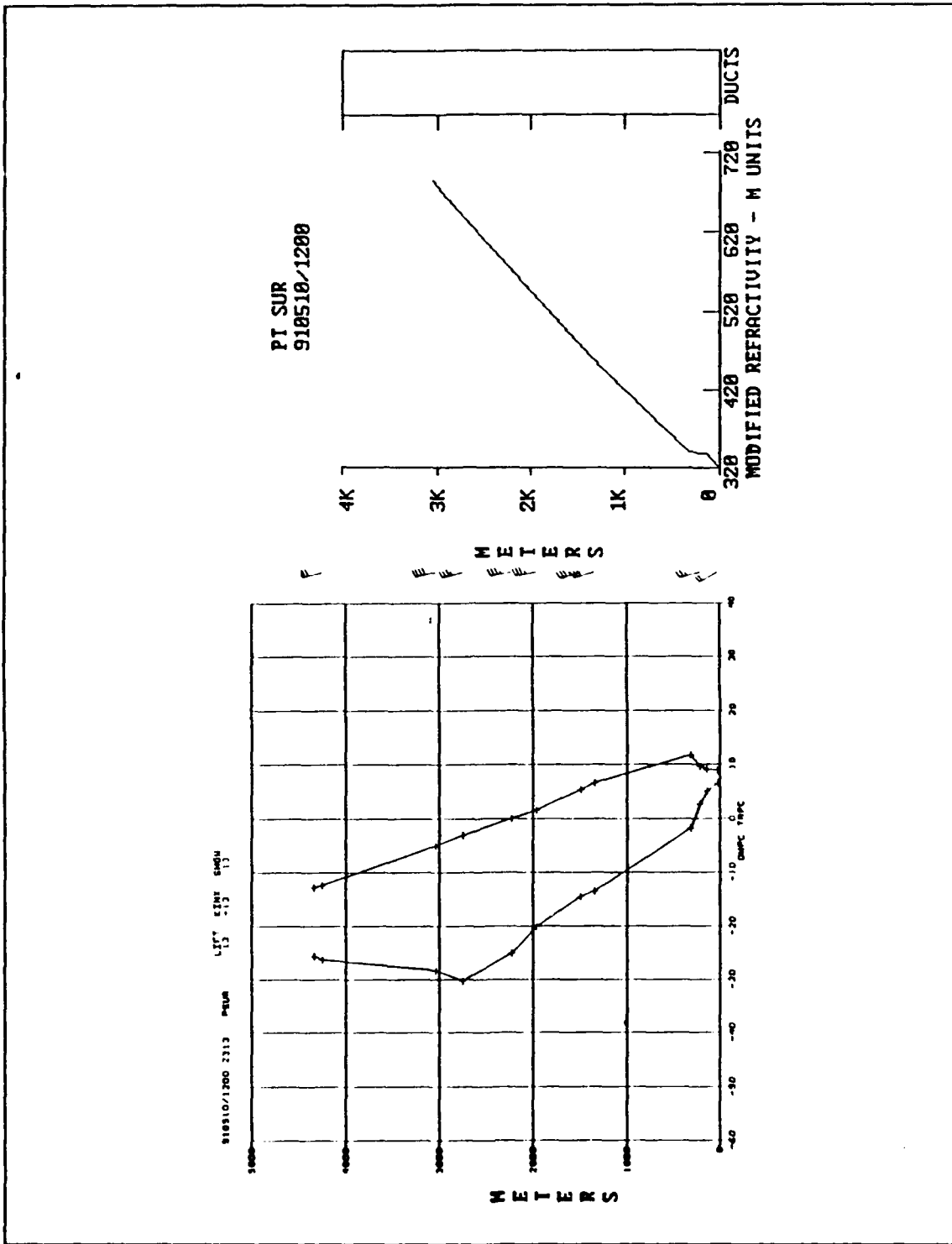
Fig. 37. 10/1200Z PSUR sounding and IREPS profile. Fig. 35a (left) is the sounding and Fig. 35b (right) is the IREPS profile.
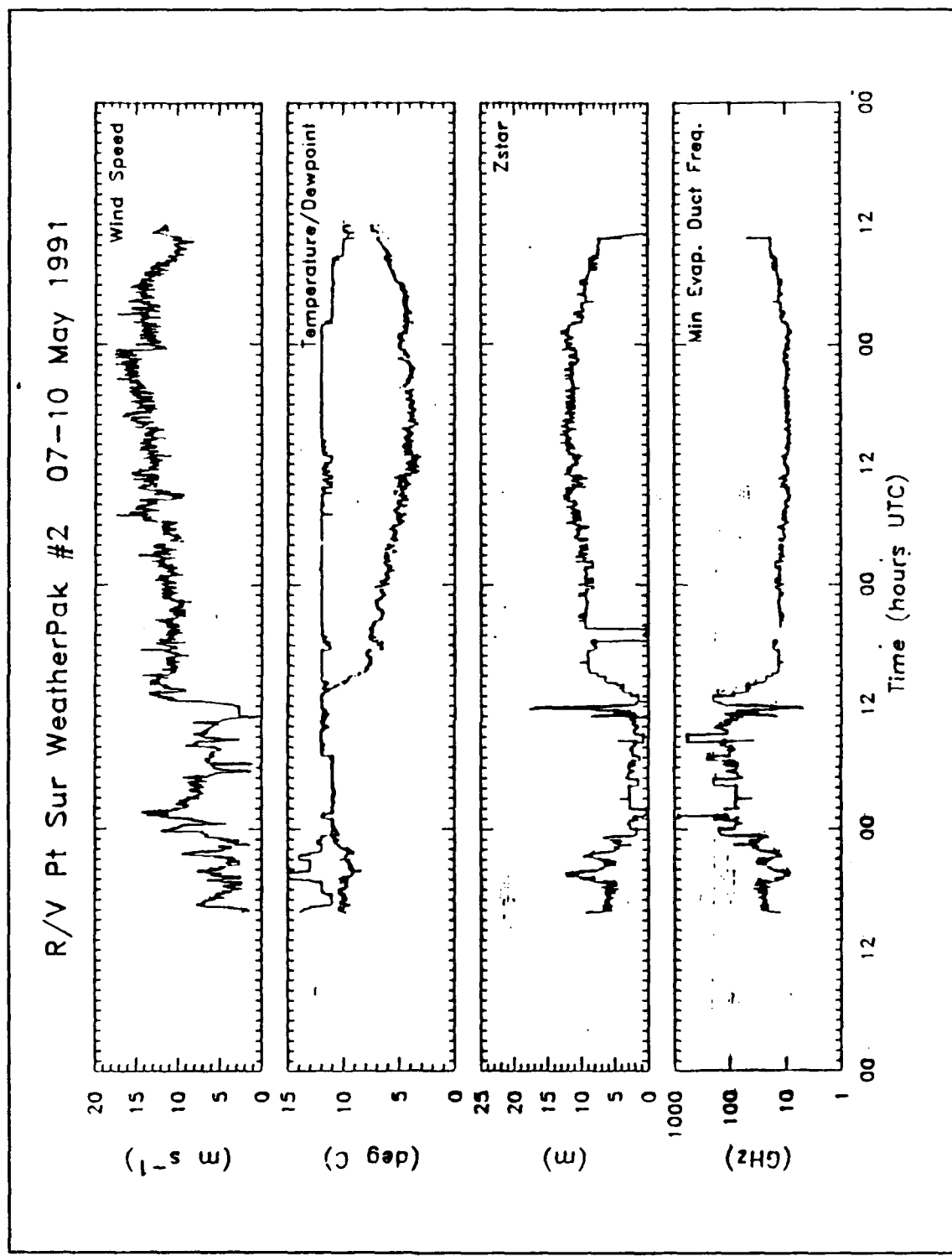
Fig. 38. PSUR surface time series. Plots of wind speed, temperature, dewpoint temperature, evaporation duct height (Z_*) and minimum evaporation duct frequency (f_{min}).
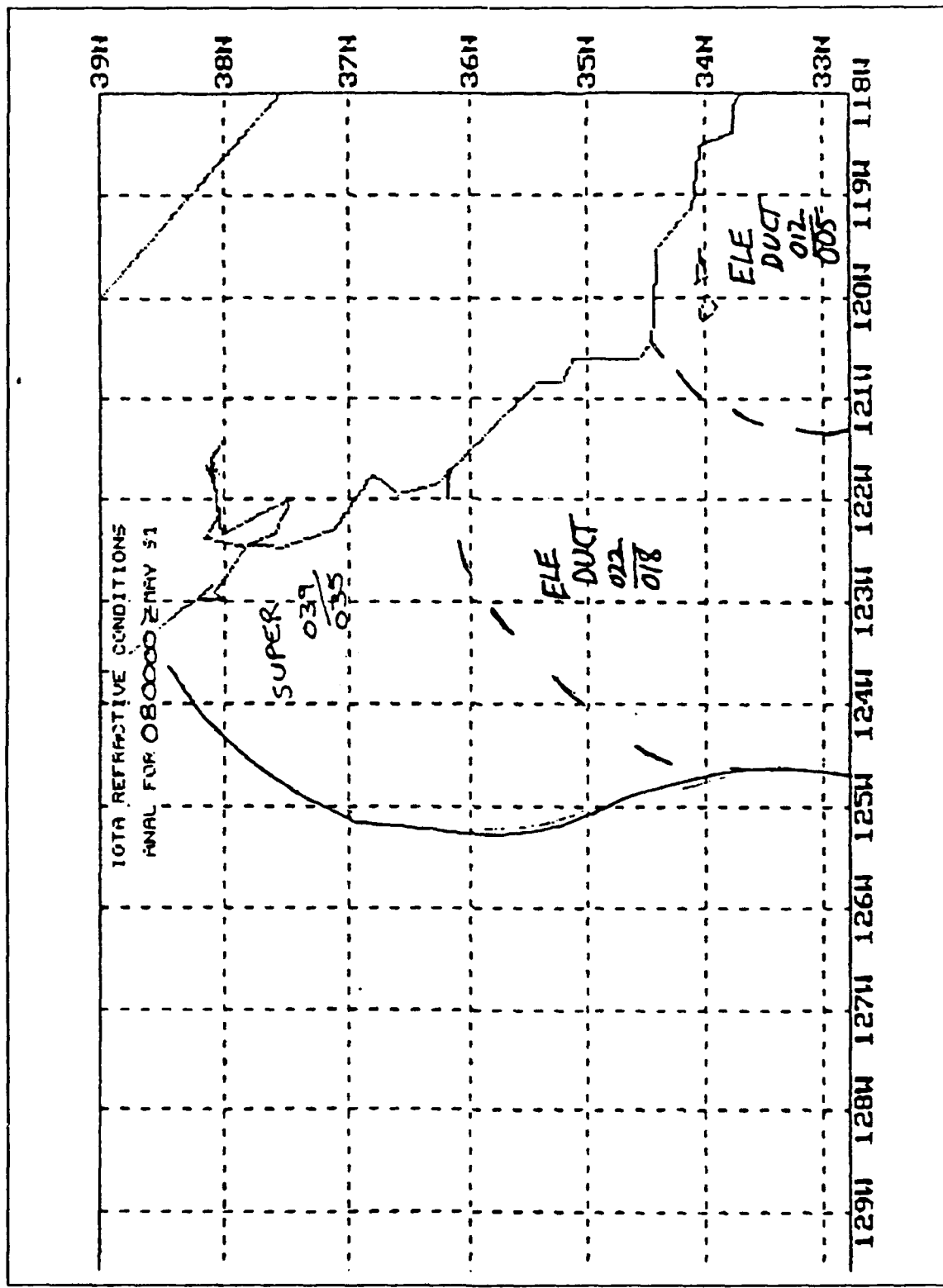
Fig. 39. 08/0000Z NWOC refractive assessment.
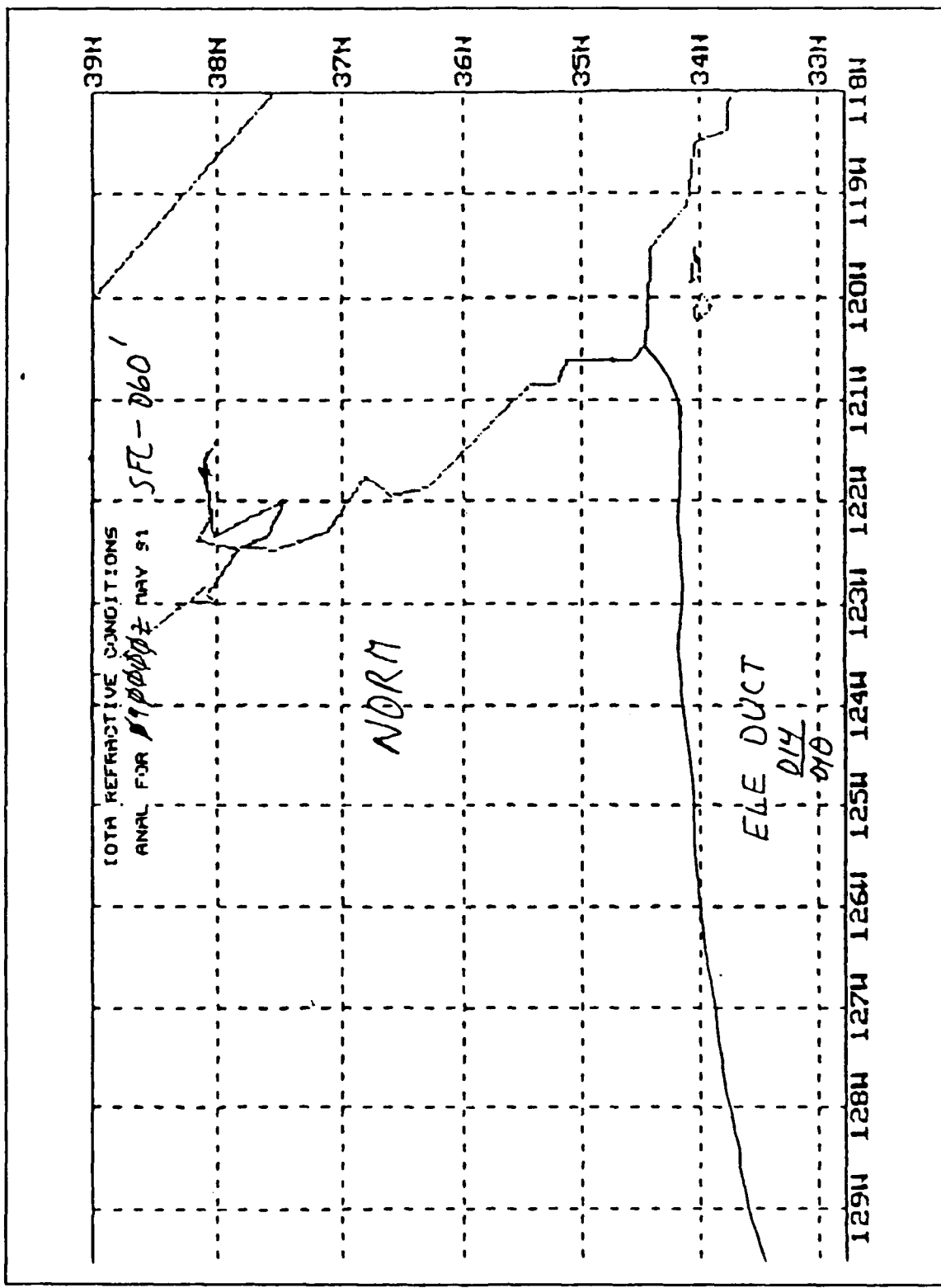
**Fig. 40.** 09/0000Z NWOC refractive assessment.

Fig. 41. 10/0000Z NWOC refractive assessment.
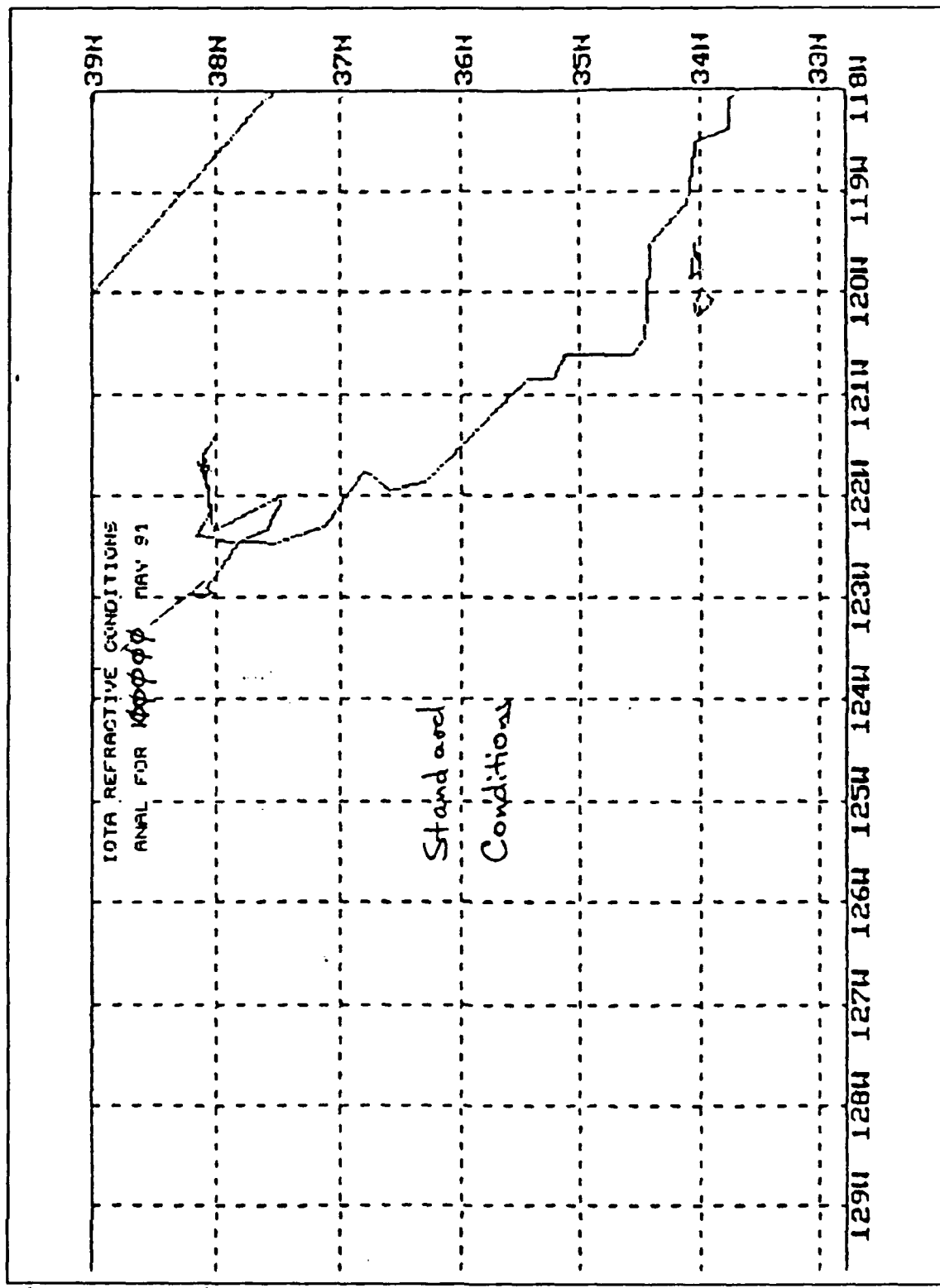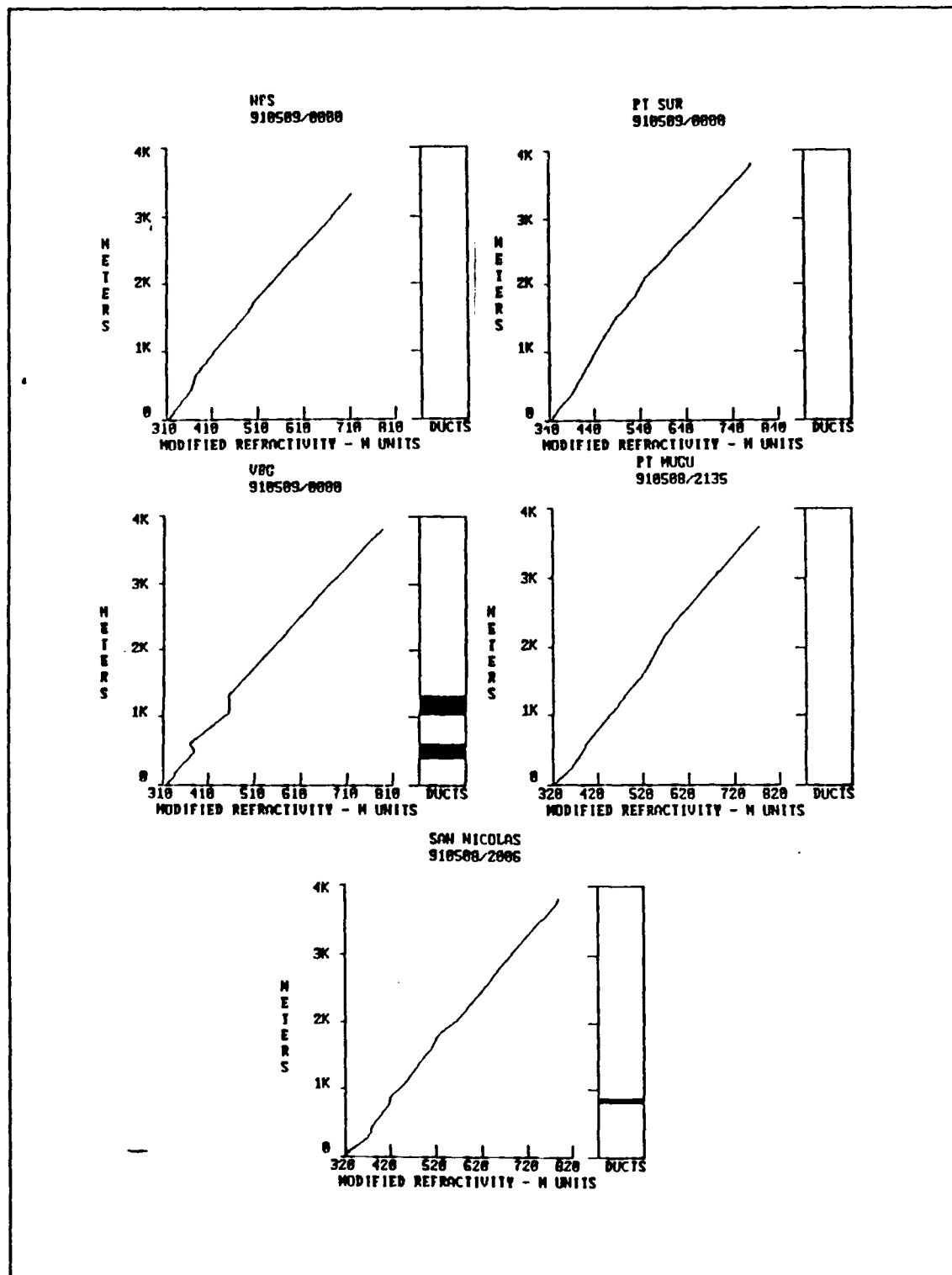
Fig. 42. 09/0000Z IREPS profiles. Survey station IREPS profiles for 09/0000Z time period.
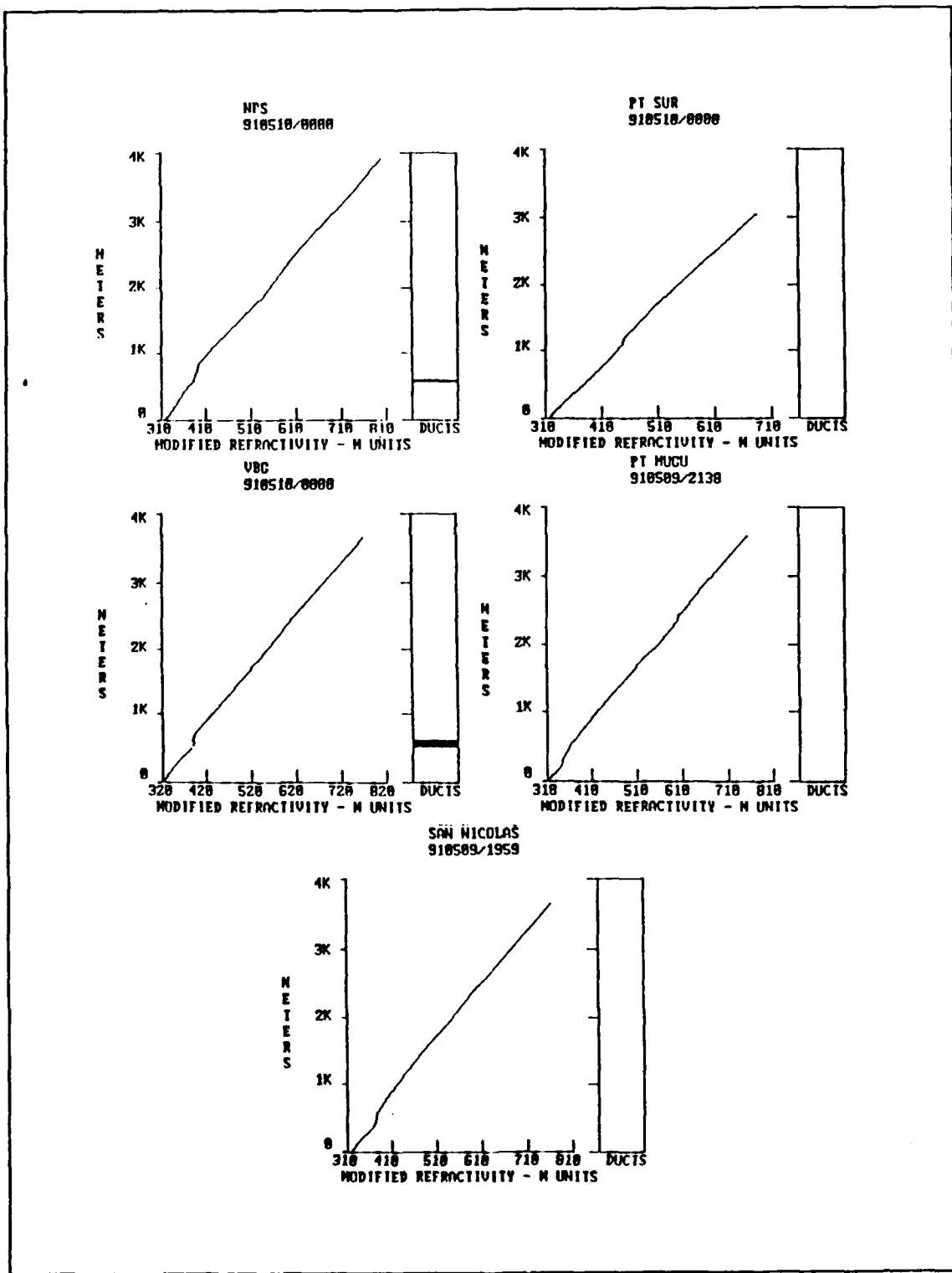
**Fig. 43.** 10/0000Z IREPS profile. Survey station IREPS profiles for 10/0000Z time period.
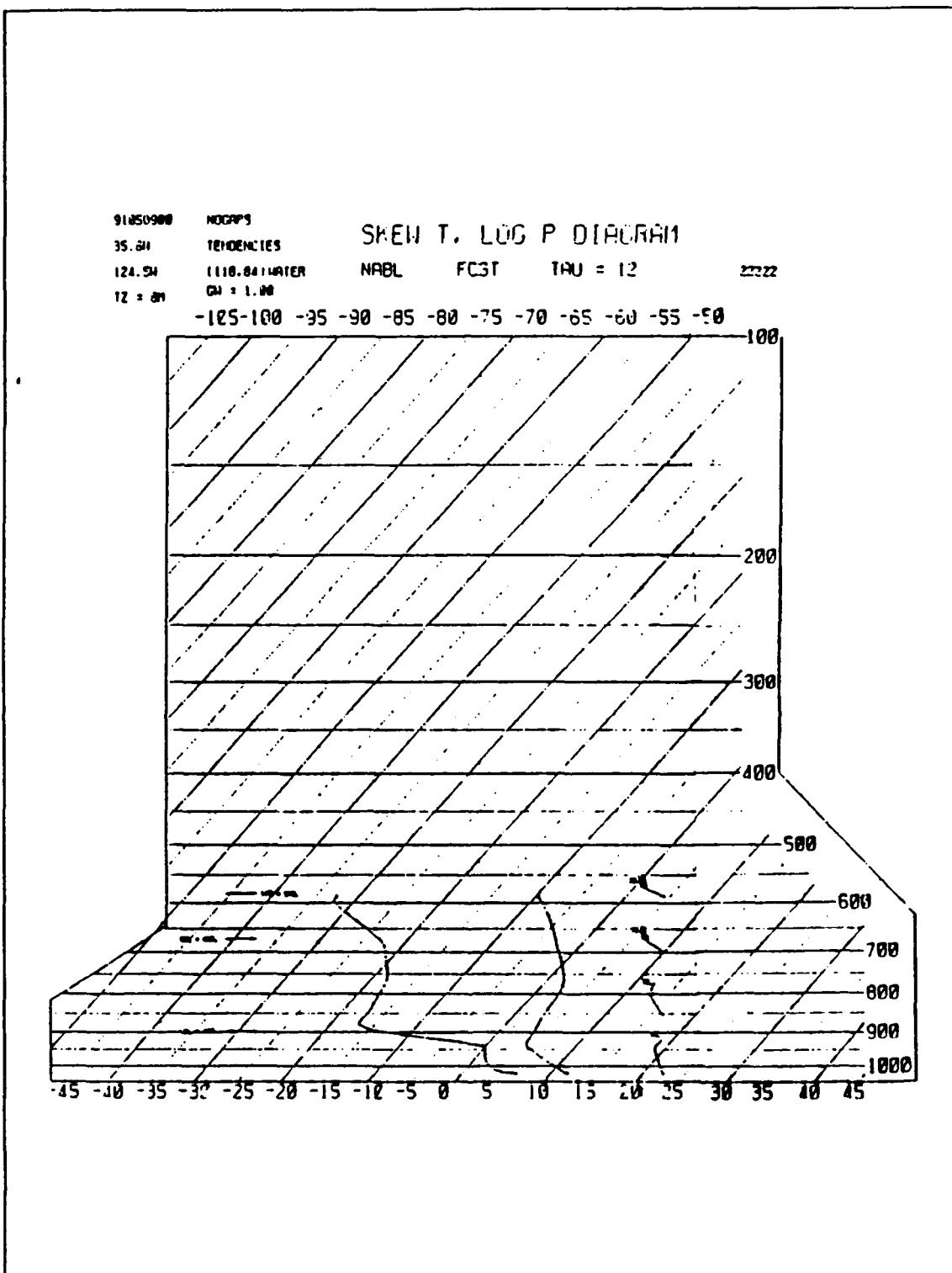
Fig. 44. 09/0000Z NABL sounding forecast. NABL 09/0000Z 12 hour sounding forecast for 09/1200Z.

81
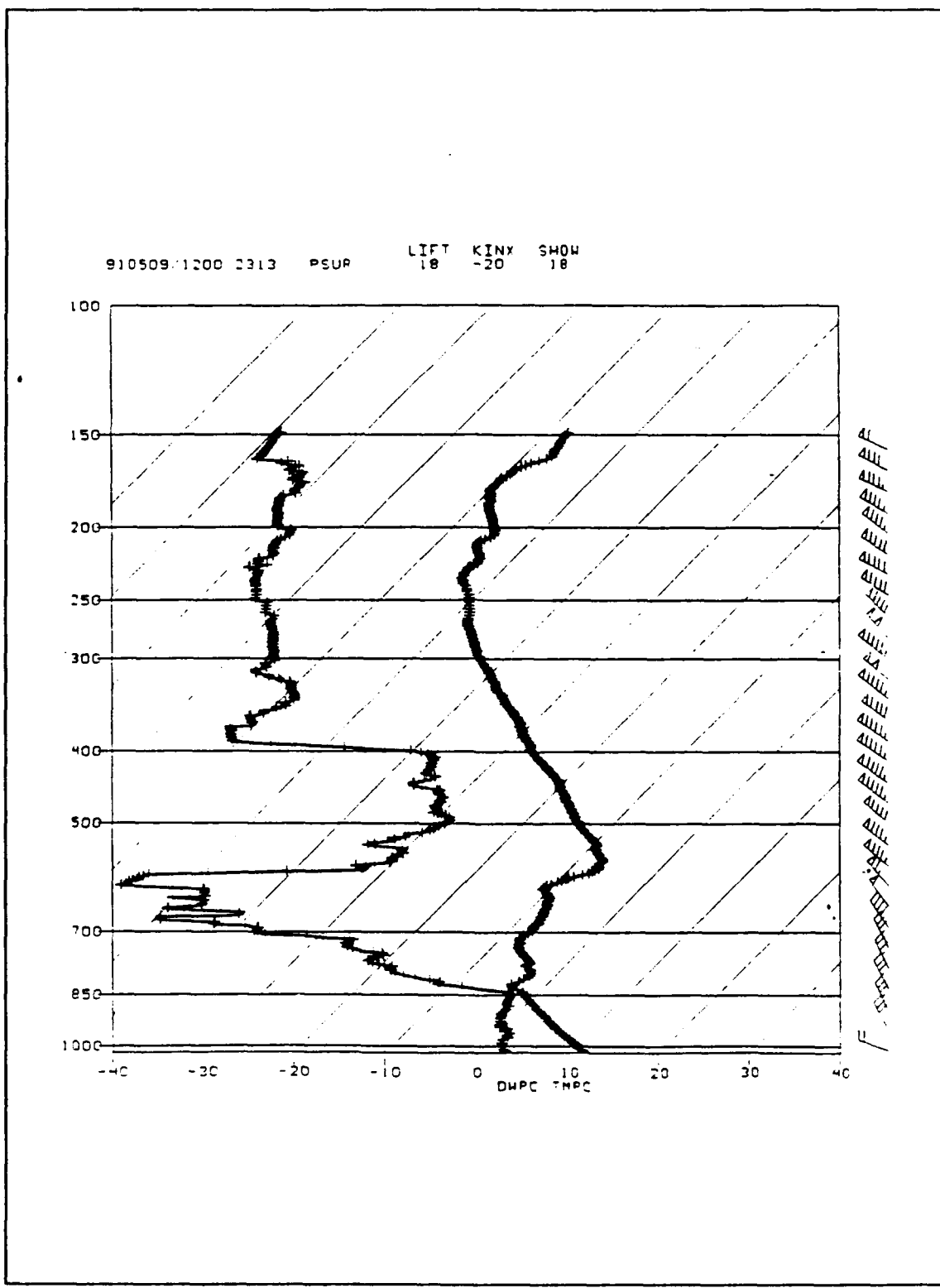
**Fig. 45.** 09/1200Z PSUR sounding.
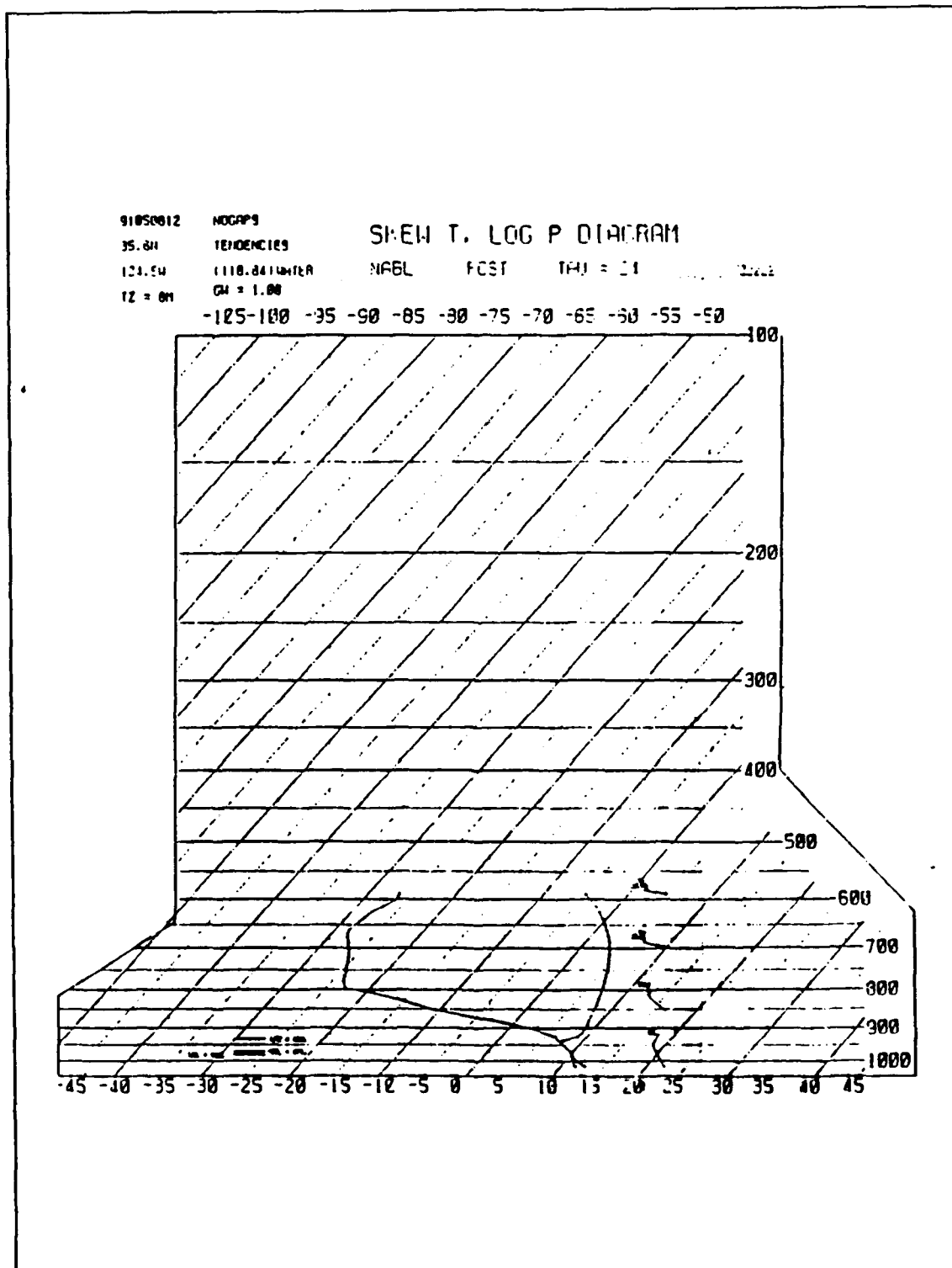
Fig. 46. 08/1200Z NABL sounding forecast. NABL 08/1200Z 24 hour sounding forecast for 09/1200Z.
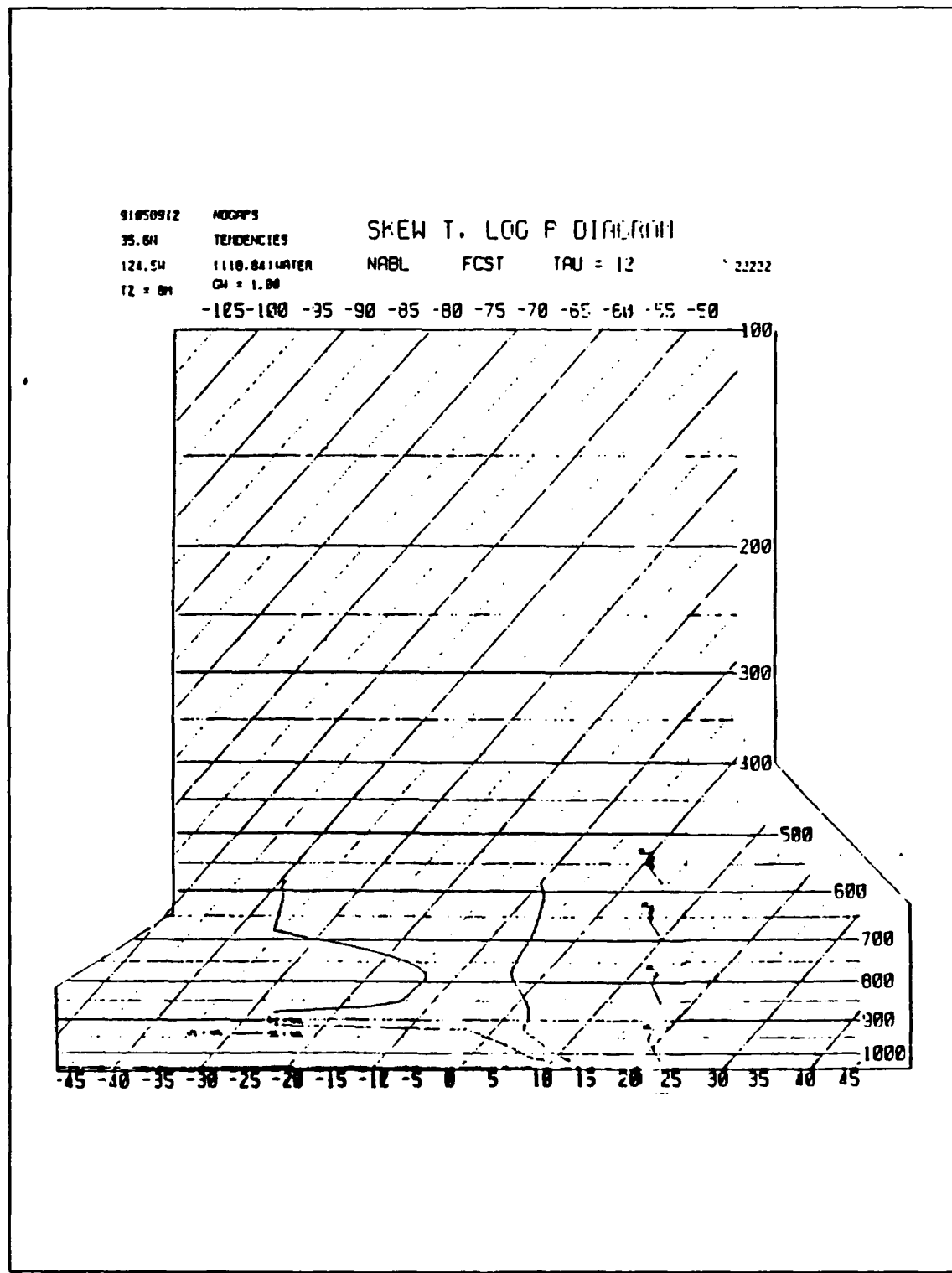
**Fig. 47.** 09/1200Z NABL sounding forecast. NABL 09/1200Z 12 hour sounding forecast for 10/0000Z.
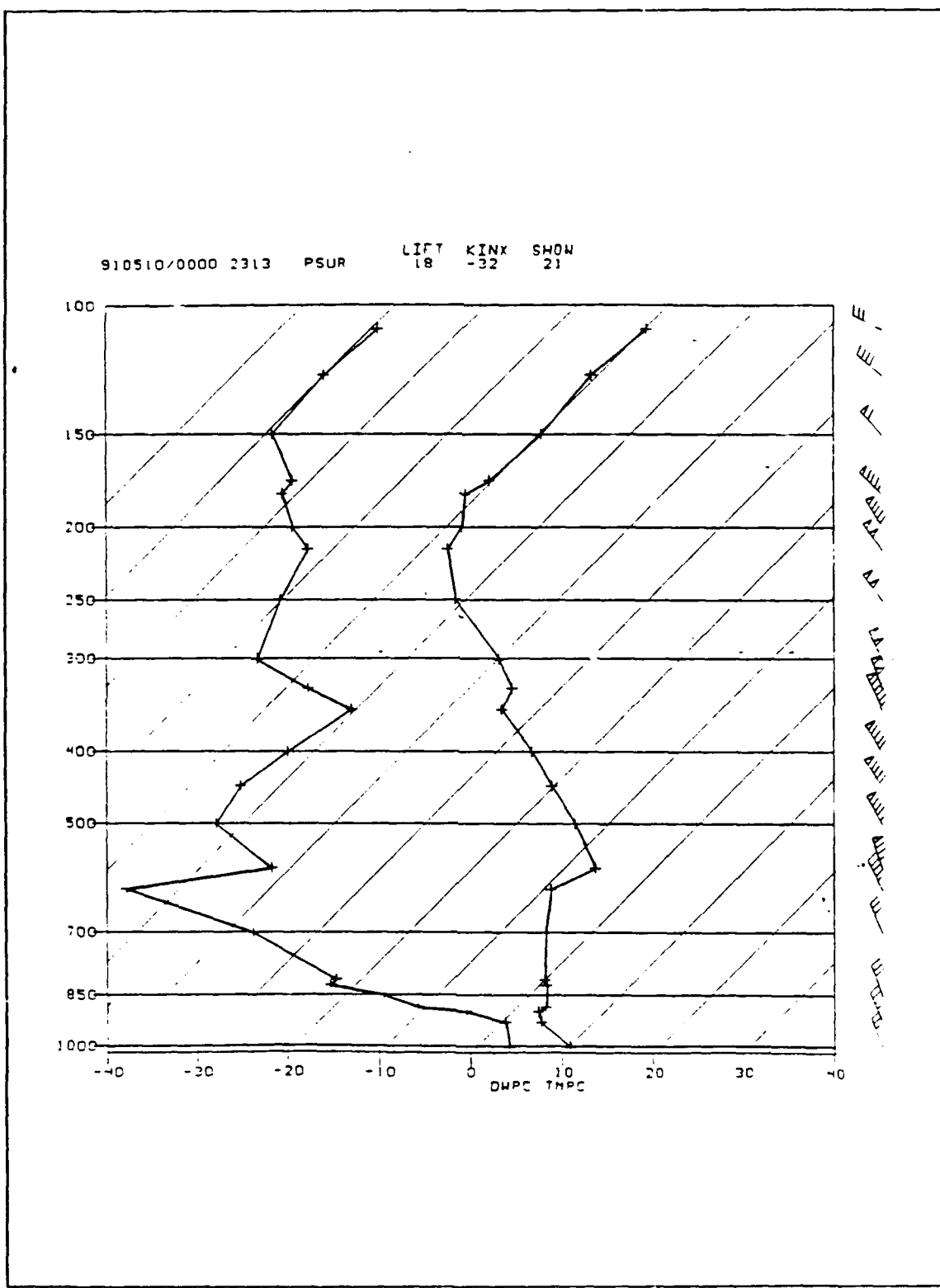
**Fig. 48.** 10/0000Z PSUR sounding.
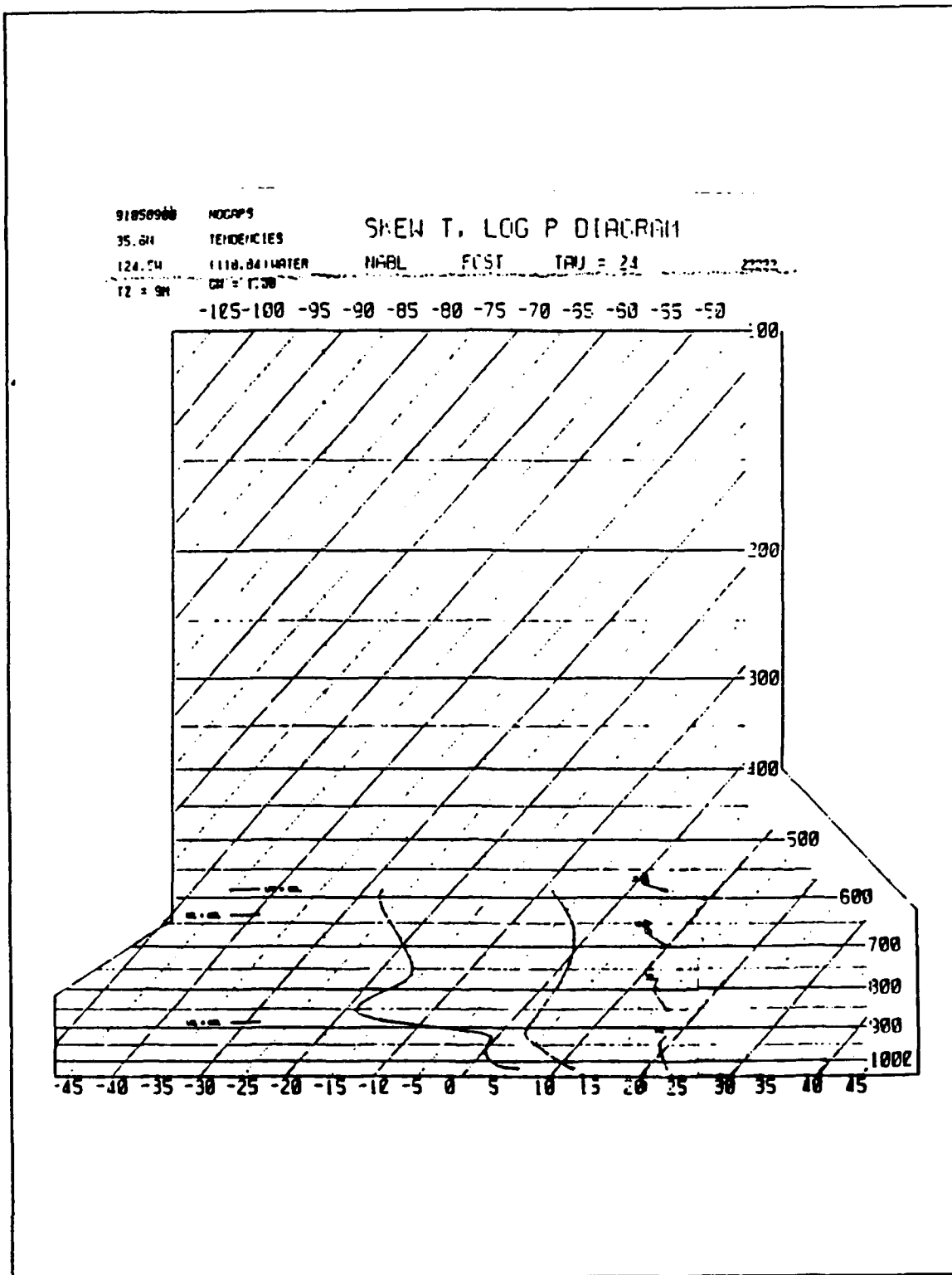
Fig. 49. 09/0000Z NABL sounding forecast. NABL 09/0000Z
24 hour sounding forecast for 10/0000Z.

LIST OF REFERENCES

Davidson, K. L., Lectures on electromagnetic propagation. Lecture notes from refractivity course at the Naval Postgraduate School, Monterey, CA, April 1991.

Fairall, C. W., Davidson, K. L., Schacher, G. E., and Houlihan, T. M., Evaporation Duct Height Measurements in the Mid-Atlantic, Naval Postgraduate School Report NPS61-78-005, pp. 11-24, 15 August 1978.

Farrell, Robert J., Jr., The Caribbean Basin--A Refractivity Study, USAF Environmental Technical Applications Center USAFETAC/TN-89/007, p. 5, December 1989.

Ko, H. W., Sari, J. W., and Skura, J. P., "Anomalous Microwave Propagation Through Atmospheric Ducts," John Hopkins APL Technical Digest, Vol. 4, No. 3, pp. 12-26, January-March 1983.

Patterson, W. L., and others, Engineer's Refractive Effects Prediction System (EREPS) Revision 2.0, NOSC Technical Document 1342 Rev. 2.0, Naval Ocean Systems Center, San Diego, CA, February 1990.

Patterson, W. L., Effective Use of the Electromagnetic Products of TESS and IREPS, NOSC Technical Document 1369, Naval Ocean Systems Center, San Diego, CA, October 1988.

----------, Integrated Refractive Effects Prediction System (IREPS) User's Manual Revision PC-2.0, NOSC Technical Document 1874, Naval Ocean Systems Center, San Diego, CA, August 1990.

Paulus, R. A., Specification for Environmental Measurements to Assess Radar Sensors, NOSC Technical Document 1685, Naval Ocean Systems Center, San Diego, CA, November 1989.

Rosenthal, J., and Helvey, R., "Some Synoptic Considerations Relative to the Refractive Effects Guidebook (REG)," Proceedings of Conference on Atmospheric Refractive Effects Assessment 23-25 January 1979 San Diego, California, NOSC Technical Document 260, Naval Ocean Systems Center, San Diego, CA, 1979.

INITIAL DISTRIBUTION LIST

No. Copies

1. Defense Technical Information Center   2
   Cameron Station
   Alexandria, VA 22304-6145

2. Library, Code 52   2
   Naval Postgraduate School
   Monterey, CA 93943-5000

3. Chairman (Code MR/Hy)   1
   Department of Meteorology
   Naval Postgraduate School
   Monterey, CA 93943-5000

4. Chairman (Code OC/Co)   1
   Department of Oceanography
   Naval Postgraduate School
   Monterey, CA 93943-5000

5. Professor Carlyle H. Wash (Code MR/WX)   3
   Department of Meteorology
   Naval Postgraduate School
   Monterey, CA 93943-5000

6. Professor Ken L. Davidson (Code MR/WX)   2
   Department of Meteorology
   Naval Postgraduate School
   Monterey, CA 93943-5000

7. LCDR Anthony A. Martinez   1
   NOCC/JTWC
   PSC 489, Box 2
   FPO AP 96540-0051

8. Director Naval Oceanography Division   1
   Naval Observatory
   34th and Massachusetts Avenue NW
   Washington, DC 20390

9. Commander   1
   Naval Oceanography Command
   Stennis Space Center, MS 39529-5000

10. Mr. Michael Pastore   1
    NOARL
    Monterey, CA 93943-5006